ROLE OF IL-6 AND OSM ON TUMOR DEVELOPMENT IN MOUSE MODELS FOR LUNG CANCER

THE ROLE OF GP130 CYTOKINES IL-6 AND OSM ON TUMOR DEVELOPMENT IN MOUSE MODELS FOR LUNG ADENOCARCINOMA

By SEAN LAUBER, B.Sc.

A Thesis Submitted to the School of Graduate Studies in Fulfillment of the Requirements for the Degree Master of Science

McMaster University MASTER OF SCIENCE (2012) Hamilton, Ontario

TITLE: The role of gp130 cytokines IL-6 and OSM on tumor development in mouse models for lung adenocarcinoma AUTHOR: Sean Lauber, B.Sc. (Concordia University) SUPERVISOR: Dr. Carl Richards NUMBER OF PAGES: xi, 143

Abstract

Lung cancer is the leading cause of cancer related deaths in both the US and Canada and efforts still need to be made towards understanding the disease. The role of inflammation in the promotion of cancer development represents a newer avenue of research. The glycoprotein (gp)-130 cytokine interleukin-6 (IL-6) has a well established role in promoting inflammation and recent evidence suggests roles in development of certain tumors in animal models. Less is known of the related family member oncostatin M (OSM) and the functions of either IL-6 or OSM in lung cancer development is not known. Based on the hypothesis that these cytokines promote lung cancer development, IL-6 and OSM were overexpressed in the lungs of two separate mouse models for lung cancer utilizing adenovirus vectors encoding IL-6 or OSM. The first mouse model utilized a Cre-conditional oncogene KRAS G12D (developed by Tyler Jacks) in which endotracheal administration of adenovirus (Ad)-encoded Cre-recombinase resulted in increases in lung densities in a dose-dependent fashion over a period of 6 weeks that were measurable by CT scanning and histology. Increases in cytokines IL-6 and kertinocyte chemoattractant (KC) were detectable in the bronchoalveolar lavage (BAL) by week 4, as well as marked increases in alveolar macrophage numbers. Macrophages were also shown as a possible target for Cre-mediated recombination and mutant KRAS expression. Administration of either AdIL-6 or AdOSM as well as AdCre resulted in a trend toward increases in tumor burden with AdOSM based on experiments terminated at 4 weeks. The second

mouse model involved endotracheal administration of the lewis lung carcinoma (LLC) cell line, which after 7 days resulted in detectable tumor burden. Administration of either AdIL-6 or AdOSM and LLC cells simultaneously was shown to increase tumor burden relative to AdDl70 co-administration. These results suggest a possible role of IL-6 or OSM in promoting lung tumor development in animal models and may ultimately reveal gp130 cytokines IL-6 or OSM as a possible therapeutic target for the treatment of lung cancer.

Acknowledgements

I would like to thank Dr. Carl Richards for his support and for providing a wonderful work environment in which to complete this work. I would also like to thank my committee members: Dr. Kjetil Ask, Dr. Jonathan Bramson and Dr. Martin Stampfli for their helpful advice that ultimately resulted in a finished thesis. I must also thank the friends who made me laugh and supported me throughout this work (Mike Dorrington, Jessica Guerette, Jessica Kafka, Tamara Krneta, Rocky Lai, Graeme Richards, Rebecca Rodriguez, David Schnittker, Fiona Whelman, Stephen Wong and Celine Yeung). A special thanks to Jane Ann Smith for taking the time (and patience) to train me on various animal techniques which made this work possible. Additionally, I'd like to thank Trish VanHoek in animal quarters for her helpful advice and for her efforts regarding the KRAS G12D line. Finally I'd like to thank Alice Morrison for her patience and long-lasting support over these past two years as well as my family (Mom, Dad, Nina, Tanya, JP as well as Cynthia and Reggie) and friends (Steve, Paul, Trevor) back home.

List of Abbreviations

AAH	Atypical adenomatous hyperplasia
BAL	Bronchoalveolar lavage
BRAF	V-raf viral oncogene homolog
CCR	C chemokine receptor
CSF	Colony stimulating factor
CT	Computed tomography
DNA	Deoxyribonucleic acid
ECM	Extracellular matrix
EGF	Epidermal growth factor
ERCC1	Excision repair cross-complementing 1
GTP	Guanosine triphosphate
G-CSF	Granulocyte colony stimulating factor
GM-CSF	Granulocyte macrophage colony stimulating factor
GP130	Glycoprotein 130
HPV	Human papillomavirus
IKK	IκB kinase
IL-	Interleukin
JAK	Janus kinase
KRAS	Kristen rat sarcoma
KC	Kertinocyte chemoattractant
LIF	Leukemia inhibitory factor
LKB	Liver kinase B1
LLC	Lewis lung carcinoma
LPS	Lipopolysacharide
LSL	Lox-Stop-Lox
mAB	Monoclonal antibody
MAP	Mitogen-activated protein
MCP	Monocyte chemotactic protein
MIP	Macrophage inflammatory protein
mRNA	Messenger RNA
mTOR	Mammalian target of rapamycin
MMP	Matrix metalloproteinase
MYC	Myelocytomatosis viral oncogene homolog
NFκB	Nuclear factor κB
NSCLC	Non-small cell lung carcinoma
OSM	Oncostatin M
PI3K	Phosphoinositide 3-kinase
PKB	Protein kinase B
P53	Protein 53
RAF	Rapidly accelerated fibrosarcoma viral oncogene homolog
RAS	Rat sarcoma viral oncogene homolog

RNA	Ribonucleic acid
ROS	Reactive oxygen species
SCLC	Small cell lung carcinoma
sIL-6	Soluble IL-6
shRNA	Short hairpin RNA
siRNA	Small interfering RNA
SOCS	Suppressor of cytokine signaling protein
SRC	Sarcoma viral oncogene homolog
STAT	Signal transducer and activator of transcription
TAM	Tumor associated macrophage
TAN	Tumor associated neutrophil
TIMP	Tissue inhibitor of metalloproteinase
TLR	Toll-like receptor
TNF	Tumor necrosis factor
VEGF	Vascular endothelial growth factor

List of Figures

Table of Contents

Chapter 1: Introduction

1.1 Lung cancer

Cancer of the lung and bronchus is most prevalent among cancers and is the leading cause of cancer related deaths in the US (Jemal et al., 2009). In 2011, lung cancer claimed nearly 160,000 lives equal to approximately 30% of the total deaths due to cancer with an additional 220,000 new cases reported for that year (American Cancer Society, 2011). Other prevalent cancer types such as those targeting the colon, pancreas, breast, or prostate have claimed significantly fewer lives (50,000, 38,000, 40,000, and 34,000 respectively) (American Cancer Society, 2011). Similar proportions of mortality are seen in Canada when accounting for population differences (Canadian Cancer Society, 2011).

Lung cancer can be categorized into small-cell lung cancer (SCLC) and non-small-cell lung cancer (NSCLC) groups, with NSCLC constituting 85% of all cases (Herbst et al., 2008). NSCLC is heterogeneous and composed of squamous-cell carcinoma, large-cell lung carcinoma and adenocarcinoma. Of these, adenocarcinoma is the major subtype, representing approximately 35% of all lung cancers (Bryant and Cerfolio, 2007). Tobacco use contributes to all forms of lung cancer, in particular to SCLC and squamous cell carcinoma with adenocarcinoma being present most frequently in never-smokers (Herbst et al. 2008).

1.1.1 Common pathways in lung cancer

The majority of lung cancers arise as a result of smoking. Many carcinogens in tobacco smoke (such as polycyclic aromatic hydrocarbons and

nitrosaminoketones) may result in DNA adduct formation and eventually this could lead to a mutation (Brambilla and Grazdar, 2009). One of the more deregulated signaling pathways in lung cancer involves epidermal growth factor (EGFR) and its downstream partners, consisting of a number of genes that are commonly associated with lung cancer. EGFR is composed of an extracellular ligand binding domain, a transmembrane section and an intracellular tyrosine kinase (TK) domain. The receptor, once activated, is phosphorylated by the tyrosine kinases intracellularly and acts as a docking site for a number of downstream signaling proteins including RAS, BRAF, and PI3K (Brambilla and Grazdar, 2009). Mutations in EGFR and RAS (specifically the KRAS gene) can occur in as many as 30% of NSCLC cases, while BRAF and PI3K mutations are less common (4%) (Brambilla and Grazdar, 2009). Interestingly, when the same tumors are analyzed in separate patients, only one of three possible genes (EGFR, KRAS, BRAF) is found to be mutant, suggesting that simultaneous mutations of different genes in the EGFR pathway may not be necessary for lung cancer development (Shigematsu and Grazdar, 2006). Generally, mutations associated with lung cancer include those involved in apoptosis (p53), cell proliferation (EGFR, KRAS, LKB1, PI3K), and DNA repair (ERCC1, p53), with p53 mutations being the most prevalent in all lung cancer types (more than 50%), EGFR mutations secondly most common in squamous cell carcinoma (30%) and KRAS mutations most common in adenocarcinoma (30%) (Herbst et al. 2008).

1.1.2 Mutations in KRAS

In NSCLC, mutations in KRAS are frequently found in codons 12 or 13 and this leads to a constitutively active form of KRAS due to ablation of a GTPase regulatory domain (Riley et al., 2009). These mutations in RAS have previously been shown to promote tumorigenicity in a number of ways. Increased proliferation and pro-survival signals are mediated by elevated RAF/MAP kinase activity and Pkb/Akt signaling pathways which are associated with passage through the cell cycle (Downward, 1997; Marte and Downward, 1997). Tumor invasiveness and angiogenesis have also been shown to be promoted by oncogenic RAS in a variety of cell types, for example through the induction of (matrix-metalloproteinase) MMP-9 as in NIH/3T3 fibroblasts which lead to collagen IV degradation (Ballin et al., 1988), VEGF in colorectal cell lines (Okada et al., 1998), IL-8 in cervical, breast and lung lines (Sparrman and Bar-Sagi, 2004) as well as the repression of the anti-angiogenic TSP-1 factor in many cell types (Watnick et al., 2003). Furthermore, CC10-Cre/Lox-Stop-Lox (LSL) G12D KRAS mouse models of lung adenocarcinoma (in which oncogenic KRAS is only expressed in lung derived Clara cells due to the tissue specific CC10 promoter) have an associated inflammatory phenotype (Ji et al., 2006) and this may promote cancer development. RAS induced inflammation may be due to increases in the activation of its downstream target NF-κB (Meylan et al., 2009; Basseres et al., 2010) in a process that is not fully understood but is known to

depend on IKK (a protein involved in activating NF-κB) through non-canonical pathways during endometrial carcinogenesis (Mizumoto et al., 2011). Additionally, increases in IL-8, which can act as both a chemokine and angiogenic factor, may play a role in promoting inflammation as has been found in human NSCLC samples (Luppi et al., 2007). Mutations in KRAS have been studied in lung adenocarcinoma since 1987 and efforts still need to be made to develop effective therapeutics (Rodenhuis et al., 1987).

1.2 Inflammation and tumor promotion

The awareness surrounding the impact of inflammation on cancer has been increasing, mainly as a mediator for tumor promotion. Many cancers have been linked to conditions of chronic inflammation, for example inflammation associated with exposure to cigarette smoke or asbestos, inflammation upon various infections (*H. pylori* in stomach cancer, Hepatitis B and C in liver cancer), as well as a result of the tumor itself (Coussens et al., 2002; Grivennikov et al., 2010). A tumor can initiate inflammation by its associated antigenicity, tissue damage due to tumor growth, hypoxia, as well as aberrant production of chemokines and pro-inflammatory molecules (Tlsty et al., 2006). Major cellular mediators of inflammation (including macrophages and neutrophils) are then recruited to the tumor site and may lead to an optimized environment for tumor development through the generation of a variety of pro-tumorigenic factors and/or immunosuppressive actions. For instance, growth factors and DNA damaging

agents (such as the macrophage-derived EGF and ROS), factors capable of extra-cellular matrix (ECM) degradation (such as MMP), as well as increased production of angiogenic factors (such as VEGF) are characteristically produced by these inflammatory cells (Wislez et al., 2010; Coussens et al., 2002).

One population of these inflammatory cells, the macrophage, is found within many tumors and is also referred to as tumor associated macrophage (TAM, dating back as far as 1975) (Wood and Gillespie, 1975). More recently this paradigm has been extended to neutrophils where tumor associated neutrophils (TANs) are also believed to play an important role in tumor development (Fridlender et al. 2009). The importance of these cells and inflammation in general in tumor promotion has been suggested in multiple studies. Both macrophages and neutrophils have been shown to restore progression to malignancy by re-establishing MMP9 production after transplantation in bone marrow deficient MMP9-/- K14-HPV16 mouse models for invasive squamous cell carcinoma (Coussens et al., 2000). Furthermore, decreases in angiogenesis were observed in studies that depleted neutrophils (antibody-mediated) in a RIP1-Tag2 mouse model for pancreatic cancer (Nozawa et al., 2006) as well as macrophages in CSF -/- PyMT mouse models for breast cancer (Lin et al., 2006). Moreover, in KRAS driven mouse models for pancreatic adenocarcinoma, caelurein-induced pancreatic inflammation (through upregulation of NF-κB) was shown to be required for progression to advanced

tumors, and this was associated with increases in both macrophages and neutrophils (Guerra et al., 2007).

Under normal circumstances, acute cellular inflammation is resolved through apoptosis or clearance of the relevant cells. Some tumors have appeared to develop ways to sustain inflammation in order to take advantage of its tumor promoting benefits. This can be accomplished by persistent tumor-derived cytokine production that can aid in recruitment and survival. For instance, the macrophage chemoattractant MCP-1 is upregulated in bladder, cervix, ovary, lung, and breast tumors and can be correlated to the grade of the tumor, with highly invasive tumors secreting the highest levels of MCP-1 (Vicari and Caux, 2002). Macrophage survival/migration factors VEGF and M-CSF (Mantovani et al., 2002) as well as the neutrophil stimulae G-CSF and BV8 (Shojaei et al., 2007, 2008, 2009) are also upregulated in many tumors. Furthermore, in ovarian cancers, retention of TAMs may be possible by downregulation of the MCP-1 receptor CCR2 (effectively preventing further chemotaxis of the cell), which may be due to the action of TNF-α and other pro-inflammatory cytokines at the tumor site (Sica et al., 2000).

1.2.1 Inflammatory cells in lung cancer

Numbers of macrophages and neutrophils present, as an indication of the extent of inflammation, are enhanced in both mouse and human lung adenocarcinomas. Oncogenic CC10-Cre/LSL G12D KRAS mouse models of lung

adenocarcinoma show increased numbers of both macrophages and neutrophils in the broncho-alveolar lavage fluid, correlating with increased levels of the chemokines that recruit such cells (MCP-1, MIP-1 and KC, MIP-2, respectively) (Ji et al., 2006; Ochoa et al., 2011). Similar observations were noted in assessing human NSCLC biopsies which were shown to display increased levels of MCP-1 and MIP-1b (by analysis of RNA in tissue homogenates); furthermore an *in vitro* chemotaxis assay showed that NSCLC macrophages (from tissue homogenates) displayed reduced migratory ability when MCP-1 and MIP-1b were blocked using neutralizing antibodies (Arenberg et al., 2000). Similarily, the neutrophil chemoattractant IL-8 (orthologous to murine KC and MIP-2) was shown to be increased consistently in NSCLC samples (Smith et al., 1994; Seike et al., 2007; Yuan et al., 2000), although IL-8 may function predominantly as a stimulator of angiogenesis rather than a neutrophil chemoattractant (Smith et al., 1994; Yuan et al., 2000). Furthermore, in a $KRAS^{LA1}$ mouse model for lung adenocarcinoma (which carries a latent oncogenic KRAS G12D allele that is stochastically activated by homologous recombination); increased numbers of alveolar macrophages have been associated with malignancy (Wislez et al., 2005). Recruitment and enhanced survival of macrophages and neutrophils may be possible by increased GM-CSF and G-CSF secretion by the tumor or surrounding stromal cells (Wislez et al., 2001; Seikie et al., 2007; Asselin-Paturel et al., 1998).

1.3 Gp130 cytokines and inflammation

The gp130 cytokine family includes a variety of cytokines, that are both structurally and functionally similar, such as interleukin-6 (IL-6), interleukin-11 (IL-11), interleukin-27 (IL-27), leukemia inhibitory factor (LIF) and oncostatin-M (OSM) among others. These cytokines are involved in a variety of biological processes including hematopoiesis, immune response, inflammation and cellular differentiation (White and Stephens 2011). The gp130 family is named due to members sharing the common receptor component glycoprotein 130 (gp130). The differences in signaling by each cytokine is manifested through a second receptor component that is unique to the cytokine (for example, IL-6 initially binds to IL-6R which then associates with a gp130 homodimer) (Taga and Kishimoto 1997). Ligand binding can then result in recruitment and activation of the primary downstream signal transducer STAT3, although other pathways can become activated depending on the cell type (including MAPK, PI3K, and mTOR pathways) (White and Stephens 2011, Heinrich et al. 2003).

IL-6 has long been known to play a key role in establishment of the acute inflammatory response and is considered to be the major stimulator of acute phase protein production (Gauldie et al. 1987, Gabay, 2006). IL-6 is produced in response to a variety of known inflammatory modulators such as IL-1β, TNF-α, and various TLR ligands such as LPS, and is elevated in nearly every disease associated with chronic inflammation (Naugler and Karin, 2008).Transgenic mice

overexpressing IL-6 (linked to the CC10 promoter in lung derived Clara cells) have shown increased levels of T and B cell infiltrates (DiCosmo et al., 1994) and increased polyclonal IgG (when human IL-6 was fused downstream of a highly active human immunoglobulin heavy chain enhancer) (Suematsu et al., 1989). Genetic ablation of IL-6 in a mouse model for arthritis show reduced tissue damage and inflammatory cell recruitment in the knee joint (Alonzi et al., 1998). Analysis of IL-6 deficient mice (by homologous recombination) revealed impaired T- and B-cell functions (reduced cytotoxic T cell levels in response to vaccinia virus, reduced IgG and IgA responses) as well as a severe reduction in the inflammatory acute response (reduced liver haptoglobin, α-1 acid glycoprotein, and serum amyloid-A) (Manfredi et al. 1998, Kopf et al., 1994).

Given the scope of IL-6 functions in inflammation, the role of gp130 signaling in inflammation comes as no surprise and was examined in an experiment involving conditional ablation of gp130 in a mouse model for colitis. Deletion of gp130 resulted in a dramatic improvement in colitis symptoms and decreased colonic inflammatory infiltrate as evidenced by reduced cellular infiltrate (macrophages, neutrophils), pro-inflammatory cytokines (TNF, IL-6, IL-17, KC, MIP2) (Sander et al. 2008) and displayed features associated with IL-6 deficient animals (impaired T- and B-cell functions, reduced inflammatory acute response) (Ernst et al. 2001). Toshio Hirano's group has focused on creating mutant variants of gp130 in mice such as the activating $gp130^{F759/F759}$ mutation

that results in ablation of negative regulation by SOCS3 (the suppressor of cytokine signaling (SOCS)-3 protein) and these mice develop splenomegaly, lymphoadenopathy, enhanced inflammatory phase response and arthritis that is accompanied by autoantibody production and T cell abnormalities (Atsumi et al. 2002). Furthermore, in a study examining inflammatory hepatocellular adenomas (IHCA, characterized as benign tumors associated with obesity or alcoholism), 60% of samples were found to carry mutations in gp130, resulting in constitutive signaling of the receptor that is thought to promote the inflammatory nature of the disease (Rebouissou et al. 2009).

Other gp130 cytokines such as IL-11 and OSM appear to have overlapping functions with IL-6 in terms of inflammation (reviewed in Silver and Hunter, 2010). IL-11 can be secreted by epithelial cells, fibroblasts, smooth muscle cells and antigen-presenting cells in the lung, and has been shown to regulate neutrophil recruitment during pulmonary tuberculosis infection (Kapina et al. 2011) as well as Th2 type responses and eosinophilic inflammation in mouse models for asthma (Kuhn et al. 2000). The related gp130 family member Oncostatin M (OSM) is secreted by a variety of inflammatory cells including activated macrophages, T cells and neutrophils and has marked effects in modulating the inflammatory environment (through induction of chemokines and recruiting inflammatory cells) and tissue remodeling (through induction of TIMP-1 and MMP-1, 3 and 9) (Tanaka and Miyajima, 2003). OSM has been implicated

in a number of inflammatory diseases including arthritis (Cawston et al., 1998, Langdon et al., 2000, Hui et al. 2005), asthma (O'Hara et al. 2003), and pulmonary fibrosis (Mozaffarian et al. 2008). Transgenic mice overexpressing OSM in the pancreatic β-islet cells show severe fibrosis and inflammatory cell recruitment that is not dependent on IL-6 (Bamber et al., 1998). Furthermore, previous work by the Richards laboratory has shown that adenovirus delivery of OSM (AdOSM) in articular joints can lead to worsened arthritic phenotype (Langdon et al., 2000) while AdOSM delivery to the lungs can lead to a dramatic inflammatory response characterized by extracellular matrix deposition and eosinophil accumulation (Langdon et al. 2003, Fritz et al. 2011).

1.4 Gp130 cytokines and cancer

1.4.1 Interleukin-6

The association of IL-6 with cancer is strong, with its overexpression being linked to nearly every tumor studied (Trikha et al. 2003). IL-6 has been associated with a variety of pro-tumorigenic cell activities including cellular proliferation, migration, angiogenesis and invasiveness (Guo et al. 2012). The importance of IL-6 in provoking tumorigenicity was illustrated by Ancrile et al. (2007) in a variety of *in vitro* and *in vivo* experiments which made use of RAS G12V transformed cell lines that were tested for tumor growth in immunocompromised mice. These researchers found that decreasing IL-6, either by shRNA knockdown of the transformed cell line or by injection of neutralizing

antibody at the tumor site, resulted in a reduction in tumor load when transformed cell lines were transplanted to mice. In addition, Ancrile et al. (2007) also tested the requirement of IL-6 in the development of carcinogen-induced skin tumors in mice and found that tumor burden in IL6-/- mice was reduced 30-fold compared to wildtype animals. In mouse models for colitis-associated colon cancer, researchers have found elevated IL-6 secreted by lamina propria macrophages and CD4+ T cells which was shown to be involved in promoting tumor cell proliferation and survival (Grivennikov et al., 2009) while use of anti-IL-6R was shown to suppress tumorigenesis in this model (Becker et al., 2004). In an oncogenic CC10-Cre/LSL G12D KRAS mouse model for lung adenocarcinoma, increases in IL-6 protein levels in the BAL and mRNA levels in lung tissue are evident relative to wildtype mice (Ochoa et al., 2011). Furthermore, through its major signal transducer STAT3, IL-6 may influence cellular proliferation, suppression of apoptosis and angiogenesis by increased production of VEGF (Lin and Karin, 2007, Yeh et al., 2006).

In addition to the classical IL-6 signaling pathway (mediated through membrane-bound IL-6R and gp130) an alternative mode of signaling exists termed IL-6 transsignaling (Jostock et al., 2001). This mechanism relies on soluble IL-6R (sIL-6R) that can form a complex with IL-6 (sIL-R/IL-6) and this complex can signal through gp130 on cells that lack the IL-6R. Recently, IL-6 transsignalling has been implicated in models of pancreatic cancer. In this system,

LSL G12D KRAS animals were crossed with sgp130^{tg} animals to generate progeny that have abrogated IL-6 transsignalling (Lesina et al. 2011). It was found that double transgenic animals showed a reduction in tumor number and grade compared to LSL G12D KRAS mice upon Cre activation (Lesina et al. 2011). Interestingly, LSL G12 KRAS animals were also crossed to IL-6 -/- animals (abrogating both classical and transsignalling) in this study and the same results were seen with the sgp130^{tg} cross, suggesting that in this model IL-6R transsignaling is principally responsible for IL-6 mediated tumor enhancement.

The importance of IL-6 in cancer, as well as its role in other diseases, has warranted the development of therapeutic agents designed to block IL-6 signaling. Known inhibitors of IL-6 expressionsuch as corticosteroids and cytokines (like IL-4), as well as mAbs designed to block IL-6 and IL-6R have been used to treat various diseases including cancer (Trikha et al. 2003). More recent and specific targeting therapies such as CNTO 328 (an anti-IL-6 mAb) show promise in ovarian, renal and prostate cancer as it is well tolerated and results in stabilized disease symptoms (all in phase I/II) (Guo et al. 2012). Clearly, a role of IL-6 in a variety of cancers (as well as other diseases) is evident, however the importance of IL-6 in lung cancer is not yet clear.

1.4.2 Oncostatin M

Due to its role in promoting inflammation and tissue remodeling, OSM may thus have important roles in modifying the tumor environment, in particular

in ways that promote angiogenesis and metastasis. Vasse et al. determined that human OSM acts as a pro-angiogenic factor that can induce proliferation of endothelial cells as well as lead to VEGF expression *in vitro* and that OSM-induced effects were more marked than IL-6 (Vasse et al., 1999). In breast cancer cell lines, tumor-derived GM-CSF induces human OSM in neutrophils and this leads to VEGF production, breast cancer cell detachment, and increased invasive potential (Queen et al., 2005). OSM acts at a receptor complex composed of gp130 and OSMRβ (Tanaka and Miyajima, 2003), and researchers have recently found that high levels of OSMRβ can be indicative of poor prognosis in breast cancer (West et al., 2012). In a study involving cervical squamous cell carcinoma (SCC), OSMRβ was found to be upregulated in a number of human cervical SCC lines and knockdown with OSMRβ siRNA resulted in reduced endothelial tube formation in an *in vitro* angiogenesis assay and decreased invasiveness through matrigel (Winder et al. 2011). All of these findings suggest that OSM may act as a promoter of tumorigenesis in select cancers, however its role in lung cancer is not known.

1.4.33 Gp130 signaling by STAT3

Gp130 receptor complex engagement by IL-6 or OSM results in activation of receptor-associated kinases such as the JAK or SRC proteins which then leads to phosphorylation of tyrosine residues on the receptor thus creating docking sites for SH2-containing protein STAT3 (Gerhartz et al., 1996). STAT3 monomers can

then become phosphorylated by the associated receptor kinases and dimerize, enabling the protein to pass through the nucleus and associate with transcriptional activation elements to promote expression of genes such as those involved in cancer like cell proliferation (through upregulation of c-MYC and cyclin D-2), cell survival (increased BCL-X_L expression, reduced p53), angiogenesis (VEGF), and promotion of inflammation (NF-κB) (Yu and Jove 2004). Importantly, STAT3 in tumors can induce a number of factors which in turn can be secreted to activate STAT3 in the surrounding stroma, leading to a feedforward loop resulting in STAT3 activation in non-transformed cells (Yu et al. 2009). These increases in STAT3 activation can result in a constitutively inflammatory environment, potentiating tumor development.

Many studies have investigated the importance of STAT3 in tumor progression. A constitutively active form of STAT3 (termed STAT3-C) was shown to transform 3Y1 fibroblasts *in vitro* and intradermal injection of these cells into nude mice resulted in large tumors over a period of 6 weeks (Bromberg et al. 1999). Furthermore, a large number of human cancer cell lines and tissues have been shown to overexpress STAT3 (lymphomas, melanomas, as well as breast, lung, prostate, ovarian, and pancreatic cancers) (reviewed in Yu and Jove 2004). Non-small-cell lung cancer (NSCLC) tissues show increased levels of activated STAT3 and correlate with higher clinical stage (Jiang et al. 2011). These increases in STAT3 signaling may be a result of activating mutations in the upstream EGFR and KRAS (Yu et al. 2009, Meylan et al. 2009). In KRAS-based

mouse models for pancreatic cancer, increased levels of activated STAT3 are detected and correlate with disease progression, and transgenic mice with decreased STAT3 signaling ($STAT3^{Y705}$) show a dramatic reduction in tumor progression (Lesina et al. 2011). Furthermore, similar reductions in tumor burden were found in STAT3-deficient (by genetic ablation) mouse models for colitis-activated colon cancer (CAC) compared to STAT3 proficient mice (Bollrath et al., 2009).

In an effort to understand how STAT3 hyperactivation may be initiated in cancer, Ernst et al. (2008) examined the necessity of IL-11 in a $gp130^{Y757F/Y757F}$ mouse model for gastric cancer (IL-11 acts at a receptor complex of gp130 and IL-11R (Dahman et al., 1998)). The $gp130^{Y757F/Y757F}$ mutation renders STAT3 unresponsive to negative regulation by its natural inhibitor SOCS3 (and therefore once STAT3 signaling is initiated it cannot be repressed). Normally, $gp130^{Y757F/Y757F}$ mice develop gastric cancer due to the overactive STAT3 but when these mice were crossed to IL-11R -/- the stomachs of these mice were completely free of any signs of gastric cancer or chronic inflammation. This suggests that the IL-11R is required for STAT3 initiation which then supports progression to gastric cancer. Moreover, when $gp130^{Y757F/Y757F}$ mice were crossed to IL-6 KO animals, little effect was seen with regard to gastric tumor suppression or inflammatory infiltrate compared to the $gp130^{Y757F/Y757F}$ mice. These data suggest a strong role for IL-11 and not IL-6 in the $gp130^{Y757F/Y757F}$ mouse model for gastric cancer in initiating STAT3 signaling, suggesting that different gp130

cytokines may play alternative roles in cancers of different origin or different organs.

An important aspect of STAT3 signaling is its ability to undergo crosstalk with the important inflammatory modulator NF-κB. NF-κB is a transcription factor composed of several Rel-related proteins which is normally sequestered in the cytoplasm by IκBα; IκB kinases (IKK) can phosphorylate IκBα allowing for its degradation and subsequent liberation of NF-κB which then undergoes nuclear translocation (Karin et al., 2002). The half-life of NF-κB in the nucleus is determined by the acetylation status of its RelA subunit, which acts as a target for p300/CBP acetyltransferases or histone deacetylases (Chen et al., 2001). Under conditions of acetylation, RelA associates weakly with IκB and its nuclear presence is favored, however when deacetylated RelA can associate more strongly with IκB and this favors RelA nuclear export (Chen et al., 2002). Importantly, activated STAT3 has been shown to lead to hyperacetylation of RelA due to its suggested interaction with p300 which allows for increased retention in the nucleus where it can act to activate transcription of a number of important inflammatory regulators (Lee et al., 2009). NF-κB is often overexpressed in many cancers due to its ability to upregulate genes involved in proliferation, survival, angiogenesis and invasiveness (Yu et al. 2009). Like STAT3, many tumor cell lines and primary tumor samples show increased levels of NF-κB (Barkett and Gilmore, 1999) and inhibition of NF-κB can result in increased sensivity to chemotherapy (Amit and Ben-Neriah, 2003). In an article published by Tyler

Jacks' group, researchers found that inhibition of NF-κB (achieved by overexpressing the surpressor IκB-SR) resulted in dramatic reduction in tumor burden in a KRAS G12D mouse model for lung adenocarcinoma (Meylan et al. 2009). Additionally, a crucial inducer of tumorigenesis downstream of NF-κB is the gp130 cytokine IL-6 (Libermann and Baltimore, 1990) while it is known that OSM can induce NF-κB (Nishibe et al., 2001). Collectively, these findings suggest STAT3 and NF-κB to be involved in promoting a variety of cancer types.

1.4 Thesis Project Proposal

Much remains unknown with regard to the lung adenocarcinoma environment, specifically how the gp130 cytokines IL-6 and OSM contributes to tumor development. In certain model systems, recent evidence suggests a role for these cytokines in enhancing tumor development although their role in lung cancer is not yet clear. This thesis work is centered on the general hypothesis that lung inflammation is a critical driving force for lung tumor development. Through the infiltration of a variety of cell types involved in producing proliferative, DNA damaging, angiogenic, and ECM degrading factors, the tumor can take advantage of this environment in its growth and progression towards malignancy. Specifically, the work is focused on whether gp130 members IL-6 and OSM contribute to lung tumor development and the hypothesis is that local elevation of these cytokines will correlate with the promotion of tumor development.

A mouse model for adenocarcinoma (harboring a conditional LSL G12D mutation in the KRAS gene) will be utilized and the effects of overexpression of gp130 related cytokines in the lung mucosa and how this relates to tumor development will be examined. Modification of the local lung environment will be made possible by delivery of adenovirus encoding IL-6 or OSM proteins. The degree to which local IL-6 and OSM elevation influence tumor development will be evaluated on the basis of CT scanning and histology. Tumor development will be assessed on a four-stage grading system for the LSL G12D KRAS mouse model for adenocarcinoma (DuPage et al., 2009; Johnson et al., 2001; Jackson et al., 2005, see figure 1). The earliest lesions, termed grade 1 are atypical adenomatous hyperplasia (AAH) or small adenomas, grade 2 lesions are large adenomas, grade 3 lesions are non-invasive adenocarcinomas, and grade 4 are invasive. The mouse model that will be used is attractive due to the predominance of KRAS mutations in human lung adenocarcinoma and the likelihood of it being an initiating mutation (Westra , 2000).

In addition to the LSL G12D KRAS mouse model; a second model was developed using the lewis lung carcinoma (LLC) cell line. This cell line was derived from a spontaneous lung tumor in a C57Bl/6 animal that has been adapted for use in culture. This second model will rely on intubation of these LLC cells into the lungs of C57Bl/6 mice which will then form lung tumors within 7 days. This model has been used by several groups who have directly intubated the cells

(Savai et al. 2005) or surgically implanted them into the lungs (Yamaura et al. 1999). Importantly, this second model will allow for comparison of results with the KRAS based mouse model.

Figure 1. Histological grading of KRAS G12D tumors. Representative H&E micrographs KRAS G12D tumors of varying grade (taken fromDupage et al. 2009).

A) Grade 1 tumors showing diffuse hyperplasia.
B) Grade 2 tumors showing a defined area of dense tissue.
C) Grade 3 tumors showing a mixed cellular phenotype.
D) Grade 4 tumors showing desmoplasia and invasiveness.

Figure 1

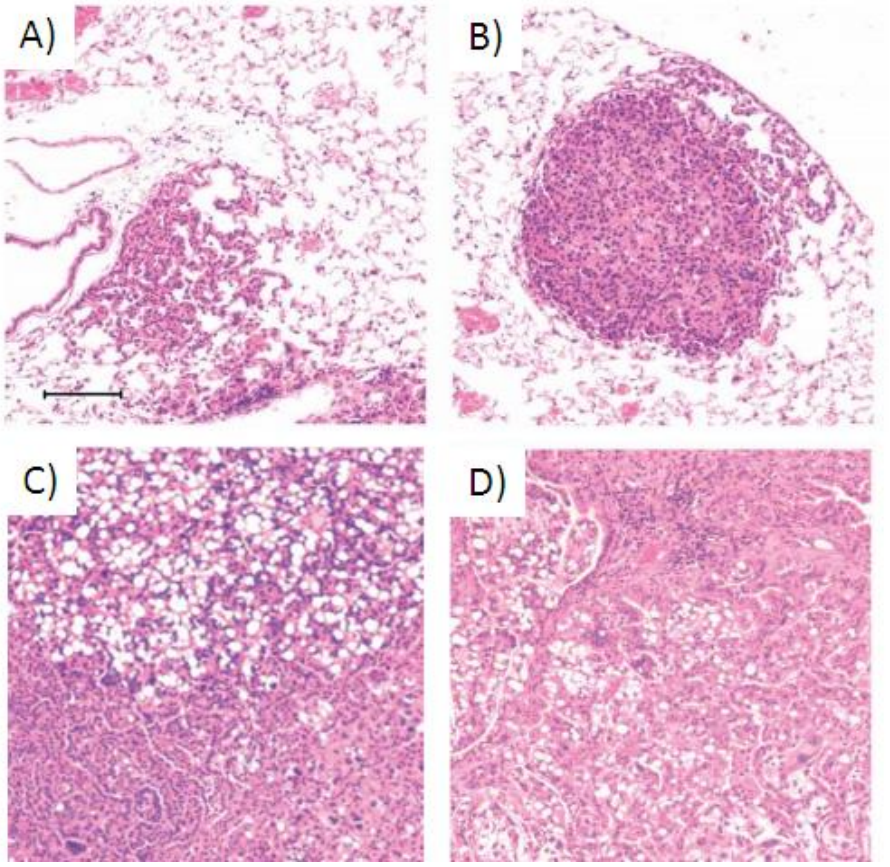

Chapter 2: Materials and Methods

2.1 Transgenic mice

Transgenic LSL G12D KRAS mice (6-8 weeks old) were purchased from The Jackson Laboratory (strain B6.129S4-KRAStm4Tyj/J) originally generated by Tyler Jacks (Jackson et al., 2001). These animals are heterozygote and have an activating glycine to aspartic acid mutation at codon 12 of the KRAS gene which is silenced due to an upstream flanking LoxP-Stop-LoxP (LSL) transcription stop cassette. This can be removed by Cre-mediated recombination, yielding the constitutively active KRAS oncogene upon transcription (Figure 2).

2.2 Genotyping of KRAS G12D mice

Template for genotyping was obtained from DNA extracted from 5 mm tail snips using the DirectPCR Lysis Reagent (Viagen Biotech, Los Angeles, CA) according to the manufacturer. Primers were developed as recommended by the Jackson Laboratory for this strain (purchased from Sigma-Aldrich, Oakville, Ontario):

oIMR8272 (5'-GTCGACAAGCTCATGCGGG-3')

oIMR8273 (5'-CGCAGACTGTAGAGCAGCG-3')

oIMR8274 (5'-CCATGGCTTGAGTAAGTCTGC-3')

PCR was performed in 25 µl reactions using Platinum Taq (Life Technologies, Burlington, Ontario) according to the manufacturer delivering 1 µl of both oIMR8272 and oIMR8273 (to amplify the common region – see figure 3), or 1 µl of both oIMR8274 and oIMR8273 (to amplify the LSL region – see figure

3) all at an initial primer concentration of 25 µM. PCR was then performed using the Mastercycler Gradient thermocycler (Ependorff, Mississauga, Ontario) using the following conditions: initial denaturation (94℃ for 3 min – 1 cycle), amplification (94℃ for 0.5 min, 55℃ for 1 min and 72℃ for 1 min – 35 cycles), final extension (72℃ for 2 min).

5 µl of the PCR reaction was combined with 1 µl of EZ Vision loading buffer (Amaresco, Solon, OH) (acts as a loading and fluorescent dye) before loading onto a 1.5% agarose (Biotechnology grade, BioShop) gel. 1 µl of 100 bp ladder (GeneRuler 100 bp Plus DNA-ladder, Fermentas, Burlington, Ontario) was loaded alongside and ran for 1.5 hours at 80V in 1X TBE (from 5X: 216 g Tris (BioUltraPure, BioShop, Burlington, Ontario), 110 g Boric acid (Biotechnology grade, Bioshop, Burlington, Ontario), 80 ml 0.5M EDTA, pH 8.06 in 4 L dH2O; the EDTA solution was prepared from 93.05 g disodium salt dihydrate-EDTA (Fisher Scientific, Ottawa, Canada) and brought to pH 8.06 by addition of NaOH (Bioshop, Burlington, Ontario) to a final volume of 500 ml (Sambrook et al., 1989)). The gel was then imaged using the Alpha Innotech camera (Fisher Scientific, Ottawa, Canada). Bands of approximately 500 bp and 600 bp were indicative of the heterozygote and these animals would be used for subsequent experiments.

The primer binding sites, the expected PCR product sizes, and a more detailed analysis of the LoxP-Stop-LoxP site is shown in figure 3; along with this in figure 4 are the results of a typical genotyping experiment.

2.3 Infection of lungs with AdCre

Adenovirus-encoded Cre (AdCre) was used to activate expression of the LSL G12D KRAS gene. Calcium phosphate precipitation of the virus was utilized as in Jackson et al. 2001. To prepare 10 ml of the calcium phosphate media, 1 ml of 10X EMEM (Sigma-Aldrich, Oakville, Ontario, catalog M0275) was combined with 0.1 ml 0.2 M L-glutamine and 8.9 ml sterile water. The virus was then diluted in this solution and 2 µl of a 2M calcium chloride solution was then added. Following a 20 minute incubation at room temperature, 50 µl of virus (containing the appropriate pfu) was delivered to the lungs by intubation.

2.4 CT scanning analysis

Computed tomography (CT) scans were performed before intubation (week 0) and at the indicated times by the McMaster Center for Pre-clinical and Translational Imaging (MCPTI) facility. CT scan images were analyzed using Amira v 5.0 (purchased from Visage Imaging, San Diego, CA). Files were saved as big endian with a resolution of 1x1x1 mm voxel size. Lung label fields were generated by a segmentation process that separated the lung region from the rest of the animal. Lung labels were drawn to exclude ribs, heart and the diaphragm. This label field was used to generate a histogram of densities in the lung label using the following settings: Range = -1000 → +250, Bins = 26, Histogram Options = Absolute, Plot Options = all unchecked.

The histogram was saved under the .csv format and the Histogram.y column was analyzed by Microsoft Excel (2010). The Histogram.y values were

then expressed as percentage of the whole lung volume (after summing the total voxels) and this data was used for all subsequent analyses. These histograms were loaded into Prism v5.00 for graphical and statistical analysis.

To generate the color overlays, the lung labels were loaded along with its respective .raw file. Two new materials were generated in addition to the material containing the lung label. The lung label material was selected and the range -200 → 0 and also 0 → +200 HU was selected using the Threshold function (current material only selected) and then extracted from the lung label material and individually added to the new materials. The old lung label (lacking the -200 → 0 and 0 → +200 HU densities) was colored blue, -200 → 0 colored yellow and 0 → +200 colored red using the color presets. Each colored range was displayed using the Dotted Draw Style.

2.5 Histological processing and analysis by ImageJ

The left lung from each animal was cut transversely at the point where the trachea undergoes its first bifurcation and the cut edge was embedded. 5 µm sections were made 700 µm apart and 3 of these sections were placed on a single slide (for a total of 6 lung slices representative of 1 animal). The slide was then stained with H&E by the McMaster Immunology Research Center Histology Core.

For quantification using ImageJ, photographs of the H&E stained slides were taken at 1.6 X magnification. The images were loaded into Photoshop CS2

and the magnetic lasso tool was used to extract the lung from the rest of the image. This lung image was then loaded into ImageJ v1.45s where the higher density area was approximated by varying the threshold tool. This area was the measured and the whole lung was then measured before being represented as % high density of total lung area. This was repeated for the 6 lung slices on a single slide and averaged for that animal.

2.6 Immunohistochemistry using pan-cytokeratin

Pan-cytokeratin (Dako, Burlington, Ontario) was used to stain lung epithelial cells and regions of hyperplasia as recommended by Dr. J.C. Cutz (McMaster University). Briefly, 3 μm sections were deparafinized at 60°C for 45 minutes before being subjected to xylene, alcohol, and water washes. The sections were then soaked in TBS and digested with proteinase K (Dako, Burlington, Ontario) before washing with TBS and blocking with 5% normal goat serum. The sections were then stained with 1:500 dilution of the pan-cytokeratin antibody for 1 h at room temperature, washed and then developed using Envision+ (Dako, Burlington, Ontario). The sections were counterstained with Mayer's Hxt and mounted in glycerin.

2.7 Tumor grading and enumeration

Grading was performed as indicated in section 1.5 and was assisted by Dr. J.C. Cutz (McMaster University). Tumors were enumerated from histological sections using three 5 μM sections (300 μM apart) from the upper right lobe for

section 3.2 and nine 5 µM sections (300 µM apart) from the left lobe for section 3.3.

2.8 Verification of Cre-mediated recombination

As noted previously, removal of the upstream transcription stop cassette allows for expression of the mutant KRAS gene (refer to figure 2). Through this recombination a single LoxP site remains, resulting in a PCR product approximately 50 bp larger than the amplicon from the homologous chromosome (containing the wildtype KRAS gene, see figure 5A). Template for genotyping was obtained from total lung extracts from AdCre infected ($5x10^8$ pfu) and uninfected lungs. The lungs were homogenized in Trizol (Life Technologies, Burlington, Ontario) and DNA was extracted according to the manufacturer's instructions. Primers were designed to flank the lox-stop-lox cassette (purchased from Sigma-Aldrich, Oakville, Ontario):

CreRecF (5'-AGCAAGGCAGAAGTCACAGAGGTT-3')

CreRecR (5'-TTACAAGCGCACGCAGACTGTAGA-3')

The PCR reaction was performed as in section 2.2 with the following conditions: initial denaturation (94°C for 3 min – 1 cycle), amplification (94°C for 0.5 min, 60°C for 0.5 min, 72°C for 1 min – 35 cycles), final extension (72°C for 2 min – 1 cycles). The products were then loaded on a 2% agarose gel and ran for 2 h at 80V. After imaging the gel, bands of approximately 1000 bp were assessed to be derived from template that did not undergo recombination; whereas bands of

approximately 1050 bp were assessed as indicating recombination. As shown in figure 5B, only animals that were treated with AdCre showed a product 50 bp larger, indicative of the recombination.

2.9 Analysis of broncho-alveolar lavage fluid

Animals were anesthetized using isoflurane and then sacrificed. The lungs were removed and 0.5 ml of sterile room temperature PBS was infused as standard procedure in the laboratory (Fritz et al., 2011). To loosen the cells, the lungs were gently bounced and massaged before the bronchalveolar lavage (BAL) was recovered; this process was repeated 2 times per animal to recover a final volume of approximately 1 ml. The BAL was then centrifuged for 2 minutes at 10,000 RPM and the supernatant was removed from the pellet and stored at -80°C for subsequent ELISA analysis. The pelleted cells were resuspended in 100 µl PBS and 10 µl of this was used for total cell counts using Trypan Blue (Gibco) and a hemocytometer. Approximately 100,000 cells were loaded into the cytospin for differential staining.

2.10 Isolation of macrophages for cre-mediated recombination

For isolation of the adherent population (mostly macrophages), approximately 1,000,000 cells were plated per well on a 6-well plate and incubated for 2 h at 37°C and 5% CO2 on 10% FBS DMEM. The non-adherent population was washed off twice using sterile PBS and the adherent population was used for subsequent studies. For AdDl70/AdCre/AdGFP infection to verify

Cre-mediated recombination in the macrophage population, cells were treated with 100 M.O.I. of the relevant virus for 1 h in serum-free DMEM, after which the virus-containing media was removed and 10% FBS DMEM was added. Approximately 10% infection was achieved using this approach as estimated by visualization of GFP+ cells.

2.11 Sequencing of KRAS gene in lewis lung carcinoma

Template for genotyping was obtained from KRAS positive and negative genotyped mouse tail DNA (as positive and negative controls), as well as from LLC cells. The DNA from LLC was extracted using Trizol ((Life Technologies, Burlington, Ontario) according to the manufacturer's instructions. Primers were designed to flank codons 12 and 13 in the KRAS gene (purchased from Sigma-Aldrich, Oakville, Ontario):

X38F (5'-GTCCACAGGGTATAGCGTACTATG-3')

X38R (5'-GAGCAGCGTTACCTCTATCGTA-3')

The PCR reaction was performed as in section 2.2, with the following conditions: initial denaturation (94°C for 3 min – 1 cycle), amplification (94°C for 0.5 min, 55°C for 1 min, 72°C for 1 min – 35 cycles), final extension (72°C for 2 min). The products were then loaded on a 1% agarose gel and ran for 1 h at 80V. Bands of approximately 500 bp were excised and the Wizard SV Gel and PCR Clean-up System (Promega, Madison, WI) was used to purify the DNA from the gel. The DNA was then run on a 1% agarose gel alongside a marker of known

concentration and subsequently diluted to approximately 10 ng/µl (recommended concentration for 500 bp fragments). Primers X38F and X38R were diluted to 1 µM and submitted along with the DNA to the MOBIX McMaster sequencing facility. Analysis of DNA sequence was assisted using Serial Cloner v2.1.

2.12 *In vitro* studies involving lewis lung carcinoma (LLC)

LLC cells were obtained from ATCC (Manassas, VA) and regularly cultured and passaged in 10% FBS DMEM. These cells were typically grown in T-75 flasks and once confluent were washed once with PBS before lifting off the flask surface using trypsin-containing media (standard laboratory procedure (Fritz et al. 2011)). After 5 minutes at room temperature, the flask was knocked several times to dislodge highly adherent cells. The trypsin was quenched with 10% FBS DMEM and the suspension was pipetted up and down several times to obtain a single cell suspension before splitting into new T-75 at a 1:10 dilution. After 3 days the cells were split again. Approximately 1,000,000 LLC cells were frozen in a single cryovial using DMEM supplemented with 20% FBS and 5% DMSO and stored at -80°C for 2 days (in a Mr. Freeze container) before being stored in liquid N_2. To thaw cells, a single vial was brought out of liquid N_2 on ice and then quickly thawed in a 37°C water bath. 1 ml of sterile PBS was added to the cells and then brought up to 10 ml using PBS before spinning at 1200 RPM for 3 minutes. The supernatant was discarded and the pellet was resuspended in warm 10% FBS DMEM before being added to a T-75.

For proliferation studies, 2000 LLC cells (from ATCC, Manassas, VA) were seeded onto a 96-well plate and stimulated with mOSM, mIL-6, mTNF-α, hTGF-β1, mIL-13, mIL-1β and mIFN-γ (all R&D) at concentrations of 0.2, 2 and 20 ng/ml. After 72 h, these cells were treated with 20 µl of MTT (5 mg/ml, Sigma-Aldrich, Oakville, Ontario) and placed at 37°C and 5% CO2 for 4 h. Afterwards, the cells were lysed and MTT was solubilized using 120 µl of the MTT solvent (8 mM HCl, 0.2% IGEPAL CA-630 in isopropanol). After pipetting up and down vigorously to lyse the cells, the plate was placed on a shaker for 15 minutes before reading the absorbance at 540 nm. Changes in cell number were measured as % growth increase relative to the absorbance of untreated control cells. Supernatants were also taken at these times and stored at -20°C before being analyzed for cytokine levels by ELISA. For proliferation experiments these cells were cultured in 2% FBS DMEM.

2.13 *In vivo* studies involving lewis lung carcinoma (LLC)

For in vivo experiments involving intubation of live LLC cells a protocol from Dr. Bowdish's laboratory was employed. For intubation of 15 animals, 3 vials of 1,000,000 cells were thawed and washed using 10% FBS DMEM before being plated on three 100 mm non-tissue culture treated petri dish and placed at 37°C at 5% CO2. After three days, each petri dish was split 1:3 (being careful not to disrupt cell clumps) into two new 100 mm non-tissue culture treated petri dishes (for a total of 9 plates) and placed again in the incubator overnight. The following day the cells were pipetted into 50 ml falcon tubes and centrifuged at

10,000 RPM for three minutes and then resuspended in 10 ml of 10% FBS DMEM and combined into a single 50 ml falcon tube. The cell suspension was then centrifuged at 10,000 RPM for 3 minutes and then resuspended to a final volume of 0.5 ml PBS. Cells were assessed using trypan blue for viability (normally 60-70%) and high cell clump content. Cells were then resuspended (by tapping the vial) before being split equally into 3 ependorffs. Immediately before intubation, the cells were mixed with adenovirus expressing mOSM or mIL-6 in a ratio of approximately 25 µL cells to 25 µL virus before 50 µL of cells/virus were intubated into wildtype C57Bl/6 (Charles Rivers) for a period of 1 week.

2.14 ELISA

All ELISAs (mIL-6, mKC, mMCP-1, purchased from R&D, Minneapolis, MN) were completed according to the manufacturer's instructions.

Figure 2. Illustration of cre-mediated recombination resulting in expression of oncogenic KRAS. The inserted transcriptional stop cassette (in red) prevents transcription of the oncogenic KRAS G12D allele. Two LoxP sites flank the stop cassette which is removed when Cre-recombinase is added, allowing for transcription of KRAS G12D.

Figure 2

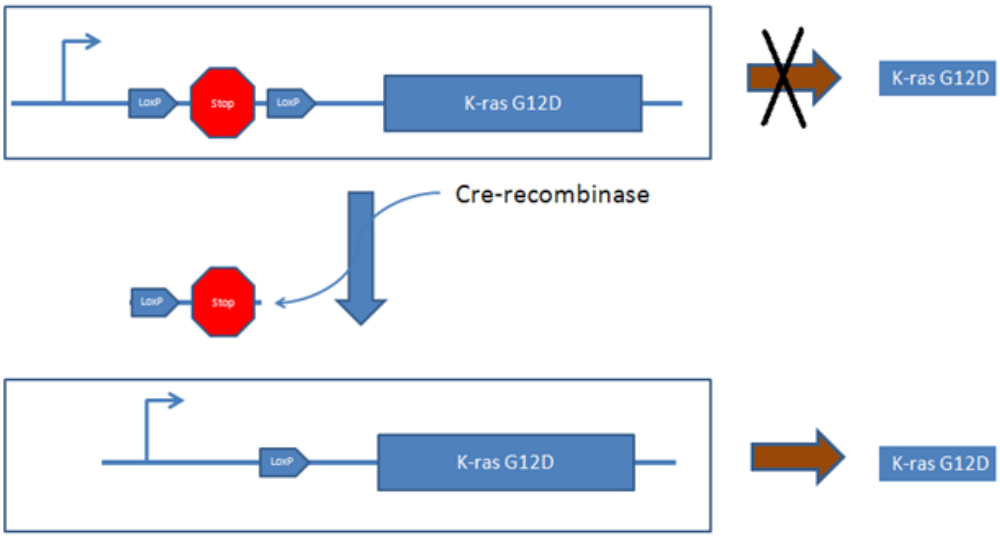
LoxP
Stop
LoxP
K-ras G12D
K-ras G12D
Cre-recombinase
LoxP
Stop
LoxP
K-ras G12D
K-ras G12D

Figure 3. LoxP-Stop-LoxP sequence and primer binding sites for genotyping KRAS G12D mice. Primers oIMR8272 (yellow arrow), oIMR8273 (green arrow), and oIMR8274 (blue arrow) are shown above their respective positions within the LSL-KRAS G12D gene along with the expected amplicon sizes (below). The corresponding sequence is shown above illustrating the primer binding sites (same colors as before), the LoxP-Stop-LoxP site (LoxP in grey, Stop in red), and the nucleotide position (left of sequence) from the plasmid that was used to develop the transgenic (Jackson et al. 2001) (Addgene plasmid 11585).

Figure 3

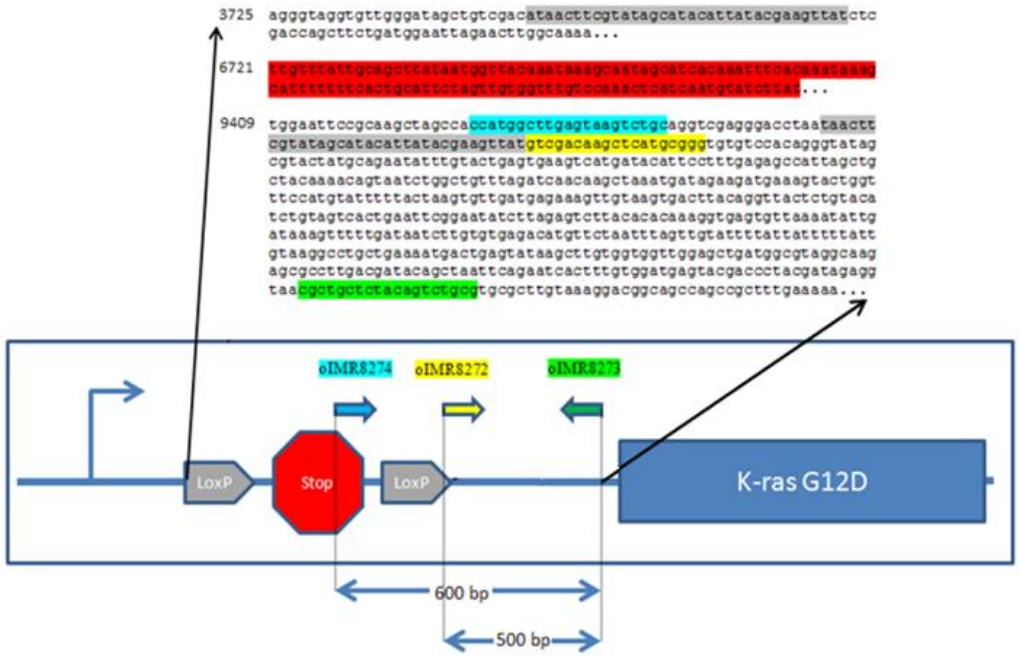
3725
6721
9409
oIMR8274
oIMR8272
oIMR8273
LoxP
Stop
LoxP
K-ras G12D
600 bp
500 bp

Figure 4. Results of genotyping experiment. DNA was extracted from six separate 5 mm tail snips from KRAS G12D mice and these samples were assayed for the common 500 bp fragment (1a-6a, spanning oIMR8272/73, on the left half of the figure), and the LSL 600 bp fragment (1b-6b, spanning oIMR8274/73, on the right). As expected, products were obtained using the common primer set (1a-6a), while samples 1b-3b showed product using the LSL primer set, indicating that animals 1-3 carry the LSL KRAS G12D allele and are heterozygote. A 100 bp ladder (L) was run alongside with the indicated basepair (bp) length.

Figure 4

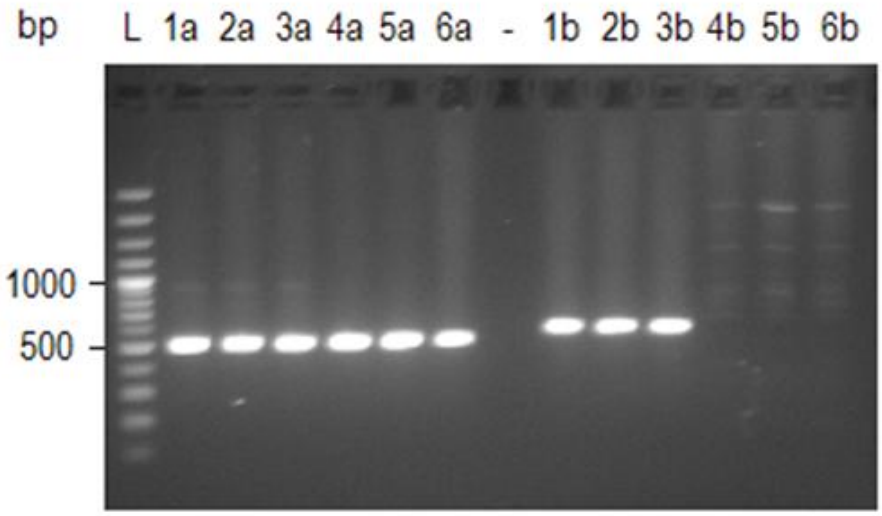

Figure 5. Verification of Cre-mediated recombination. 2 KRAS G12D animals were intubated with $5x10^8$ pfu adenovirus expressing Cre-recombinase (AdCre) and 2 without. After 4 weeks, the lungs of these animals were removed and assessed for Cre-mediated recombination by PCR.

A) Cre-mediated recombination PCR strategy. KRAS G12D mice are heterozygous for the KRAS mutation and one chromosome carries the mutant copy (left) which after Cre-mediated recombination will contain a residual LoxP site that makes amplification of that region approximately 50 bp larger than amplification of the same region on the chromosome carrying the wildtype KRAS allele (right).

B) DNA sequence of relevant region, showing the portion of the LSL casette that is excised due to Cre-recombinase (yellow), the Cre recognition sites (underlined) and the primer binding sites (boxed).

C) Products of the PCR reaction were loaded onto a 2% agarose gel along with a 100 bp DNA ladder (L). Samples from animals treated with AdCre (+Cre) show an additional product that is not seen from samples from animals that were not treated with AdCre (-Cre), indicating cre-mediated recombination occurs on addition of Cre-recombinase.

Figure 5

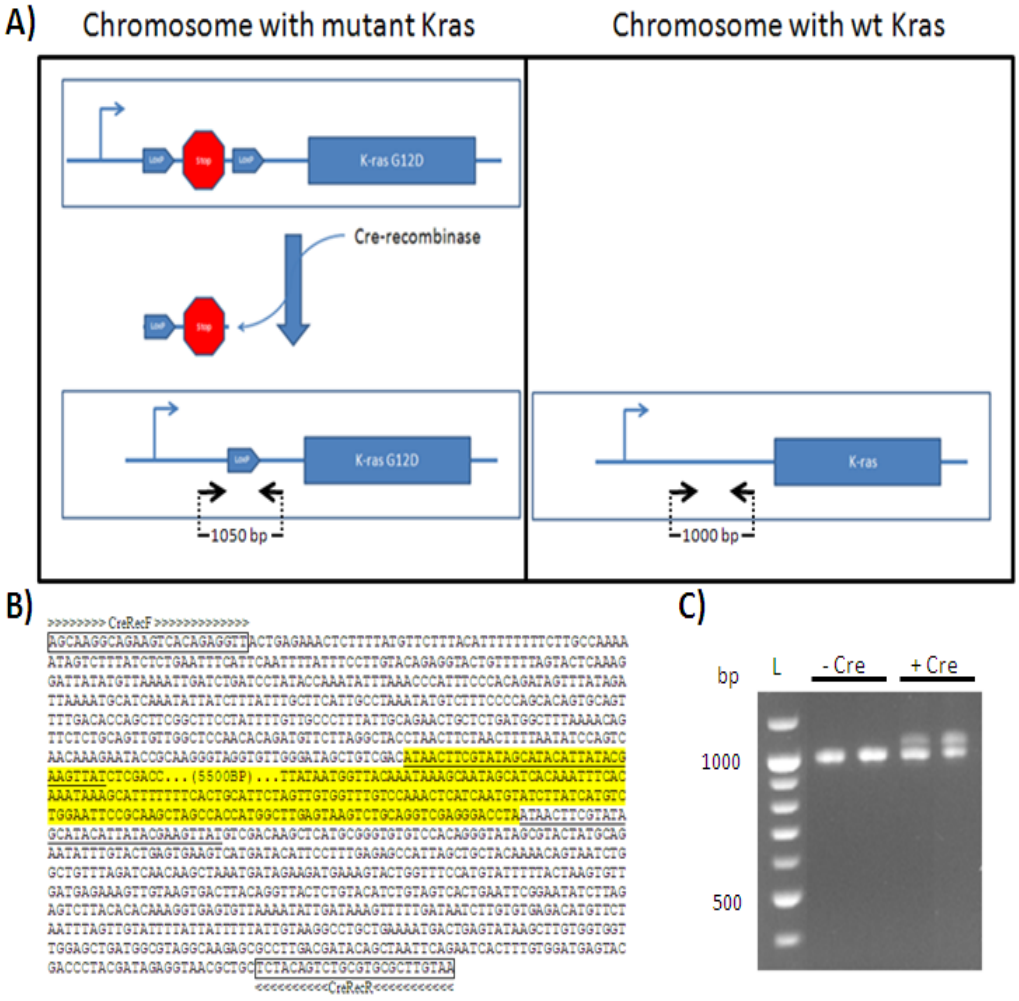
A)
Chromosome with mutant Kras
Chromosome with wt Kras
K-ras G12D
Cre-recombinase
K-ras G12D
K-ras
1050 bp
1000 bp
B)
>>>>>>>> CreRecF >>>>>>>>>>>>>
AGCAAGGCAGAAGTCACAGAGGTTACTGAGAAACTCTTTTATGTTCTTTACATTTTTTTCTTGCCAAAA
ATAGTCTTTATCTCTGAATTTCATTCAATTTTATTTCCTTGTACAGAGGTACTGTTTTTAGTACTCAAAG
GATTATATGTTAAAATTGATCTGATCCTATACCAAATATTTAAACCCATTTCCCACAGATAGTTTATAGA
TTAAAATGCATCAAATATTATCTTTATTTGGTTCATTGCCTAAATATGTCTTTCCCCAGCACAGTGCAGT
TTTGACACCAGCTTCGGCTTCCTATTTTGTTGCCCTTTATTGCAGAACTGCTCTGATGGCTTTAAAACAG
TTCTCTGCAGTTGTTGGCTCCAACACAGATGTCTTAGGCTACCTAACTTCTAACTTTTAATATCCAGTC
AACAAAGAATACCGCAAGGGTAGGTGTTGGGATAGCTGTCGACATAACTTCGTATAGCATACATTATACG
AAGTTATCTCGACC...(5500BP)...TTATAATGGTTACAAATAAAGCAATAGCATCACAAATTTCAC
AAATAAAGCATTTTTTTCACTGCATTCTAGTTGTGGTTTGTCCAAACTCATCAATGTATCTTATCATGTC
TGGAATTCCGCAAGCTAGCCACCATGGCTTGAGTAAGTCTGCAGGTCGAGGGACCTAATAACTTCGTATA
GCATACATTATACGAAGTTATGTCGACAAGCTCATGCGGGTGTGTCCACAGGGTATAGCGTACTATGCAG
AATATTTGTACTGAGTGAAGTCATGATACATTCCTTTGAGAGCCATTAGCTGCTACAAAACAGTAATCTG
GCTGTTTAGATCAACAAGCTAAATGATAGAAGATGAAAGTACTGGTTTCCATGTATTTTTACTAAGTGTT
GATGAGAAAGTTGTAAGTGACTTACAGGTTACTCTGTACATCTGTAGTCACTGAATTCGGAATATCTTAG
AGTCTTACACACAAAGGTGAGTGTTAAAATATTGATAAAGTTTTTGATAATCTTGTGTGAGACATGTTCT
AATTTAGTTGTATTTTATTATTTTTATTGTAAGGCCTGCTGAAAATGACTGAGTATAAGCTTGTGGTGGT
TGGAGCTGATGGCGTAGGCAAGAGCGCCTTGACGATACAGCTAATTCAGAATCACTTTGTGGATGAGTAC
GACCCTACGATAGAGGTAACGCTGCTCTACAGTCTGCGTGCGCTTGTAA
<<<<<<<<<<CreRecR<<<<<<<<<<
C)
bp
L
- Cre
+ Cre
1000
500

Chapter 3: Results

3.1 Characterization of KRAS G12D mouse model

3.1.1 Initial dose response experiment

An initial adenovirus encoding Cre-recombinase (AdCre) dose response experiment was performed and found to be unsuccessful. Ten 6-8 week old KRAS G12D mice were treated with a low dose of AdCre ($5x10^5$ pfu, n=2), a high dose ($5x10^7$ pfu, n=4), and a high dose of control vector AdDl70 ($5x10^7$ pfu, n=4). Originally 12 mice were used but 2 had died due to causes unrelated to tumor development. After performing histology it was clear that there was no apparent difference at the histological level of the high dose group (AdCre $5x10^7$ pfu) compared to the control (AdDl70). The results of CT scans were similar in that no difference was detected between AdDl70 and AdCre at the doses used here.

3.1.2 Refined dose response experiment (CaPi)

The AdCre dose response experiment was subsequently repeated subjecting the AdCre virus to calcium phosphate (CaPi) precipitation. This methodology was used by Jackson et al. (2001), the developers of this mouse model, as this was shown to increase the ability of the adenovirus to infect its target cells (Fasbender et al. 1998; Yi et al. 2001). The highest dosage was also increased 10-fold and a group without CaPi precipitation was also included. Using n=18, the modified experimental approach included a low dose ($5x10^6$ pfu, n=4), a medium dose ($5x10^7$ pfu, n=4), and a high dose ($5x10^8$ pfu, n=3) of CaPi precipitated AdCre along with a high dose of control vector AdDl70 ($5x10^8$ pfu,

n=4) and a high dose of AdCre ($5x10^8$ pfu, n=3) without CaPi precipitation for comparison.

3.1.3 CT scan analysis

The animals were then CT scanned at 2 week intervals until the 6^{th} week. Half of the animals were sacrificed for histology at week 4 leaving only 9 animals for scanning at week 6. Figures 6-8 show complete lung CT scans of representative animals from each group at week 2 (figure 6), week 4 (figure 7) and week 6 (figure 8). In each of these figures, (A) shows the unmodified CT scan image while (B) incorporates a colored overlay consisting of intensifying colors to highlight density changes (all voxels that are colored blue are between -1000 and -200 HU, yellow between -200 and 0 HU, and red between 0 and +200 HU).

Lung density histograms were generated from the CT scan data over the range -1000 → +250 HU for each animal (figure 9). By averaging histograms from unaffected control animals (n=18, all week 0) and AdCre-treated animals (n=14, all week 4 or 6 AdCre $5x10^8$ or $5x10^7$ pfu that showed obvious increases in lung density) and then subtracting the control histogram from the AdCre-treated histogram, one observes that on average increases in density occur between -200 → +200 HU and corresponding decreases over -500 → -200 HU (figure 10).

In an attempt to quantify these increases in density as seen by CT scanning, each week 0 histogram was subtracted from the corresponding week 4 or 6 histogram and the area under the curve was calculated over the range -200 → +200 HU (the range that is increased in AdCre affected animals, see figure 10). This number was then averaged for each group and the results of this are shown in figure 11. This data represents the percentage of the lung that includes voxels between -200 → +200 HU and in the higher AdCre treatment groups this can be as high as 70% (compared to AdDl70 which is typically about 5-10%).

3.1.4 Histological and ImageJ analysis

As mentioned previously, of the 18 animals that were used for the dose response experiment, half of them were sacrificed at week 4 and the other half at week 6 for use in histology. Serial sections of the lung were stained with H&E and representative animals showing varying levels of affectedness are shown in figure 12. As can be seen in this figure, the AdCre $5x10^7$ pfu lungs show regions of denser tissue, especially towards the periphery of the lung and around some airways whereas the AdCre $5x10^8$ pfu lungs (both with and without CaPi precipitation, data not shown) show a much more dramatic and diffuse pattern of this staining through the whole of the lung. There were no detectable increases in density with the $5x10^6$ pfu treatment group at these time points.

These regions of densely staining tissue were quantified with the aid of the ImageJ software. As illustrated in figure 13A, using the threshold feature of this program allows the user to select various densities of the lung and then measure the area. By comparing the higher density regions of the lung to the total area, it is possible to determine the % high density of the lungs. It should be pointed out that these higher densities include blood vessels and some darker staining areas of the epithelial border of airways, which although do not constitute affected densities are still included by the threshold feature in AdDl70 animals. The % high density of 6 individual sections for one animal was averaged and these values were then averaged by group as is shown in figure 13B. As expected, increasing dosage of AdCre results in a greater % high density value. These densities were also graded, according to criteria described in the introduction, and this is shown in figure 13C and D. Grade 2 tumors were detected primarily in AdCre $5x10^8$ pfu at week 4, and $5x10^7$, $5x10^8$ and $5x10^8$ without CaPi at week 6 (figure 13D).

3.1.5 Immunohistochemistry using pan-cytokeratin

As a suggestion by Dr. J.C. Cutz (McMaster University) to better resolve regions of hyperplasia and to confirm the epithelial nature of the AdCre-associated increases in density, immunohistochemistry using pan-cytokeratin was used. Cytokeratin is a component of the intermediate filament in the eukaryotic cytoskeleton and has an important role in human tumor diagnosis (Broers et al., 1988). Immunohistochemistry of cytokeratin specifically stains epithelial cells

and allows for visual separation from high density regions associated with mononuclear/inflammatory cell accumulation. As can be seen in figure 14, treatment with AdCre ($5x10^8$ pfu without CaPi precipitation for 4 weeks) resulted in regions of increased density that positively stain for pan-cytokeratin compared to AdDl70 treatments. This further confirms the functionality of this model.

3.1.6 Analysis of broncho-alveolar lavage fluid

As indicated in the introduction, it has been reported that a variety of pro-inflammatory cytokines (KC, MCP-1 and IL-6) have been associated with lung adenocarcinoma. It was therefore of interest to assay for these cytokines in the bronchoalveolar lavage (BAL) fluid of AdCre-treated KRAS G12D animals using ELISA-based methods. In experiments as shown in figure 15, at 4 weeks time KC and IL-6 levels were increased relative to AdDl70 treated animals while MCP-1 levels were undetectable for all samples (not shown). Interestingly, at week 4 only 2 animals had shown increased levels of OSM in the BAL and both were from the AdCre $5x10^6$ pfu group (38 and 138 pg/ml). At week 6, levels of all cytokines were undetectable (not shown).

To determine inflammatory cell infiltrate in the lung, BAL was performed followed by counting cells and cytocentrifugation. After differential staining it was clear that the majority (80-90%) of cells were macrophages with lymphocytes the second most frequent (2-15%) (figure 16). Neutrophils were relatively uncommon (0.2-5%) while the eosinophil was the most rare (0.2-2%).

Generally, increases in AdCre resulted in higher cell number in the BAL and this occurred in a dose-dependent fashion. The cell numbers are approximately equal at week 4 and 6, suggesting that a steady state had been reached.

3.1.7 KRAS G12D macrophages undergo Cre-mediated recombination

As was shown in figure 5, DNA derived from total lung lysates from AdCre treated animals showed an additional PCR product that was suggestive of cre-mediated recombination. Analysis of macrophages in the BAL of these treated animals was performed and found that the same recombination event had occurred (figure 17A). This recombination was confirmed when macrophages from the BAL of untreated KRAS G12D animals were treated with AdCre *ex vivo* and showed the same recombination (figure 17B).

Figure 6. Representative lung CT scans at week 2. KRAS G12D mice were treated with varying dosages of AdCre and subjected to CT scanning at 2, 4 and 6 weeks post-treatment. The data was analyzed using AMIRA and screen shots of representative animals were taken of the lung at 10 slice intervals from the top of the lung (towards the head) to the bottom (to the tail) to illustrate Cre-mediated effects. Lung labels were then generated using AMIRA for each representative animal and this was used to make separate colored layers (for better illustration of density ranges) over the following thresholds: blue (-1000 HU → -200 HU), yellow (-200 HU → 0 HU), red (0 HU → +200 HU). These colored layers were then overlaid over the original CT scan image.

A) Unmodified CT scan screen shots of representative animals at week 2.

B) Modified color overlay of CT scan screen shots from (A).

Figure 6

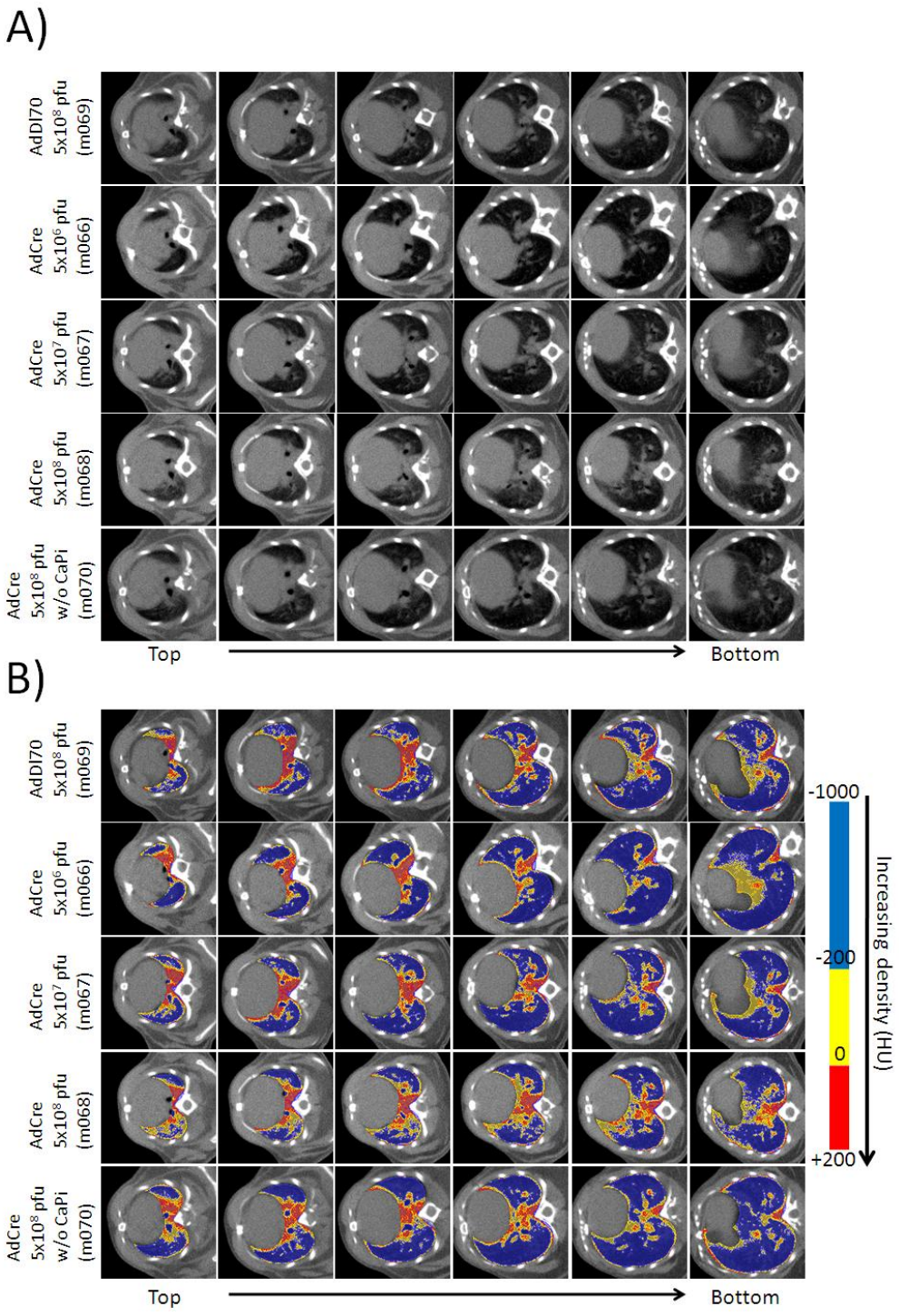
A)
AdDl70 5x10^8 pfu (m069)
AdCre 5x10^6 pfu (m066)
AdCre 5x10^7 pfu (m067)
AdCre 5x10^8 pfu (m068)
AdCre 5x10^8 pfu w/o CaPi (m070)
Top
Bottom
B)
AdDl70 5x10^8 pfu (m069)
AdCre 5x10^6 pfu (m066)
AdCre 5x10^7 pfu (m067)
AdCre 5x10^8 pfu (m068)
AdCre 5x10^8 pfu w/o CaPi (m070)
Top
Bottom
-1000
-200
0
+200
Increasing density (HU)

Figure 7. Representative lung CT scans at week 4. KRAS G12D mice were treated with varying dosages of AdCre and subjected to CT scanning at 2, 4 and 6 weeks post-treatment. The data was analyzed using AMIRA and screen shots of representative animals were taken of the lung at 10 slice intervals from the top of the lung (towards the head) to the bottom (to the tail) to illustrate Cre-mediated effects. Lung labels were then generated using AMIRA for each representative animal and this was used to make separate colored layers (for better illustration of density ranges) over the following thresholds: blue (-1000 HU → -200 HU), yellow (-200 HU → 0 HU), red (0 HU → +200 HU). These colored layers were then overlaid over the original CT scan image.

C) Unmodified CT scan screen shots of representative animals at week 4.

D) Modified color overlay of CT scan screen shots from (A).

Figure 7

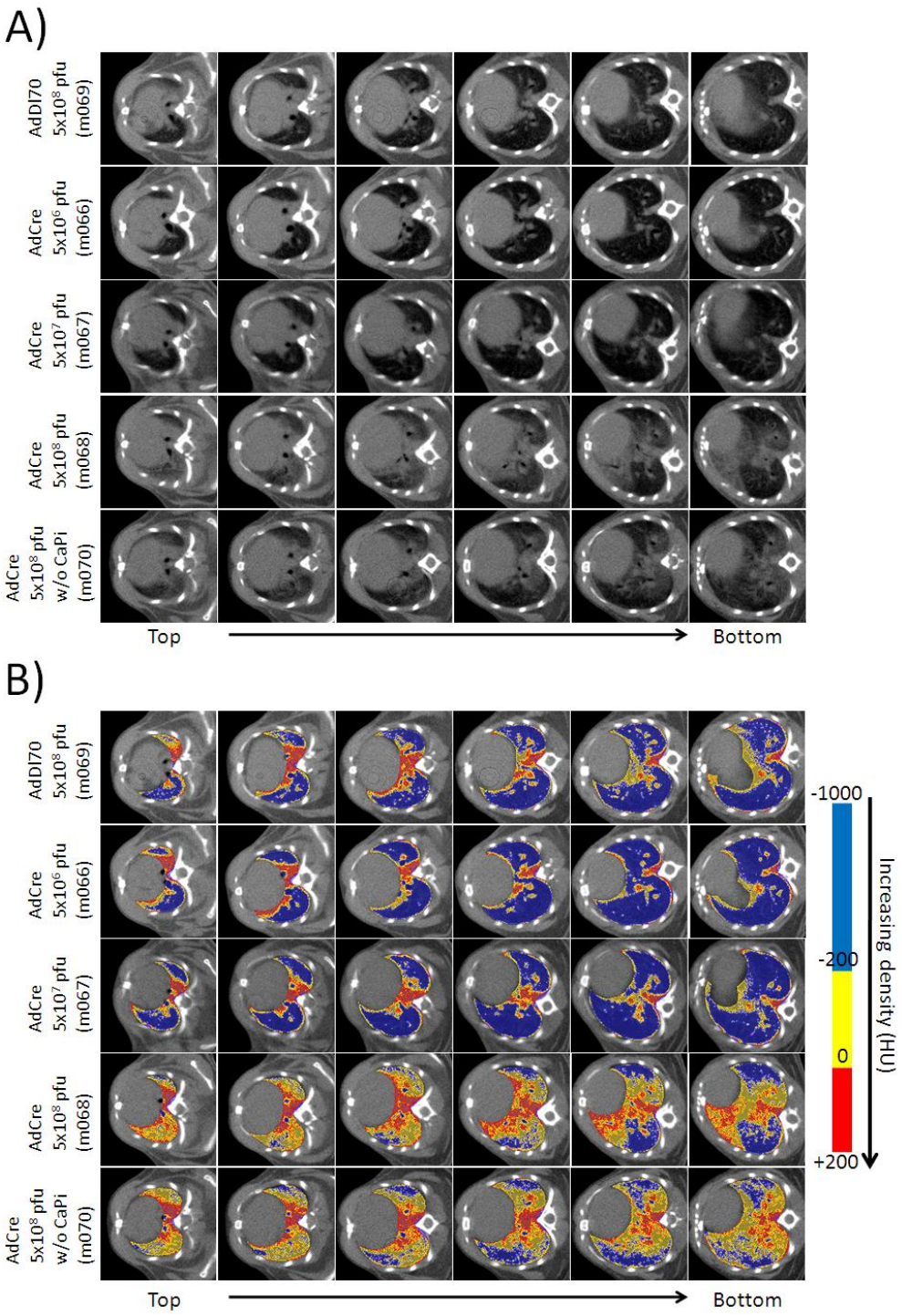
A)
AdDl70 5x10^8 pfu (m069)
AdCre 5x10^6 pfu (m066)
AdCre 5x10^7 pfu (m067)
AdCre 5x10^8 pfu (m068)
AdCre 5x10^8 pfu w/o CaPi (m070)
Top
Bottom
B)
AdDl70 5x10^8 pfu (m069)
AdCre 5x10^6 pfu (m066)
AdCre 5x10^7 pfu (m067)
AdCre 5x10^8 pfu (m068)
AdCre 5x10^8 pfu w/o CaPi (m070)
-1000
-200
0
+200
Increasing density (HU)
Top
Bottom

Figure 8. Representative lung CT scans at week 6. KRAS G12D mice were treated with varying dosages of AdCre and subjected to CT scanning at 2, 4 and 6 weeks post-treatment. The data was analyzed using AMIRA and screen shots of representative animals were taken of the lung at 10 slice intervals from the top of the lung (towards the head) to the bottom (to the tail) to illustrate Cre-mediated effects. Lung labels were then generated using AMIRA for each representative animal and this was used to make separate colored layers (for better illustration of density ranges) over the following thresholds: blue (-1000 HU → -200 HU), yellow (-200 HU → 0 HU), red (0 HU → +200 HU). These colored layers were then overlaid over the original CT scan image.

A) Unmodified CT scan screen shots of representative animals at week 6.

B) Modified color overlay of CT scan screen shots from (A).

Figure 8

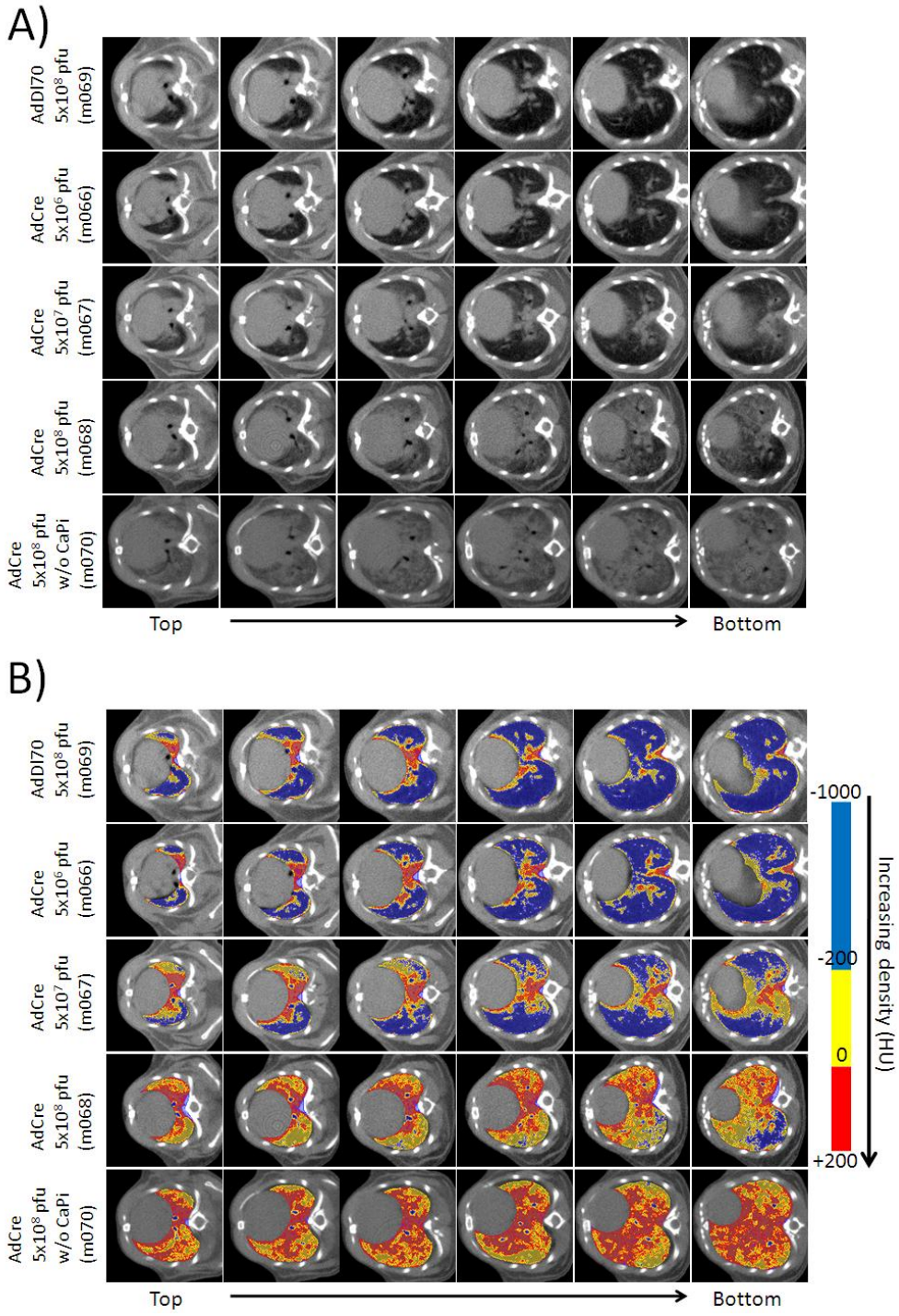
A)
AdDl70 5x10^8 pfu (m069)
AdCre 5x10^6 pfu (m066)
AdCre 5x10^7 pfu (m067)
AdCre 5x10^8 pfu (m068)
AdCre 5x10^8 pfu w/o CaPi (m070)
Top
Bottom
B)
AdDl70 5x10^8 pfu (m069)
AdCre 5x10^6 pfu (m066)
AdCre 5x10^7 pfu (m067)
AdCre 5x10^8 pfu (m068)
AdCre 5x10^8 pfu w/o CaPi (m070)
-1000
-200
0
+200
Increasing density (HU)
Top
Bottom

Figure 9. CT scan histograms showing the distribution of densities in the lung. KRAS G12D mice were treated with varying dosages of AdCre and subjected to CT scanning at 2, 4 and 6 weeks post-treatment. Using AMIRA, lung labels were generated from the CT scan data and histograms were generated over the range -1000 HU → +250 HU (26 bin resolution). Each histogram was then summed and individual bin values were expressed as percent of the total lung label sum. These percentages (for each animal for each group for each week) were then loaded into Graphpad Prism and graphs were generated and averaged by group and week (green: week 2, blue: week 4, red: week 6). Included in each graph is the average for week 0 (n=18, in black). Error bars are SEM, sample number is indicated for each graph.

A) Average histogram at week 2, 4 and 6 for animals treated with control vector AdDl70
B) Average histogram at week 2, 4 and 6 for animals treated with AdCre $5x10^6$ pfu.
C) Average histogram at week 2, 4 and 6 for animals treated with AdCre $5x10^7$ pfu.
D) Average histogram at week 2, 4 and 6 for animals treated with AdCre $5x10^8$ pfu.
E) Average histogram at week 2, 4 and 6 for animals treated with AdCre $5x10^8$ pfu without CaPi precipitation.

Figure 9

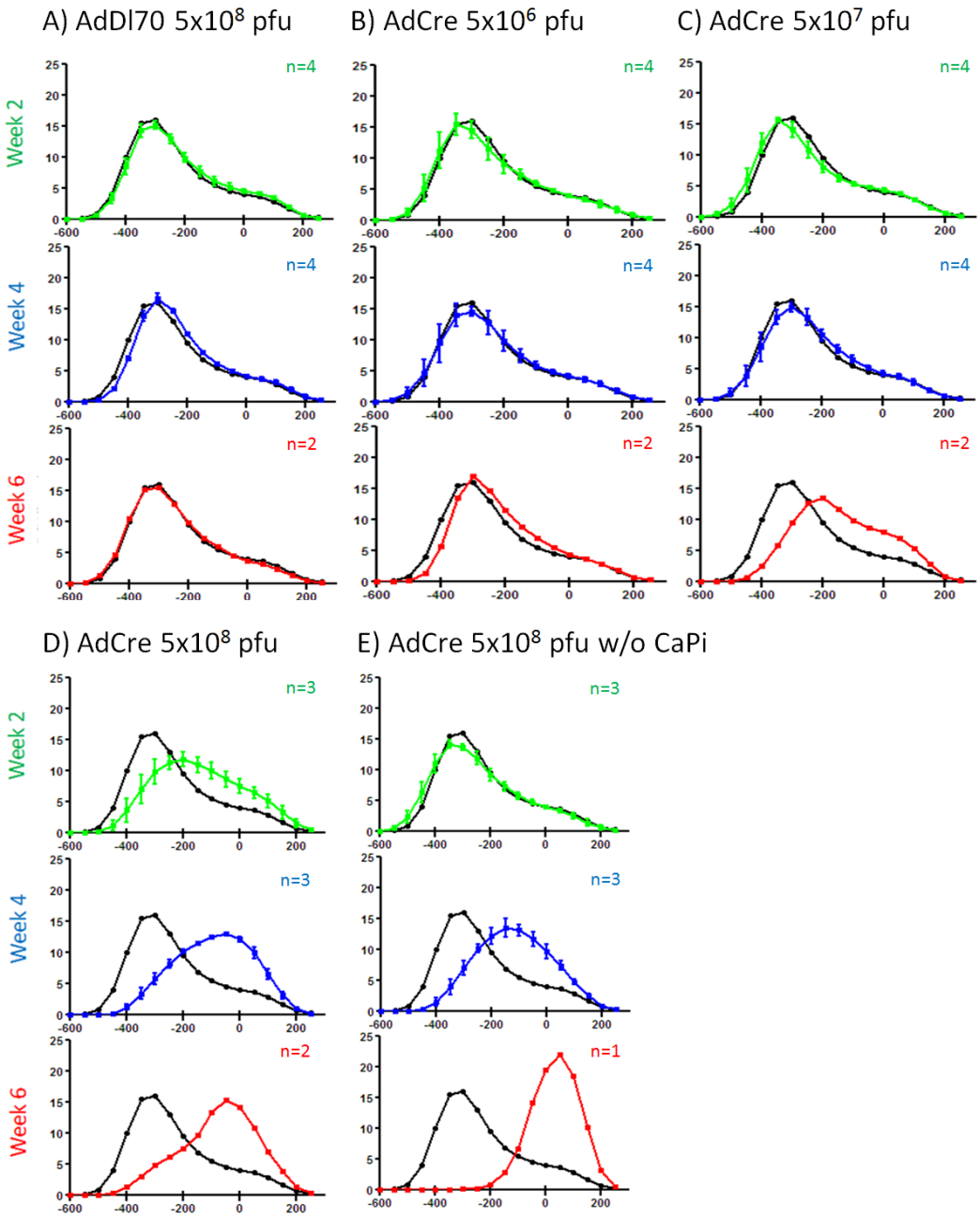
A) AdDl70 5x10^8 pfu
B) AdCre 5x10^6 pfu
C) AdCre 5x10^7 pfu
D) AdCre 5x10^8 pfu
E) AdCre 5x10^8 pfu w/o CaPi
Week 2
Week 4
Week 6
n=4
n=3
n=2
n=1

Figure 10. Determination of the range of AdCre-induced CT scan density increases. Histogram data from naïve (week 0) control lung labels was averaged and loaded into Graphpad Prism (black line) along with AdCre affected lung histograms (from AdCre $5x10^7$ pfu at 6 weeks, AdCre $5x10^8$ pfu at 2, 4 and 6 weeks, and from AdCre $5x10^8$ pfu without CaPi precipitation at 4 and 6 weeks) (red line). The AdCre affected histogram was then subtracted from the control histogram and this difference is shown (Δ(AdCre-Control) (green line). Error bars are SEM.

Figure 10

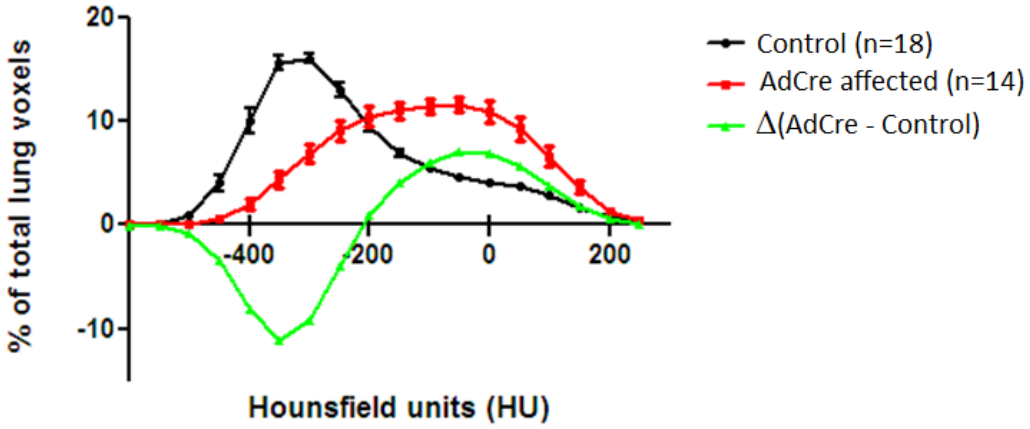
20
10
0
-10
-400
-200
0
200
% of total lung voxels
Hounsfield units (HU)
Control (n=18)
AdCre affected (n=14)
Δ(AdCre - Control)

Figure 11. Quantification of AdCre-affected densities over the range 200 → +200 HU in lung labels. KRAS G12D mice were treated with varying dosages of AdCre and subjected to CT scanning at 2, 4 and 6 weeks post-treatment. Each histogram for each animal at week 0 was subtracted from its respective histogram for week 2, 4 or 6. The resultant histogram was then summed over the range -200 HU → +200 HU and this value was averaged for each group and week. Sample numbers are indicated except for AdCre $5x10^8$ pfu (week 2-0 and week 4-0 are n=3) and AdCre 5x108 pfu without CaPi precipitation (week 2-0 and week 4-0 are n=3, week 6-0 is n=1). *<0.05, ***<0.001

Figure 11

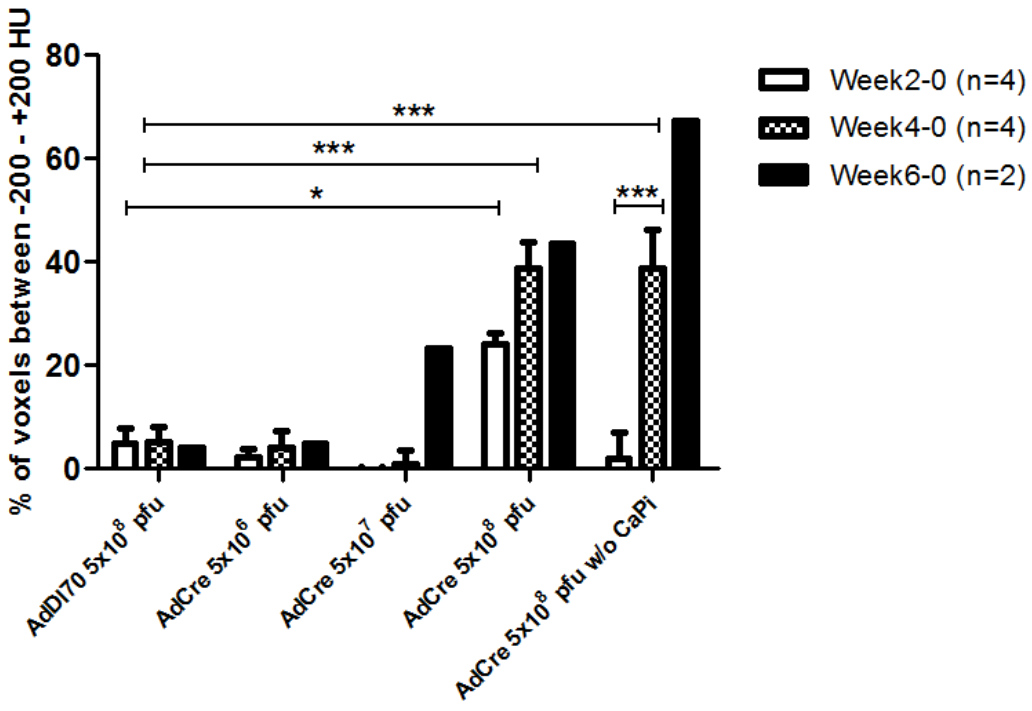
% of voxels between -200 - +200 HU
80
60
40
20
0
***
***
*
***
Week2-0 (n=4)
Week4-0 (n=4)
Week6-0 (n=2)
AdDl70 5x10^8 pfu
AdCre 5x10^6 pfu
AdCre 5x10^7 pfu
AdCre 5x10^8 pfu
AdCre 5x10^8 pfu w/o CaPi

Figure 12. Representative histology of animals from indicated groups. KRAS G12D mice were treated with varying dosages of AdCre and animals were sacrificed at week 4 and week 6. The left lung was sectioned at the major bifurcation and cut at 700 µm intervals and stained with H&E. Representative control AdDl70, $5x10^7$ pfu and $5x10^8$ pfu lungs are shown at week 6.

Figure 12

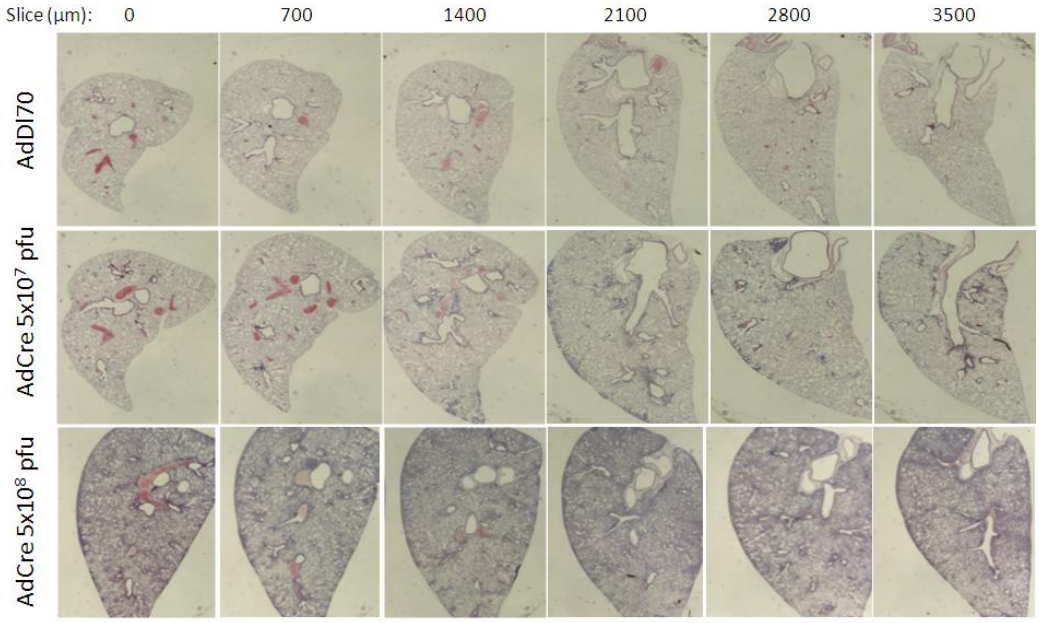
Slice (µm): 0 700 1400 2100 2800 3500
AdDl70
AdCre 5x10^{7} pfu
AdCre 5x10^{8} pfu

Figure 13. Quantifying H&E stains using ImageJ and tumor grading.

Histological samples were photographed and loaded into ImageJ where they were analyzed for increases in high density and for grade 2 tumor development.

A) Outline of quantification process using the ImageJ software for measuring % high density.
B) Averaged quantification of % high density for animals (n=2) for each group, averaging the results of 6 sections per animal.
C) H&E section of a representative AdCre $5x10^8$ pfu animal showing a well-defined and dense grade 2 tumor (black arrow) as well as diffuse and less dense grade 1 tumor (green arrow).
D) Analysis of grade 2 tumor area was quantified again using ImageJ using a drawing tool to circle in grade 2 tumor regions (and measuring the area), rather than using the threshold function. This area was then divided by the total area of the lung slice and plotted. This figure shows the area occupied by a single grade 2 tumor (the only grade 2 tumor found) in the AdCre $5x10^8$ pfu week 4 group and the AdCre $5x10^7$ pfu, $5x10^8$ pfu, and $5x10^8$ without CaPi precipitation week 6 group

Figure 13

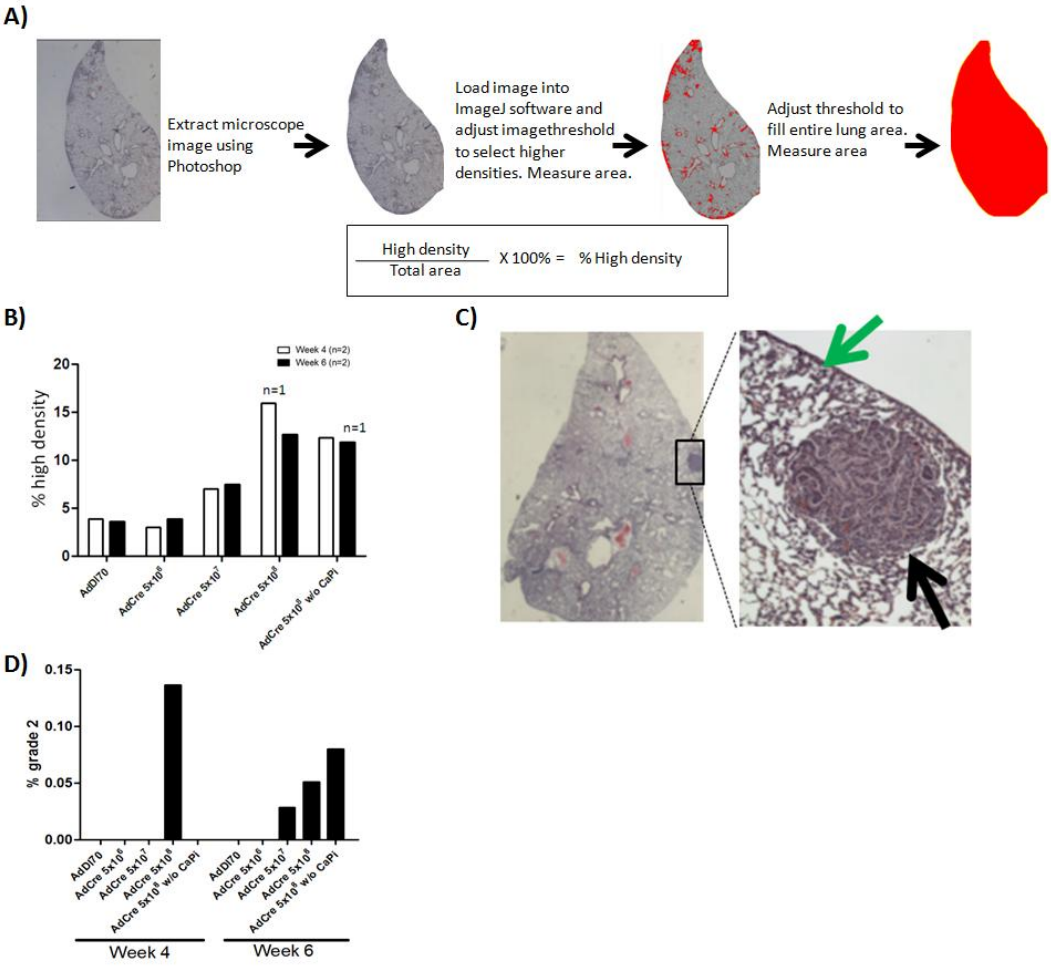
A)
Extract microscope image using Photoshop
Load image into ImageJ software and adjust imagethreshold to select higher densities. Measure area.
Adjust threshold to fill entire lung area. Measure area
High density / Total area X 100% = % High density
B)
% high density
Week 4 (n=2)
Week 6 (n=2)
n=1
n=1
AdDl70
AdCre 5x10^6
AdCre 5x10^7
AdCre 5x10^8
AdCre 5x10^8 w/o CaPi
C)
D)
% grade 2
Week 4
Week 6

Figure 14: Immunohistochemistry of AdCre-treated lung tissue using pan-cytokeratin. Histological samples were prepared from AdCre ($5x10^8$ pfu without CaPi precipitation) and AdDl70 ($5x10^8$ pfu) treated KRAS G12D mice after 4 weeks. Samples were then stained using pan-cytokeratin antibody by immunohistochemistry and photographed at 10X and 20X magnification. A negative control that was subjected to all steps of the immunohistochemistry procedure with the exception of treating with pan-cytokeratin antibody is shown below.

Figure 14

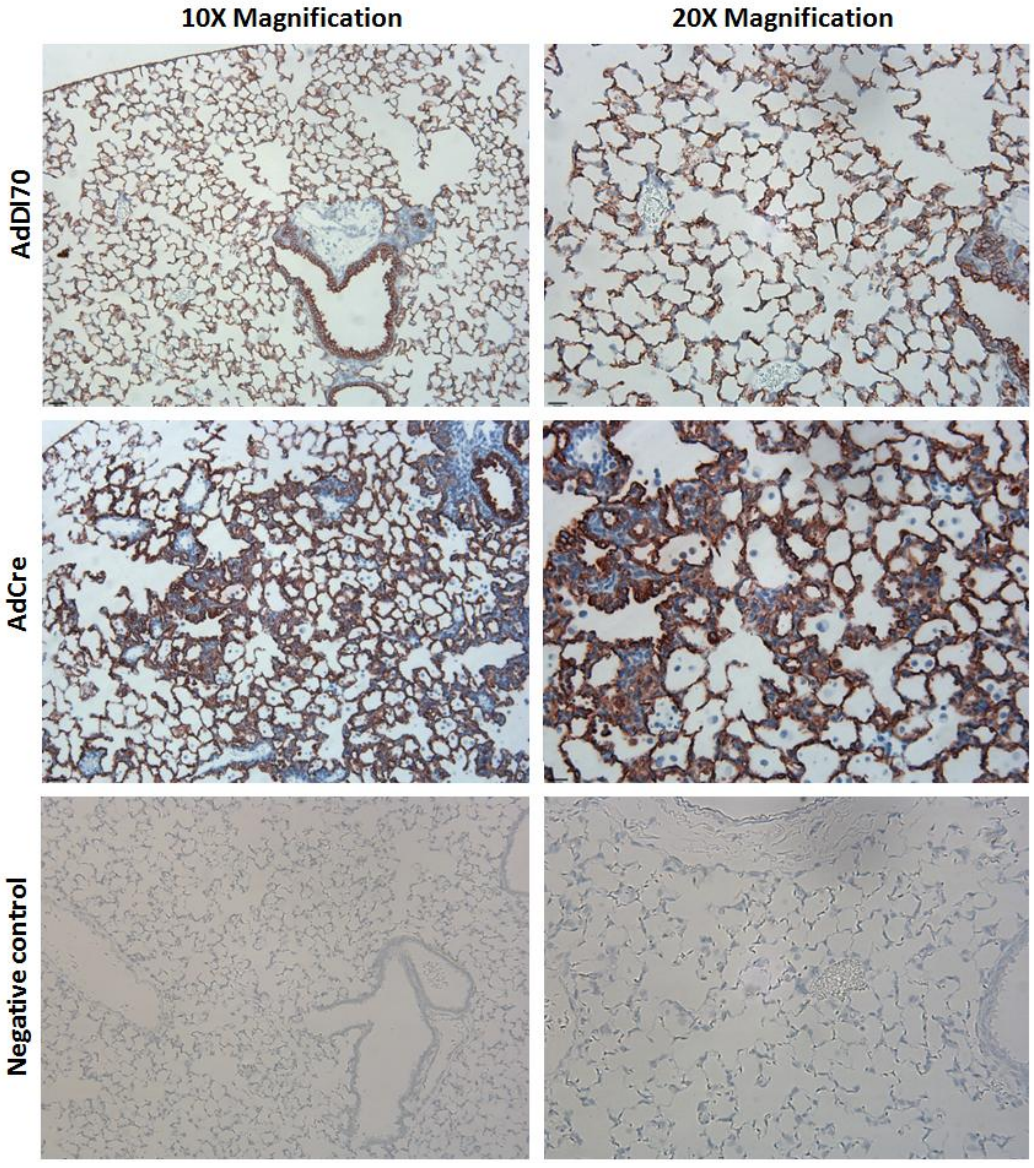
10X Magnification
20X Magnification
AdDl70
AdCre
Negative control

Figure 15: Cytokine measurement in the broncho-alveolar lavage (BAL) fluid of AdCre-treated KRAS G12D mice at week 4. Approximately 1.2 ml of BAL fluid was recovered from each animal and assayed by ELISA for IL-6 and KC. All are sample n=2 unless specified.

Figure 15

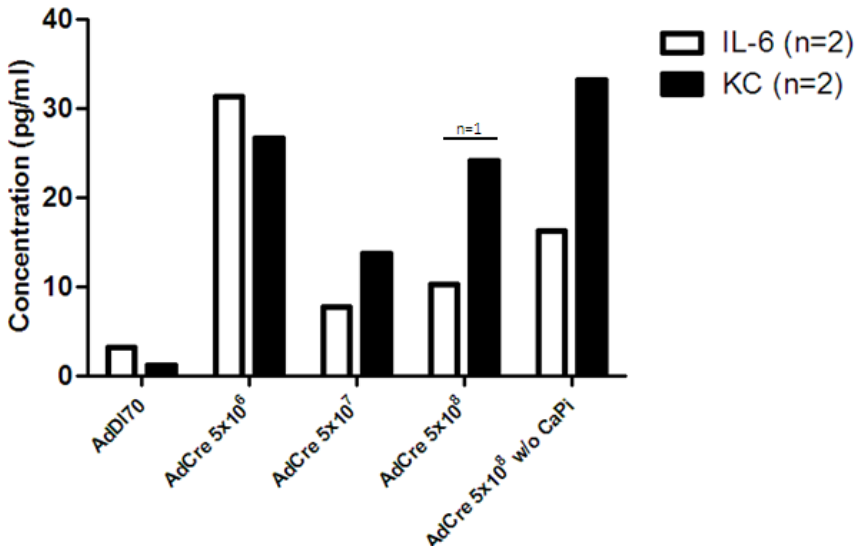
40
30
20
10
0
Concentration (pg/ml)
IL-6 (n=2)
KC (n=2)
n=1
AdDl70
AdCre 5x10^6
AdCre 5x10^7
AdCre 5x10^8
AdCre 5x10^8 w/o CaPi

Figure 16: Differential counting of cells in the broncho-alveolar lavage (BAL) fluid. Cells in the BAL were first counted to determine total cell number and then cytocentrifuged and differentially stained to identify macrophage, neutrophil, lymphocyte and eosinophil percentage. All sample n=2 unless specified.

Figure 16

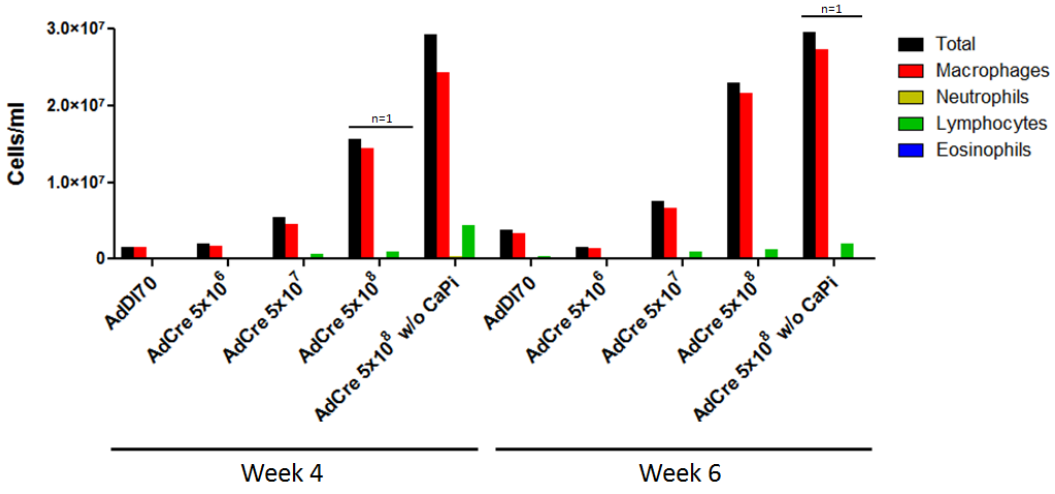
Cells/ml
3.0×10⁷
2.0×10⁷
1.0×10⁷
0
n=1
n=1
Total
Macrophages
Neutrophils
Lymphocytes
Eosinophils
AdDl70
AdCre 5x10⁶
AdCre 5x10⁷
AdCre 5x10⁸
AdCre 5x10⁸ w/o CaPi
AdDl70
AdCre 5x10⁶
AdCre 5x10⁷
AdCre 5x10⁸
AdCre 5x10⁸ w/o CaPi
Week 4
Week 6

Figure 17: Cre-mediated recombination status of macrophages.

A) Macrophages from AdCre treated mice (n=2, AdCre $5x10^8$ pfu for 4 weeks) were separated from the broncho-alveolar lavage (BAL) by adhering the cells to a 6-well plate for 2 hours before washing off the non-adherent population. The remaining adherent cells were mostly macrophages. DNA was extracted from these macrophages and PCR was run using primers specific for the Cre-mediated recombination assay (see figure 5). The products of this (MØ – Cre and MØ + Cre) were run on a 2% agarose gel along with a 100 bp ladder (L) and a positive control from a sample previously shown to undergo the recombinant (Total lung + Cre, as in figure 5).

B) Macrophages were separated from the BAL of 9 naive KRAS G12D mice and divided between 4 wells of a 6-well plate. These cells were then infected *ex vivo* using AdDl70, AdGFP and AdCre. Infection was confirmed by visual inspection of GFP+ cells (10% infection). DNA was then extracted from these cells and PCR was performed using primers specific for Cre-mediated recombination. These products were then run on a 2% gel along with a 100 bp ladder and a positive control from (A) (MØ + Cre).

Figure 17

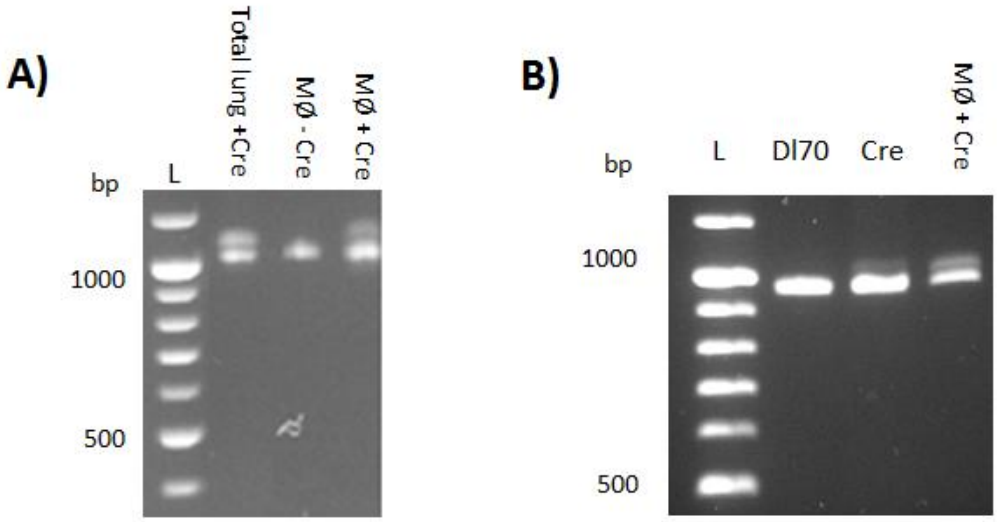
A)
bp
L
Total lung +Cre
MØ - Cre
MØ + Cre
1000
500
B)
bp
L
Dl70
Cre
MØ + Cre
1000
500

3.2 AdCre and AdIL-6/AdOSM co-treatments in KRAS G12D mice

3.2.1 Confirmation of AdOSM expression *in vivo*

An in-house mOSM ELISA was developed using a primary antibody produced by GSK (under a material transfer agreement) and a secondary biotinylated antibody (cat# BAF495) from R&D. The ELISA protocol followed was in accordance with the general guidelines stipulated by R&D and made use of all other reagents specified in recommended product protocol. This in-house ELISA was tested for its sensitivity (approximately 30 pg/ml) and specificity (no cross reaction with the gp130 cytokines LIF, IL-6, IL-31, IL-11 and CT-1 up to 10 ng/ml). The ELISA was also tested for its ability to detect mOSM secreted by LPS-stimulated RAW 267.4 macrophages (figure 18A) and in the BAL of AdOSM treated mice at day 2 and day 7 post AdOSM delivery (figure 18B and C). The results of this show that increasing concentrations of LPS can stimulate increasing mOSM secretion in RAW 267.4 cells and increasing AdOSM delivery to mice can result in increases in mOSM production *in vivo* and in both of these experiments mOSM can be assayed using the in-house ELISA.

3.2.2 AdCre and AdIL-6/AdOSM co-treatment (4 weeks)

In an effort to understand whether the gp130 cytokine IL-6 and OSM can modify the lung environment to alter tumor growth, initial experiments were performed utilizing AdCre ($5x10^8$ pfu without CaPi precipitation) along with AdIL-6 ($5x10^7$ pfu) or AdOSM ($5x10^7$ pfu). After 4 weeks, animals were

sacrificed for histology. This experiment was completed two separate times and the results of this are shown in figure 19. Tumor counts were performed blind and as shown in figure xB the AdCre/AdOSM treatment group appears to show a trend toward increased tumor burden relative to the AdCre alone or AdCre/AdIL-6 treatment group despite not reaching significance. The AdCre and AdCre/AdIL-6 treatment groups appear to show similar low levels of tumor number.

3.2.3 AdCre and AdOSM co-treatment (12 weeks)

Based on the findings in section 3.2.2, it was decided that the experiment was to be repeated using a lower dose of AdCre ($5x10^7$ pfu) for a longer period of time (12 weeks) including the CT scanning. For each group five animals were used as follows: AdCre ($5x10^7$ pfu), AdCre/AdOSM ($5x10^7$ pfu each) AdOSM alone ($5x10^7$) and AdDl70 ($1x10^8$ pfu). Unfortunately, due to limitations in animal number, the AdIL-6 treatment groups had to be dropped. CT scanning was performed on these animals at 0, 6, and 9 weeks and the animals were sacrificed at 12 weeks. Based on the CT scan findings at weeks 6 and 9, it was clear that the experiment was not successful. Confirmation of this was made when the animals were sacrificed and the lungs were processed for histology (figure 20A).

In an attempt to rationalize why the experiment did not work as planned, two KRAS G12D animals were treated with 5x107 pfu and their lungs were assayed for Cre-mediated recombination after 1 week post-treatment. As seen in figure 20B the PCR experiment shows that these lungs did not contain the

additional amplicon indicative of Cre-mediated recombination suggesting that this dose was insufficient for use to detect AdCre-mediated effects.

Figure 18. In-house mOSM ELISA confirms AdOSM expression *in vivo*. After development of an in-house mOSM ELISA, different experiments were performed to show its proficiency in detecting mOSM.

A) RAW 267.4 cells were treated with increasing concentrations of LPS and supernatants were assayed for mOSM after 48 hours.
B) BALB/c mice were intubated with increasing concentrations of adenovirus encoding mOSM and after 2 days were sacrificed and broncho-alveolar lavage was performed which was then assayed for mOSM.
C) BALB/c mice were intubated with increasing concentrations of adenovirus encoding mOSM and after 7 days were sacrificed and broncho-alveolar lavage was performed which was then assayed for mOSM.

Figure 18

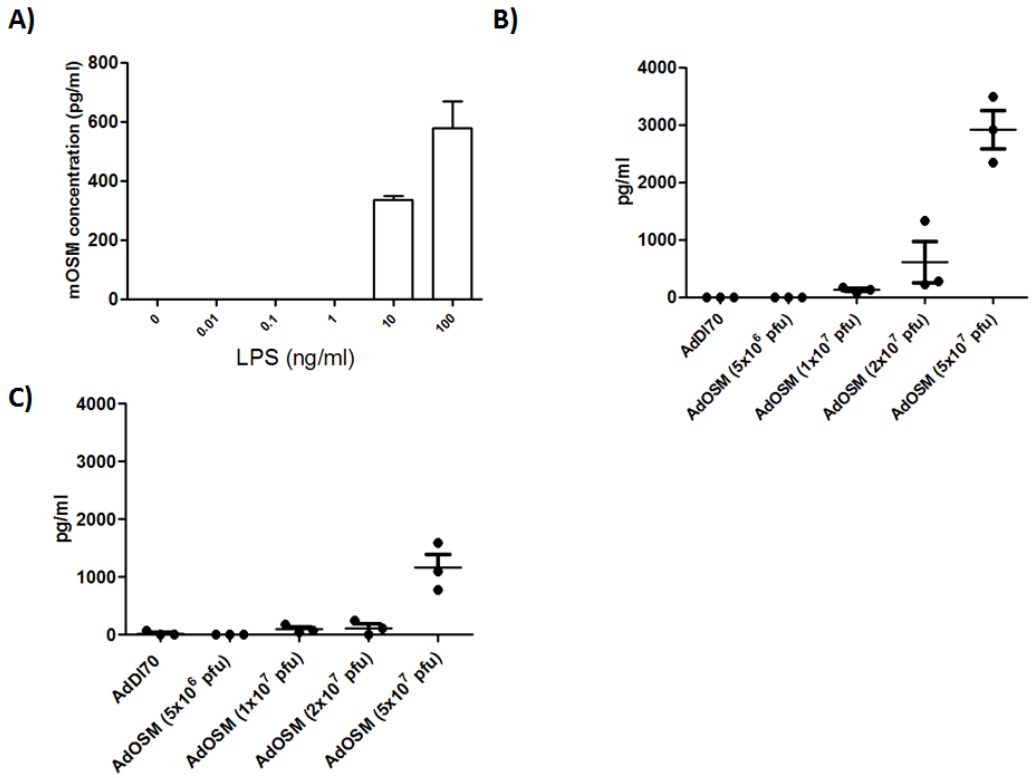
A)
mOSM concentration (pg/ml)
800
600
400
200
0
0
0.01
0.1
1
10
100
LPS (ng/ml)
B)
pg/ml
4000
3000
2000
1000
0
AdDl70
AdOSM (5x10^6 pfu)
AdOSM (1x10^7 pfu)
AdOSM (2x10^7 pfu)
AdOSM (5x10^7 pfu)
C)
pg/ml
4000
3000
2000
1000
0
AdDl70
AdOSM (5x10^6 pfu)
AdOSM (1x10^7 pfu)
AdOSM (2x10^7 pfu)
AdOSM (5x10^7 pfu)

Figure 19. Analysis of AdCre and AdIL-6/AdOSM co-treatments (4 week). Five KRAS G12D animals were treated with AdCre alone ($5x10^8$ pfu without CaPi precipitation) or in combination with AdIL-6 or AdOSM ($5x10^7$ pfu) for a period of 4 weeks before sacrificing. A single lobe of the right lung was sectioned into three slices (upper, medial and lower) and stained with H&E.

A) Representative photographs of animals from each indicated treatment group. Arrows indicate grade 2 tumors.

B) Tumors were counted blind from two separate experiments.

Figure 19

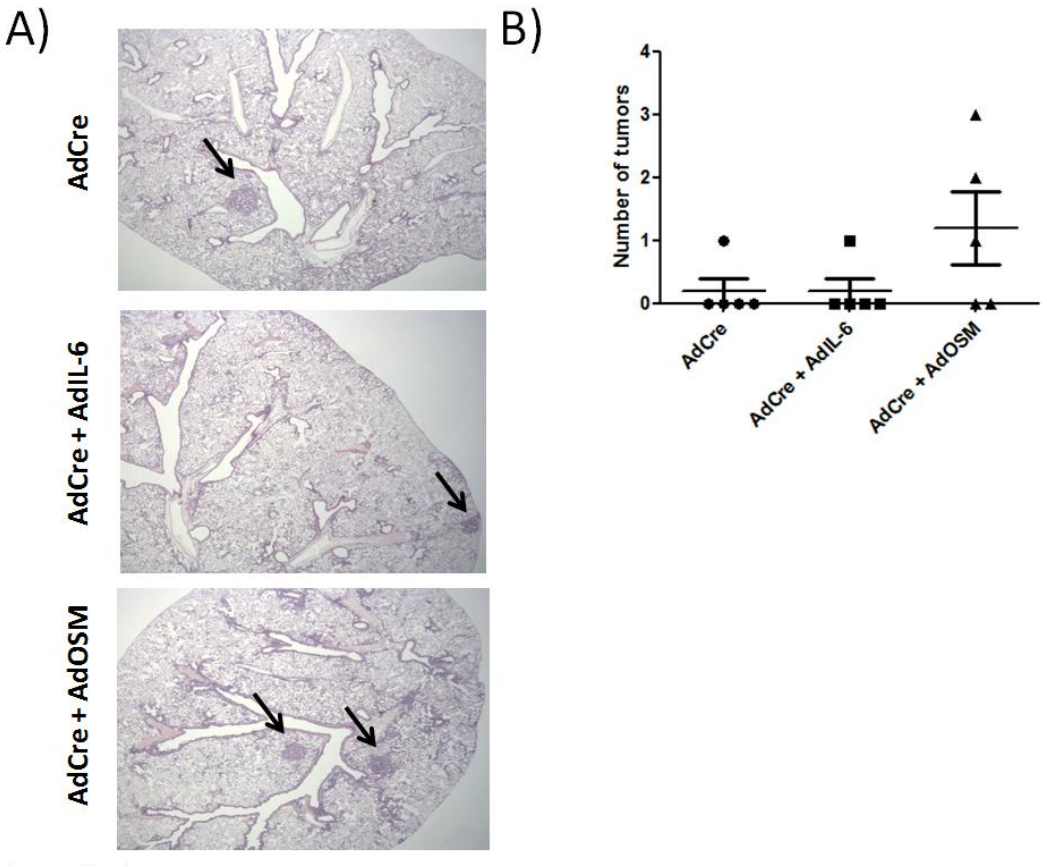
A)
AdCre
AdCre + AdIL-6
AdCre + AdOSM
B)
Number of tumors
0
1
2
3
4
AdCre
AdCre + AdIL-6
AdCre + AdOSM

F**igure 20. Analysis of failed AdCre and AdIL-6/AdOSM co-treatments (12 week).** Five KRAS G12D animals were treated with AdCre alone ($5x10^7$ pfu) or in combination with AdIL-6/AdOSM ($5x10^7$ pfu) for a period of 12 weeks before sacrificing.

A) Representative photographs of histology (H&E stained) for each treatment group (minus AdDl70).

B) Two KRAS G12D mice were treated with the same dose of AdCre ($5x10^7$ pfu) in a separate experiment for a period of 1 week before sacrificing. The lungs were processed for assaying Cre-mediated recombination (refer to figure 5) (lanes 1 and 2) and a positive control was loaded alongside (a sample previously shown (figure 5) to contain an additional amplicon indicative of Cre-mediated recombination). A 100 bp ladder was run alongside.

Figure 20

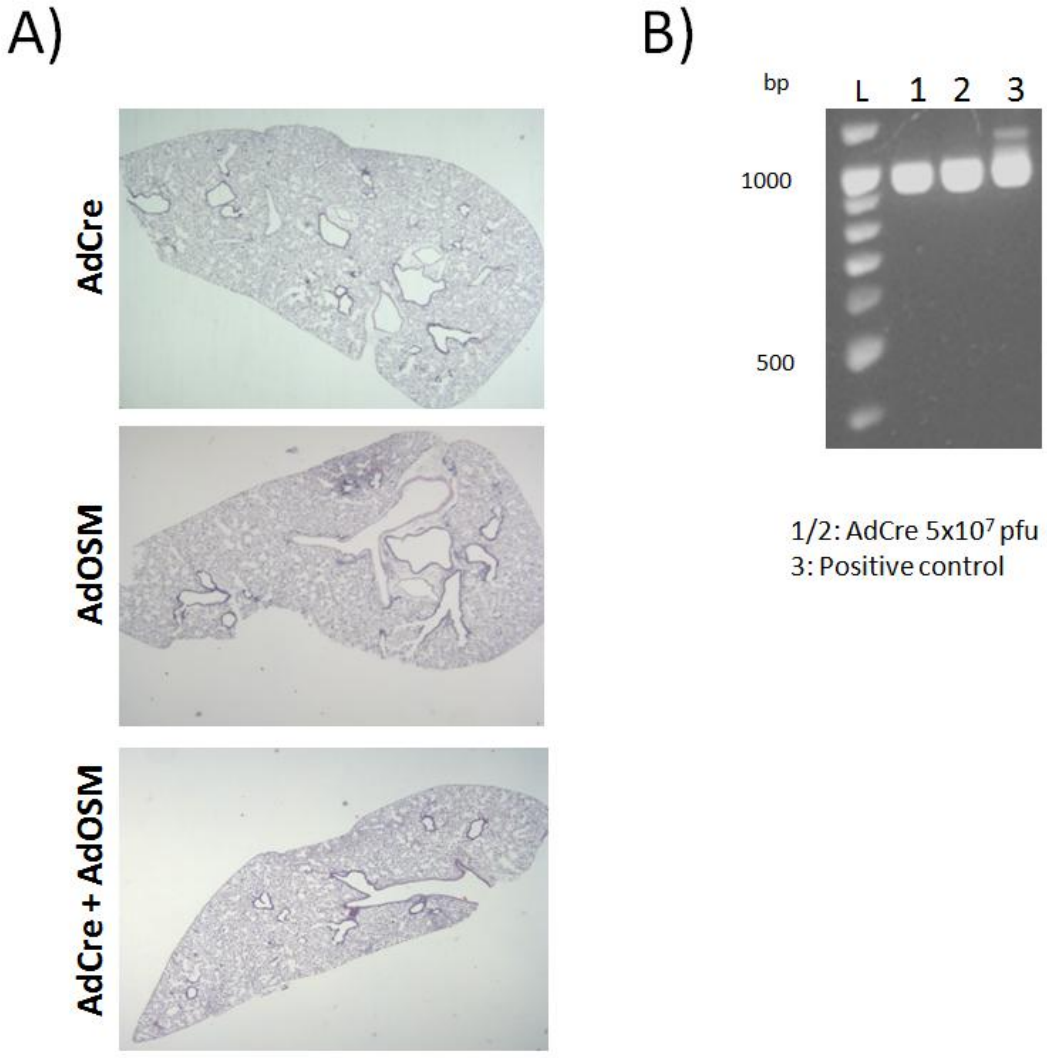
A)
AdCre
AdOSM
AdCre + AdOSM
B)
bp
L
1
2
3
1000
500
1/2: AdCre 5x10^7 pfu
3: Positive control

3.3 AdCre and AdIL-6/AdOSM co-treatments in mice treated with LLC

3.3.1 KRAS mutation status of LLC

As the LLC lung cancer model was intended to be compared to the KRAS G12D mouse model, these cells were assayed for possible mutations in KRAS. DNA was extracted from LLC cells and primers designed to flank codons 12 and 13 (the most commonly mutated regions in KRAS) were used to perform PCR. Gel purification of the relevant PCR amplicons was then performed and this product was submitted to McMaster's sequencing facility (MOBIX). In addition to LLC DNA, DNA derived from KRAS G12D animals was used as negative control (genotyping confirmed the absence of the mutant KRAS allele) as well as a positive control (genotyped heterozygote) controls. The results of this are shown in figure 21 and indicate that the LLC cell line contains a G12C mutation.

3.3.2 Analysis of *in vitro* LLC proliferation and cytokine production in response to IL-6/OSM

As the LLC lung cancer model was ultimately to be used in conjunction with cytokine overexpression in the lungs of C57Bl/6, it was therefore informative to examine the growth potential of these cells in these environments. LLC cells were stimulated with a variety of inflammatory mediators (OSM, IL-6, TNF-α, TGF-β, IL-13, IL-1β, IFN-γ) at increasing concentrations (0.2, 2 and 20 ng/ml) and measured for changes in proliferation relative to untreated cells using an MTT proliferation assay. As is shown in figure 22A, TGF-β, IL-13, and IL-1β

all seemed to decrease the proliferation of LLC while IFN-γ appeared to have this effect at its highest dose.

Cytokines IL-6, OSM, KC and MCP-1 were then assayed from the supernatants of the LLC proliferation study. IL-6 and OSM were detectable only in the samples that were treated with these cytokines and the data for this is not shown. KC and MCP-1 were detected in most of the samples and levels are shown in figure 22B and C. KC production was enhanced in a dose-dependent fashion with OSM or TNF-α treatments and there was a dramatic (5000-fold) increase in KC production as a result of IL-1β stimulation, at all three doses tested. MCP-1 was secreted at a basal level of 1000 pg/ml, TNF-α and IL-1β stimulation induced highest levels of MCP-1, whereas OSM, IL-6 and IFN-γ induced modest dose-dependent increases in MCP-1.

3.3.3 Overexpression of IL-6/OSM in mice treated with LLC

Using a protocol from Dr. Bowdish's laboratory, which instructed to keep LLC cell clumps intact (by minimizing pipetting and by growing on untreated petri dishes), allowed for sufficient tumor take once intubated into wildtype C57Bl/6. Animals were intubated with LLC cells along with a $5x10^7$ pfu of AdDl70/AdIL-6/AdOSM. After 1 week these animals were sacrificed and the lungs harvested for staining with H&E. Tumors were counted and the average area of tumor to total lung area was measured using ImageJ. This experiment was performed on two separate occasions and as shown in figure 23 the addition of

either AdIL-6 (experiment 1, figure 23B) or AdOSM (both experiment 1 and 2, figure 23B and C) increased the tumor load relative to LLC and AdDl70 treatments. Average tumor area was higher for the AdIL-6 treatment (experiment 1, figure 23B) but was most dramatic with the AdOSM treatment (experiment 2, figure 23C). When considering both experiments (figure 23D) the tumor counts and tumor area were highest with the AdOSM treatment. Total cell numbers were counted in the BAL of these treated animals and were found to show no change relative to controls (4.1×10^6, 3.3×10^6, 4.5×10^6 cells/ml for LLC/AdDl70, LLC/AdIL-6, and LLC/AdOSM respectively).

Figure 21. Results of sequencing of KRAS in LLC cells. DNA was extracted from LLC cells and primers flanking codons 12 and 13 of the KRAS gene were used for PCR. The PCR products were loaded on an agarose gel and electrophoresed before imaging. The appropriate bands were excised from the gel and cleaned before submitting for DNA sequencing. The figure shows a segment of the DNA sequence with the commonly mutant codons 12 and 13 boxed (sequence GGTGGC). "R" (red box) indicates a base that is either G or A, "n" (grey box) indicates either T or G. Numbers indicate bp.

A) Negative control DNA from a KRAS G12D animal that was genotyped Kras negative. The sequence is GGTGGC, indicating the DNA is from a homozygote wildtype animal.
B) Positive control DNA from a KRAS G12D animal that was genotyped Kras positive. The sequence is GRTGGC (G[G/A]TGGC: the GGT is a glycine, the GAT is aspartic acid), indicating the DNA is from a heterozygote source containing a G12D allele.
C) Test sample LLC DNA. The sequence is nGTGGC ([G/T]GTGGC: the GGT is glycine, the TGT is cysteine) indicating the DNA is from a heterozygote source containing a G12C allele.

Figure 21

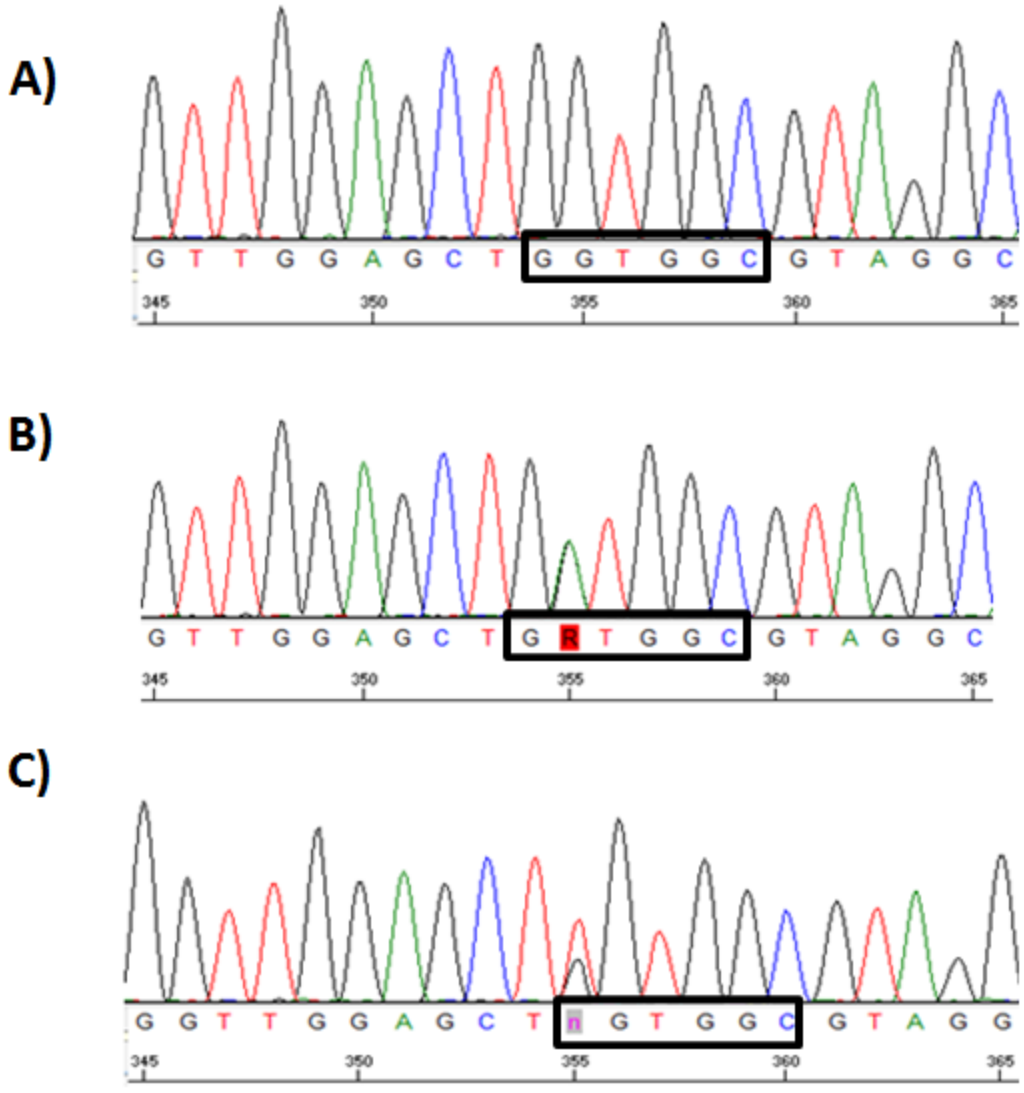
A)
G T T G G A G C T G G T G G C G T A G G C
345
350
355
360
365
B)
G T T G G A G C T G R T G G C G T A G G C
345
350
355
360
365
C)
G G T T G G A G C T n G T G G C G T A G G
345
350
355
360
365

Figure 22. Results of an *in vitro* proliferation assay and corresponding cytokine production using LLC cells. LLC cells were seeded at 2000 cells in a 96-well plate in media supplemented with 1% FBS and stimulated with the indicated concentration of cytokine (see bottom of figure for cytokine type). After 3 days the cells were incubated with MTT to measure proliferation (A) by absorbance at 540 nm. The growth increase is measured relative to unstimulated LLC cells. Data in (A) is the average of two separate experiments. In (B) cytokines KC (upper) and MCP-1 (lower) were assayed by ELISA and the dotted line indicates secretion by unstimulated cells (for MCP-1 only, KC was not secreted in unstimulated cells). Error bars are SEM.

Figure 22

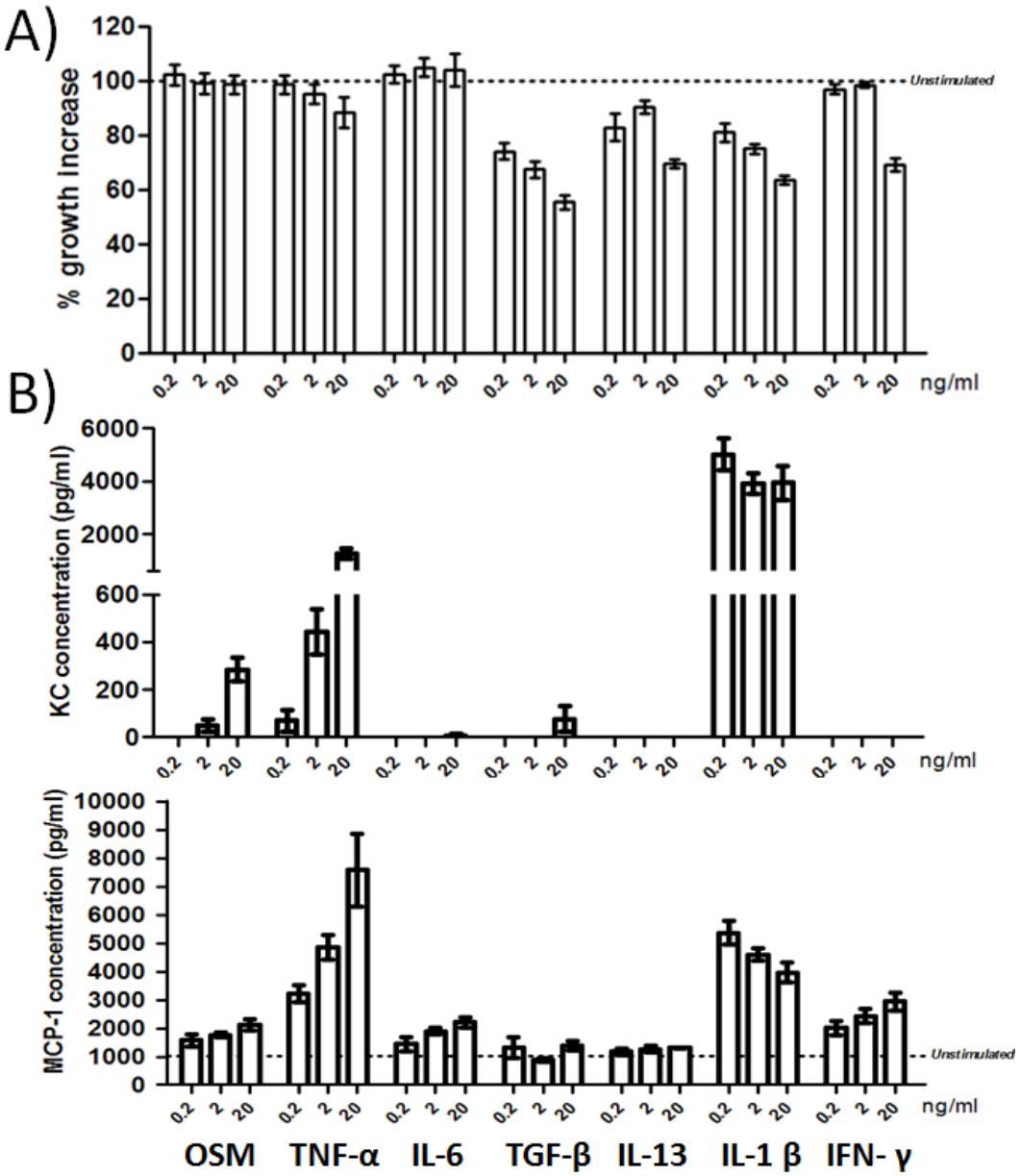
A)
% growth increase
120
100
80
60
40
20
0
Unstimulated
0.2 2 20
ng/ml
B)
KC concentration (pg/ml)
6000
4000
2000
600
400
200
0
MCP-1 concentration (pg/ml)
10000
9000
8000
7000
6000
5000
4000
3000
2000
1000
0
Unstimulated
OSM
TNF-α
IL-6
TGF-β
IL-13
IL-1 β
IFN- γ

Figure 23. Results of *in vivo* LLC and AdAdl70/AdIL-6/AdOSM co-treatments. Using a standardized protocol, LLC cells were expanded and collected ensuring high cell clump content. Before intubation in wildtype C57Bl/6 mice, the cells were mixed with $5x10^7$ pfu AdDl70, AdIL-6 or AdOSM. After one week the mice were sacrificed and the left lung was processed for histology and stained with H&E before counting tumors and measuring average area occupied by a tumor (% tumor area). The average tumor area was measured using ImageJ and involved measuring the area of tumors present and dividing that by the total lung area before multiplying by 100%. This experiment was performed two separate times. * < 0.05, ** < 0.01

A) Representative histological photographs of the various treatments from the 2 experiments.
B) Tumor counts and % tumor area from samples in experiment 1.
C) Tumor counts and % tumor area from samples in experiment 2.
D) Tumor counts and % tumor area from samples combined from both experiment 1 and 2.

Figure 23

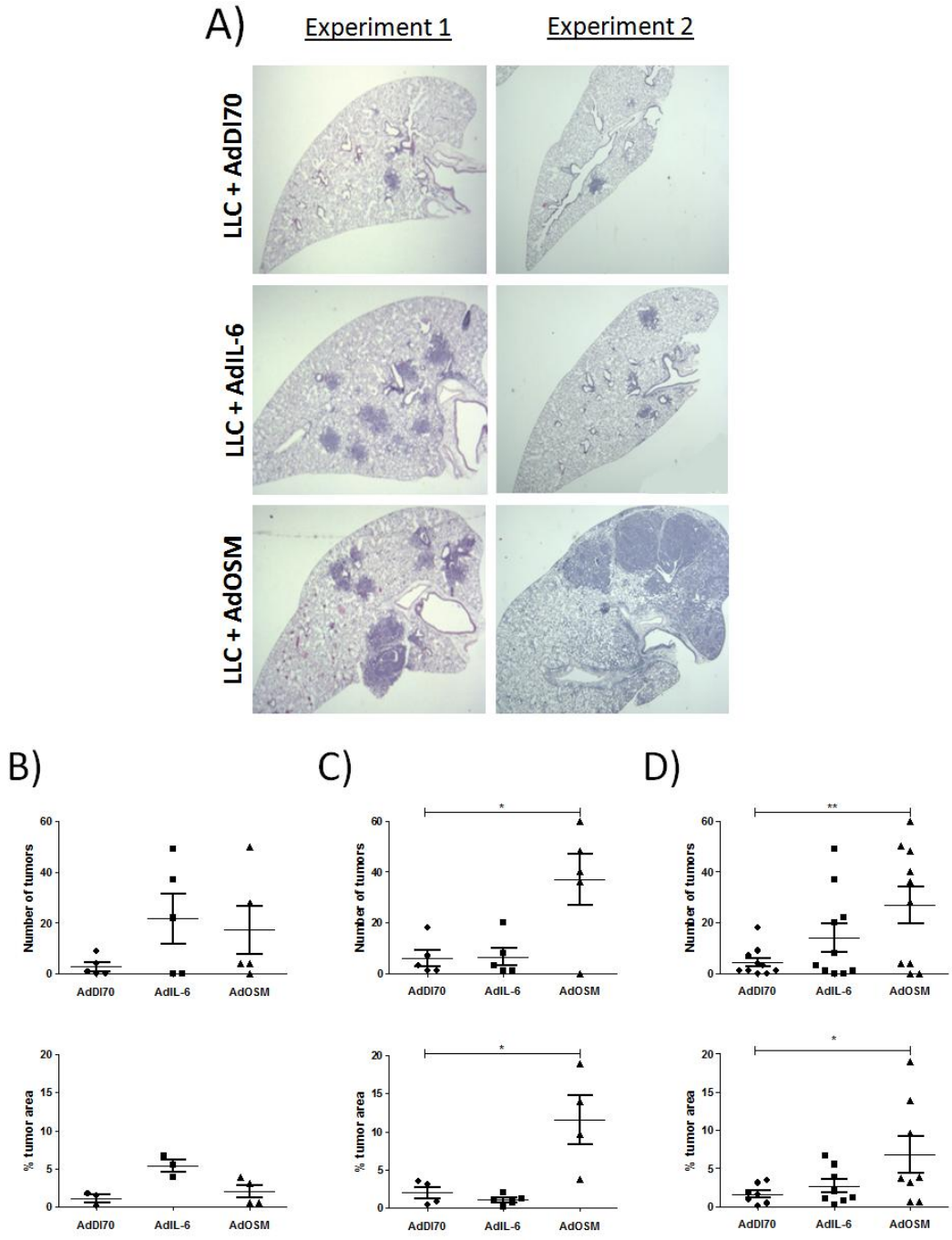
A)
Experiment 1
Experiment 2
LLC + AdDl70
LLC + AdIL-6
LLC + AdOSM
B)
C)
D)
Number of tumors
% tumor area
AdDl70
AdIL-6
AdOSM
*
**

Chapter 4: Discussion

4.1 Summary of Results

Lung cancer is a leading cause of death in the U.S. and Canada and many questions still need to be addressed regarding lung tumor development. In particular, the role of inflammation and how inflammatory cell types (such as the macrophage) may be involved in driving tumor progression are topics of current research (section 1.2). Members of the gp130 cytokine family, including IL-6 and OSM, are well characterized mediators of inflammation (section 1.3) and represent an attractive avenue for understanding inflammation and lung tumor development. Much research has been invested in understanding the role of IL-6 and its downstream signaling partner STAT-3 in various mouse tumor models (skin, colon, pancreas, gastric as well as lung) and evidence suggests a positive role for IL-6 in promoting tumor development (section 1.3.1). The role of OSM in tumor research is fundamentally lacking however select experiments have suggested that OSM may promote tumor development particularly in breast cancer by promoting angiogenesis (section 1.3.2). By modulating the lung environment to one that is inflammatory, it was then hypothesized that IL-6 and OSM would promote lung tumor development in the animal models examined.

In order to evaluate the role of gp130 cytokines IL-6 and OSM in lung tumor development, a mouse model of lung adenocarcinoma was employed. This mouse model was developed by Dr. Tyler Jacks (Jackson et al., 2001) and involves Cre-recombinase mediated expression of oncogenic KRAS G12D.

Oncogenic KRAS (carrying a point mutation in codon 12 that renders it constitutively active) in these animals is normally transcriptionally silent due to an upstream transcriptional stop cassette which can become active upon recombination mediated by Cre-recombinase (see figure 2 and also figure 5 for experimental confirmation of this recombination). KRAS is a gene involved in many aspects of tumor development and was utilized in this model due to its prevalence in human lung adenocarcinoma (section 1.1.2). As shown by Dr. Jacks' group, delivery of increasing dosages of adenovirus-encoded Cre-recombinase (AdCre) into the lungs of KRAS G12D mice resulted in increased tumor burden (Jackson et al., 2001). In order to evaluate the functionality of this model and further characterize this system using CT scanning technology, an AdCre dose response experiment was performed using a range of doses both with ($5x10^6$, $5x10^7$, $5x10^8$ pfu) and without ($5x10^8$ pfu) calcium phosphate (CaPi) precipitation and the animals were CT scanned at week 0, 2, 4 and 6. Following CT scanning, lung labels were generated from the data using the software AMIRA and lung density histograms were measured from these labels to provide quantitative data for analysis. A total of 18 animals were used (n=4 for each group including the control $5x10^8$ pfu AdDl70 group and n=3 for both the $5x10^8$ pfu groups with and without CaPi precipitation) and half the animals from each group were sacrificed at week 4 for histological analysis of the left lung (the remaining animals were sacrificed at week 6).

CT scan analysis (both visually and quantitatively) of AdCre-treated KRAS G12D animals showed varying degrees of increased lung densities relative to AdDl70 controls (figures 6-9). The low dose of AdCre ($5x10^6$ pfu) showed minimal differences by week 6 compared to AdDl70, while $5x10^7$ pfu showed moderate increases at this time point. The most obvious effects were seen with the high dose ($5x10^8$ pfu) as early as week 2 but more markedly by week 4 and 6. The high dose of AdCre ($5x10^8$ pfu) without CaPi precipitation seemed to cause similar effects however these were lacking at week 2. Analysis of histograms generated from lung labels of AdCre-treated KRAS G12D animals showed that, on average, increases in density occurred over the range -200 → +200 HU relative to untreated animals (figure 10). These density increases were then assessed for each animal over this range and found to quantify changes in lung density as a result of AdCre-treatment (figure 11). Histological analysis (both visually and quantitatively using ImageJ) of these animals showed similar degrees of increases in lung densities (figure 12 and 13) in a fashion that correlated with CT scanning and these increases are attributable to epithelial cell expansion when immunohistochemistry using an antibody to cytokeratin was used (figure 14). Thus analysis by CT scanning confirmed alterations invoked by Cre-mediated activation of mutant KRAS and indicated an additional approach to monitoring the model.

Analysis of the broncho-alveolar lavage (BAL) fluid post AdCre-treatment in KRAS G12D mice showed increased levels of cytokines IL-6 and KC relative to cytokines found in AdDl70 animals at week 4 (figure 15). OSM was also found to be increased in animals that were treated with the low dose ($5x10^6$ pfu) of AdCre at this time point. At week 6 these cytokines were not detectable. Analysis of the inflammatory infiltrate was also performed in the BAL and total cell numbers were found to increase in a dose-dependent fashion over week 4 and 6 that correlated with increases in the dose of AdCre (figure 16). Cytocentrifugation and differential staining showed that the major cell type involved in this increase was macrophages (80-90%), followed by lymphocytes (2-15%), neutrophils (0.2-5%) and eosinophils (0.2-2%). Further analysis of the macrophage population revealed that these cells may also be a target for Cre-mediated recombination and may express oncogenic KRAS (figure 17). Thus cells besides epithelial cells may act as a target for Cre-mediated recombination.

The next set of experiments involved overexpressing IL-6 or OSM (IL-6/OSM) in the lungs of KRAS G12D mice with combined AdCre treatment. Adenovirus encoding IL-6 or OSM was delivered by intubation ($5x10^7$ pfu) to create a lung environment enriched in these cytokines. An ELISA for mouse OSM was developed and the efficacy of AdOSM delivery was evaluated by measuring the concentration of OSM in the BAL after days 2 and 7 (figure 18). AdCre ($5x10^8$ pfu without CaPi precipitation) and AdIL-6 or AdOSM were then

delivered into KRAS G12D mice for a period of 4 weeks before histological analysis of a single lobe of the right lung. Tumors were counted blindly (with advice from pathologist Dr. J.C. Cutz) and no differences were found between the AdCre alone and AdCre/AdIL-6 cotreatments but there was a trend in increased tumor number in the AdCre/AdOSM cotreatment despite not reaching significance (figure 19). This experiment was then repeated using a lower dose of AdCre ($5x10^7$ pfu with CaPi precipitation) for a longer period of time (12 weeks). Analysis of the CT scans revealed no changes relative to AdDl70 controls at weeks 6 and 9 which was confirmed histologically after the animals were sacrificed at week 12 (figure 20A). A possible scenario for the experimental failure was investigated and it was found that $5x10^7$ pfu of AdCre was too low a dose to initiate Cre-mediated recombination (figure 20B).

As an additional model for lung cancer, lewis lung carcinoma (LLC) cells (derived from a spontaneous lung tumor from wildtype C57Bl/6) were utilized. These cells have previously been used in other systems to examine lung tumor biology (Savai et al. 2005, Yamaura et al. 1999). The KRAS mutation status of LLC cells was first investigated and LLC cells were found to carry a KRAS G12C mutation (figure 21). This appears to be the first identification of a KRAS mutation in this cell line. In order to determine whether or not these LLC cells proliferate directly due to cytokine stimulation, these cells were also examined *in vitro* for their growth potential in response to a variety of cytokines at 0.2, 2 and

20 ng/ml. Cytokines TGF-β, IL-13, IL-1β and IFN-γ all decreased the proliferation of LLC cells relative to unstimulated controls while cytokines IL-6, OSM, and TNF-α had no detectable effect at these doses (figure 22A). Supernatants from this experiment were assayed for IL-6, OSM, KC and MCP-1. Levels of IL-6 and OSM were not detectable in these treatments, while levels of KC were increased in response to OSM, TNF-α and most dramatically in response to IL-1β (figure 22B). MCP-1 was secreted basally by LLC cells (1000 pg/ml) and all treatments except TGF-β and IL-13 caused an increase in MCP-1 secretion in a dose-dependent manner (figure 22C). Thus, although OSM was able to induce KC production in LLC cells, neither OSM or IL-6 were able to affect proliferation directly.

LLC cells were then intubated along with AdDl70 (control) or AdIL-6/AdOSM for a period of 1 week before sacrificing and analyzing the left lung by histology. Tumors were counted and the average tumor area was measured (using ImageJ); this experiment was completed two times. AdOSM, during both experiments caused an increase in tumor number, while this was seen with AdIL-6 only during the first experiment (figure 23B and C). When considering both experiments, the effect of AdOSM clearly leads to an increase in tumor number and on average these tumors are much larger than in LLC/AdDl70 and LLC/AdIL-6 treated animals (figure 23D). Therefore it appears that IL-6/OSM

overexpression both have the ability of enhancing tumor burden in the LLC mouse model for lung cancer.

4.2 Characterization of KRAS G12D mouse model

Treatment of KRAS G12D with increasing levels of AdCre resulted in a dose dependent response on the basis of density analysis by CT scanning (both visually as in figures 6-9 and quantitatively as in figure 11), histology (visually as in figure 12 and quantitatively using ImageJ as in figure 13), grade 2 tumor development (figure 13D), and total inflammatory cell infiltrate, in particular macrophage numbers in the BAL (figure 16).

With regard to CT scanning and histology, the AdCre dose response experiment has clearly shown that KRAS G12D animals after AdCre administration can be followed by either method and both correlate with each other well. Figure 24 shows a comparison of the results of AdCre administration on density increases in the lung either by summing values between -200 → +200 HU (by histogram analysis of lung labels derived from CT scanning) or by analysis using ImageJ (histology). From this figure, it appears that the CT scanning method is more sensitive and is able to detect differences between week 4 and 6 as well as subtle increases due to low dose (AdCre $5x10^6$ pfu), which are not detected by the histology method. The basis of this may be due to the fact that the sampling size used in histology (6 slides approximately 700 µm apart in the left lung) was much smaller than the entire lung measured using the CT scan

method. It is possible that the histology method was unable to detect increases because those increases were not present in the lung samples used. In addition, by comparing the AdDl70 treated animals in figure 24, it is clear that the CT scanning method provides a lower background than the histology method and this is likely due to the presence of darkly staining tissue regions that are unchanged from controls (for instance blood in blood vessels or the thicker epithelial layer surrounding an airway) but stain to the same degree as hyperplasia and thus are measured by ImageJ. Both methods appear to correlate with one another but it should be noted that these increases in density are not necessarily due to hyerplasia of epithelial cells. As show in figure 14, while there is clearly an expansion of the cytokeratin-positive epithelial layer, there are many cells that do not stain positive for cytokeratin and are likely non-epithelial in nature, this may contribute significantly to density quantification. Thus, increases in density due to inflammation as measured by CT scanning and histology (using ImageJ) detect Cre-mediated effects in this model and should not be separated from epithelial hyperplasia.

As shown in figure 16, large numbers of macrophages were counted in the BAL of AdCre-treated animals that rise with increases in the dose of AdCre administered. Increases in macrophages and inflammation have been reported previously where a KRAS G12D mutation is involved in mouse models for lung cancer (Ji et al., 2006; Ochoa et al., 2011, Wislez et al., 2005). Bassares et al.

(2010) have shown that when KRAS G12D mice crossed with *cis*- NF-κB-EGFP mice (in which NF-κB *cis* elements are linked to EGFP expression) are treated with AdCre intranasally, dramatic increases in NF-κB activity are detected (as measured by EGFP emission) that is associated with epithelial cells. Importantly, the LKR-13 cell line (derived from a tumor in $KRAS^{LA1}$ mice, which bears the KRAS G12D mutation) has been shown to secrete high levels of MCP-1 and KC *in vitro* (Zhong et al., 2008). Given the role of NF-κB in inducing a variety of pro-inflammatory cytokines (including TNF-α, IL-1β and IL-6) and this evidence that shows a KRAS G12D cell line capable of secreting MCP-1 (Zhong et al., 2008), it is possible that the increases in macrophage number observed in this KRAS G12D AdCre dose response experiment were due to tumor-derived cytokine secretion. This may initiate and maintain an inflammatory response which ultimately may be perpetuated by the activation of the macrophage itself in this inflammatory environment. Increases in neutrophil numbers, as reported in other studies studies (Ji et al., 2006, Ochoa et al., 2010), was not observed in the KRAS G12D AdCre dose response experiment. This is likely due to these authors using a constitutively active form of the KRAS G12D oncogene (driven by the lung derived Clara cell CC-10 promoter), which is believed to provide marked increases in KRAS G12D mediated effects in comparison to Cre-based systems (Ji et al., 2006). In addition, increases in neutrophils were only detected 8 weeks in one study (Ji et al., 2006), suggesting that neutrophil increase in response to KRAS G12D activation requires substantial time to develop. Therefore, although

neutrophils have been detected in other model systems that utilize KRAS G12D, these increases were not detected in this Cre-based system.

In addition to increases in cell number in the BAL fluid there were also slight increases in pro-inflammatory cytokines IL-6 and KC 4 weeks following AdCre administration relative to AdDl70 controls (figure 15). Interestingly we did not detect MCP-1 which has been implicated in this model previously (Ji et al., 2006), however this group was only able to detect MCP-1 by week 7 and 10 and they had used a variant of the mouse model whereby the KRAS G12D oncogene is constitutively active from birth due to it being driven by the lung-derived Clara cell CC10 promoter. This same group was able to detect elevated levels of KC described in this thesis which again was only detectable by week 7 and 10. In another study by Ochoa et al. (2010) utilizing the CC10 KRAS G12D model, large increases in cytokines IL-6 and KC were detected in the BAL after 8 weeks. Perhaps in the AdCre dose response experiment described in this thesis, larger increases in cytokines would be detected after 6 weeks. It is quite possible that kinetics of cytokine expression may vary considerably over time in this model. Alternatively, perhaps there were slight differences in the way the BAL was prepared between animals in that efficiency of lavage was variable and diluted the cytokines differentially between animals.

An interesting finding in this mouse model was the possibility of cre-mediated recombination occurring in the macrophage. There is currently no

literature that reports anything similar in this mouse model and this data suggests that cell types besides epithelial may be targets for Cre-mediated recombination and generation of oncogenic KRAS. This finding might help explain the observed increase in macrophage number in animals treated with AdCre, as the macrophages may show increased proliferation or produce more chemotactic factors. However, preliminary investigation of the phenotype of these macrophages suggests that they behave similarly to macrophages derived from KRAS G12D mice treated with control AdDl70. KRAS G12D macrophages (collected from naïve mice) were collected and treated *ex vivo* with AdCre and tested for their ability to secrete IL-6, OSM, MCP-1 and KC with and without LPS stimulation as well as their ability to proliferate. No differences were detectable in comparing macrophages transduced with AdCre or AdDl70. However only 10% of cells were transduced as measured by GFP in AdGFP groups, suggesting that AdCre would transduce a similar proportion of cells. Secondly, it is possible that the recombination detected is not related to macrophages but due to a small number of contaminating epithelial cells; the signal seen in figure 17C is not strong.

With regard to the observations of effects of calcium phosphate (CaPi) precipitation, several comments can be made. CaPi precipitation appeared necessary for manifestation of AdCre-mediated effects at the lower doses of AdCre ($5x10^6$ and $5x10^7$ pfu, refer to figure 9) but unnecessary at the high AdCre

$5x10^8$ pfu dose. Figure 9 also shows that CaPi precipitation may be required for earlier onset as AdCre-mediated effects were detectable at week 2 for AdCre $5x10^8$ with CaPi but these effects were not observed without CaPi precipitation at this dose. This CaPi precipitation protocol was originally conceived by Fasbender et al. (1998) as a means to overcome low efficiency in gene transfer during gene therapy. The authors showed that CaPi precipitation increases the binding of the virus to the cell surface and suggested the virus is internalized into the cell by endosomes or phagosomes (in contrast to the usual receptor mediated pathway). They proposed that once the pH drops in the endosome the CaPi precipitate dissociates and releases the virus which can then escape the endosome and make its way to the nucleus for transcription (Fasbender et al., 1998). Adenovirus encoding β-galactosidase was precipitated with CaPi before delivery into mouse lungs (intranasally) and after 3 days these lungs were removed and stained with X-gal which showed dramatic staining along the airways compared to controls (Fasbender et al., 1998). Increases in AdCre-mediated effects that were seen using lower doses and at earlier timepoints in KRAS G12D mice can thus be explained by CaPi coprecipitation as increasing the efficiency of Cre delivery to the nucleus of target cells.

4.3 Delivery of AdCre/AdOSM may increase tumor burden in KRAS G12D mice

KRAS G12D mice were treated with AdCre $5x10^8$ pfu (without CaPi precipitation) along with $5x10^7$ pfu AdIL-6 or AdOSM for a period of 4 weeks before being sacrificed. A single lobe of the right lung was assessed for tumor burden after staining with H&E. As can be seen in figure 19, there appeared to be increases in tumor number when animals were treated with AdCre/AdOSM (3 of the 5 animals showed one or more tumors compared to 1 of the 5 that showed only one tumor in the AdCre and AdCre/AdIL-6 cotreatments) although this did not reach statistical significance. This data suggests that OSM and not IL-6 may potentiate tumor growth in this model and mechanisms of OSM-induced tumor promotion are discussed in section 4.5. It is curious that IL-6 did not appear to have any apparent effect on promoting tumor development given its involvement in other cancers (Trikha et al. 2003, Ancrile et al. 2007). Higher amounts of IL-6 levels may be required in the AdCre KRAS G12D system. On the other hand, it has been shown that IL-6 elevation in the lung environment was observed simply as a result of AdCre administration (as found in the BAL at week 4, see figure 15) so perhaps additional IL-6 has no effect. Additionally, a problem with this particular study is that the time chosen (4 weeks) may simply not be sufficient time for extensive tumor development and perhaps a longer incubation period is

necessary to observe putative effects of IL-6 or OSM induced effects in the AdCre KRAS G12D system.

The experiment involving AdCre and AdIL-6/AdOSM cotreatments was repeated using $5x10^7$ pfu (with CaPi precipitation) for a longer period of time (12 weeks) but unfortunately treatments did not induce tumor formation (CT scan and histological analysis showed no changes compared to AdDl70 controls – see figure 20A). In subsequent experiments, treating a separate set of KRAS G12D mice with the same dose of AdCre ($5x10^7$ pfu with CaPi precipitation) after one week revealed that this dose was not sufficient to induce Cre-mediated recombination in the lungs (figure 20B). It is not clear as to why $5x10^7$ pfu was insufficient to induce recombination, since earlier experiments indicated differently (see figure 9). Perhaps the efficacy of AdCre (stored at -80C diluted to $1x10^{10}$ pfu/ml in sterile PBS) decreased over time in storage.

4.4 Delivery of AdIL-6/AdOSM increases tumor burden in the LLC mouse model for lung cancer

As the LLC mouse model for lung cancer was to be compared to the KRAS G12D mouse model, it was informative to determine the KRAS mutation status of LLC. Sequencing through codon 12 (the most frequently mutated region of KRAS – see section 1.1.2) revealed a G12C point mutation. It has been reported that different mutations in KRAS can have different clinical outcomes (Janakiraman et al., 2010) and in a recent study the most common mutations in

KRAS (G12C, G12D, G12V) were shown to each display different sensitivities to various drugs used in NSCLC treatment (Garassino et al., 2011). Therefore when comparing the KRAS G12D mouse model to the LLC mouse model (harboring the G12C mutation), one might expect differences simply on the basis of the KRAS mutation. In addition, it is very possible that other mutations are present (such as p53 or EGFR – which are also commonly mutant in lung cancer – see section 1.1.1) in LLC.

LLC cells were tested for their ability to proliferate in response to a panel of cytokines at increasing concentrations (figure 22A). The effect of TGF-β was expected as it is a known inhibitor of cellular proliferation (Moses, 1992); IL-1β has been shown to induce proliferation in human airway epithelium (Murlas et al., 1997), while IFN-γ has been shown to decrease proliferation of human bronchial epithelial cells (Takami et al., 2002). It is likely that some of these effects on LLC proliferation with these cytokines (IL-13 and IL-1β) are unique to the cell type.

In addition to LLC proliferation, these cells were assayed for their ability to secrete IL-6, OSM, MCP-1 and KC (figure 22B). OSM is a known inducer of KC at least in mouse cardiac fibroblasts (Lafontant et al., 2006) and TNF-α can induce KC in lung derived Clara cells (Elizur et al., 2008) but what is interesting is the marked increase in KC after IL-1β stimulation (nearly 5000-fold as seen with the lowest concentration of 0.2 ng/ml). There are published reports indicating IL-1β is capable of inducing KC production in the lung (Lappalainen et al., 2005).

This may provide the LLC cells with a proliferative advantage in an IL-1β containing environment, since KC is involved in promoting inflammation and angiogenesis (Smith et al., 1994; Yuan et al., 2000). MCP-1 is secreted basally by LLC cells and this is consistent with the behavior of other tumor types (Vicari and Caux, 2002) while OSM, IL-6, TNF-α, IL-1β, and IFN-γ all increased production in LLC cells but was most marked with TNF-α and IL-1β (5-10 fold, see figure 22C) stimulation. TNF-α (Murao et al., 2000) and IL-1β (Parry et al., 1998) are both known inducers of MCP-1 at least in endothelial cells.

LLC cells along with $5x10^7$ pfu of AdIL-6 or AdOSM were then intubated into wildtype C57Bl/6 mice for a period of 1 week. This experiment was completed twice and the results are shown in figure 23. In the first experiment both AdIL-6 and AdOSM resulted in increases in tumor burden, however in the second experiment only AdOSM appeared to have an effect. The reason behind this is not clear although the results from the first experiment are in line with what has been published in terms of IL-6 promoting inflammation and this supporting tumor development (Trikha et al. 2003, Ancrile et al. 2007). Importantly, for the first time it was shown that AdOSM resulted in increased lung tumor burden (that were large in size) which may be attributed to a number of factors discussed in the next section.

4.5 The contribution of IL-6/OSM in promotion of lung tumor development

In the LLC mouse model for lung cancer, IL-6/OSM appeared to have the effect of increasing tumor burden. Increases in proliferation of LLC are not accomplished through IL-6 or OSM stimulation *in vitro* (figure 22A) yet figure 23 clearly shows the ability of these cytokines to induce increases in tumor burden. This then implies that IL-6/OSM mediated proliferative effects on LLC cells through an indirect mechanism which likely involves other cell types. Total cells in the BAL of animals treated with LLC and AdIL-6/AdOSM were counted and no increases in total cell number were observed (4.1×10^6, 3.3×10^6, 4.5×10^6 cells/ml for LLC/AdDl70, LLC/AdIL-6, and LLC/AdOSM respectively as shown in section 3.3.3) despite increases in tumor load. This suggests that inflammatory cell accumulation (as detected in the BAL fluid) was not associated with tumor development in the LLC model. However, it is possible that inflammatory cells were recruited at an earlier time and levels of these cells decreased around 7 days. Alternatively, inflammatory cells may be held within the tumor itself in such a way that the BAL procedure is insufficient for cell collection. To confirm the lack of inflammatory cell (macrophage/neutrophil) infiltrate, immunohistochemistry of histological samples could be performed to specifically stain inflammatory cell types. Nonetheless, there are several possible scenarios in which IL-6/OSM may promote tumor development in the LLC mouse models for lung cancer which may also be extended to the KRAS G12D mouse model.

LLC cells could be directly or indirectly stimulated by IL-6/OSM to induce secretion of factors that may be involved in promoting tumor development. As is shown in figure 22B, OSM was able to induce substantial KC production by the LLC cell line (between 50-200 pg/ml using 2-20 ng/ml OSM) as well as modest increases in MCP-1 (which is also seen when stimulating LLC cells with IL-6 – see figure 22B). KC (Smith et al., 1994; Yuan et al., 2000) and MCP-1 (Arenberg et al., 2000, Vicari and Caux, 2002) are both known to potentiate tumor development by promoting inflammation as well as angiogenesis in the case of KC (Yuan et al., 2000). Curiously, no increases in total cell number or macrophage/neutrophil number were detected in the BAL of these animals (data not shown). This may be due to differences in *in vitro* and *in vivo* conditions that alter cytokine secretion levels such that LLC cells *in vivo* do not produce sufficient MCP-1 or KC to be measured in the BAL fluid. In addition, in various gastric carcinoma cell lines, it has been shown that IL-6 can directly induce VEGF secretion in a dose-dependent manner (Huang et al., 2004) and in another study involving a prostate cancer cell line, both IL-6 and OSM were shown to induce VEGF (Weiss et al., 2011). This data suggests that both IL-6 and OSM are capable of stimulating tumor cells to produce the pro-angiogenic VEGF, and provides rationale for assessment of VEGF levels in future experiments in the LLC or KRAS G12D systems examined here.

In other possible mechanisms, tumor development may be promoted through the secretion of stromal cell (those cells not recruited to the tumor site) derived factors induced by IL-6/OSM. OSM has been shown to act on cardiac fibroblasts to produce KC (Lafontant et al., 2005), MCP-1 in human synovial fibroblasts (Langdon et al., 1997), and VEGF in human airway smooth muscle cells (Faffe et al., 2004). Importantly, these mentioned cell types (fibroblasts, endothelial cells, smooth muscle cells) that make up the tumor stroma may also be important in establishing a beneficial environment for the tumor. Significantly, it has been shown that OSM is capable of promoting angiogenesis indirectly through inducing VEGF expression in endothelial cells (Vasse et al., 1999, Queen et al., 2005). In addition, fibroblasts obtained from breast, lung and bone metastases (derived from breast cancer) were shown to secrete IL-6 and implantation of IL-6 secreting fibroblasts and the MCF-7 breast cancer cell line allowed for tumor growth which was dependent on IL-6 (Studebaker et al., 2008). In fact cancer associated fibroblasts (CAFs) have earned a reputation similar to the tumor associated macrophage (TAMs) due to their recognized role in tumor development (reviewed in Cirri and Chiarugi 2011). Thus various non-tumor cell types, altered by inflammation, may be involved in promoting tumor development.

Other pro-inflammatory cytokines have also been implicated in tumor development. IL-1β and TNF-α are known to be involved in promoting cancer

(reviewed in Lewis et al., 2006 and Balkwill, 2006) particularly in their ability to enhance inflammation and angiogenesis. OSM has also been shown to promote VEGF release by human airway smooth muscle cells, which is increased synergistically by IL-1β (Faffe et al., 2004). Moreover, matrix metalloproteases (MMPs) are another key factor in tumor development, believed to be involved in promoting invasiveness of tumors towards metastasis and to assist in permitting angiogenesis by tissue remodeling (Rundhaug 2003). IL-6 was shown to upregulate MMP-2 and -9 as well as TIMP-1 in malignant non-Hodgkin's lymphoma (Kossakowska et al., 1999) and it is known that OSM can regulate MMP-1, -3 and -9 as well as TIMP-1 (Tanaka and Miyajima, 2003). Thus there may be multiple cell types and molecular mechanisms involved in promoting tumor development.

In order to further explore the role of IL-6/OSM in their ability to promote tumor development in these animal models, a series of experiments can be conducted. The possibility of OSM or IL-6 induced VEGF production is an attractive idea since it may result in increased blood flow to the tumor, thus providing adequate nutrients allowing for hastened tumor development accounting for the observed large tumor sizes (in the LLC/AdOSM co-treatments). To support this claim experiments that measure VEGF levels in the BAL by ELSIA could be performed. Additionally, immunohistochemistry or immunofluoresence assessing VEGF or endothelial marker expression in

histological samples may further provide evidence for angiogenesis. To detect the involvement of other tumor associated cell components, assessment of various cellular markers (fibroblast, macrophage, neutrophil, smooth muscle cells) or levels of selective cytokines may reveal accumulations in the tumor mass.

Figure 24: Comparison of CT scanning and histological quantification.

KRAS G12D mice were treated with increasing amounts of AdCre for a period of 6 weeks. CT scans were performed at week 0, 2, 4 and 6 and lung labels were generated and density changes were quantified by summing the voxel values between -200 → +200 HU. Half of the animals were sacrificed for histology at week 4 while the remaining were sacrificed at week 6.

A) Results of summing lung label histograms (from CT scan data) between -200 → +200 HU. Expressed as % of the total lung volume. Adapted from figure 11.
B) Results of threshold analysis using ImageJ whereby the area of high densities was measured and related to the total lung area. Adapted from figure 13.

Figure 24

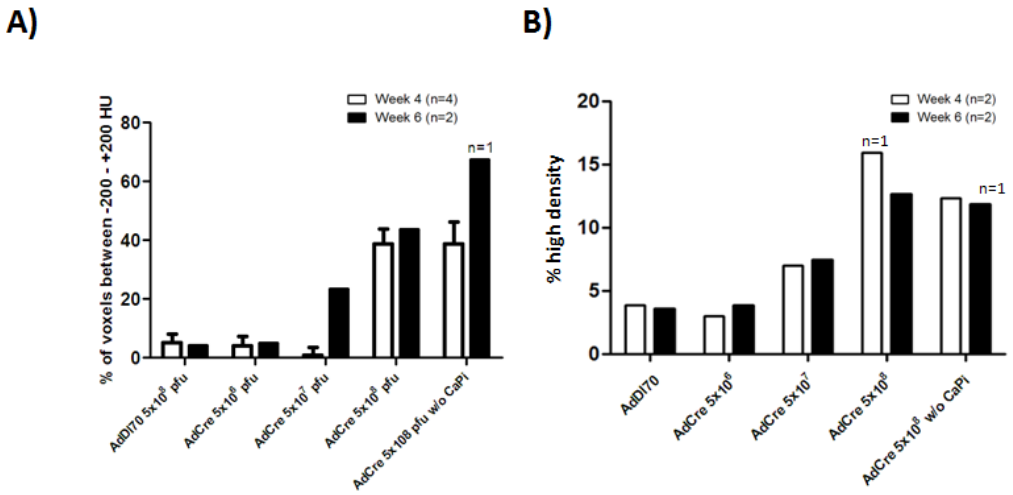
A)
B)
Week 4 (n=4)
Week 6 (n=2)
% of voxels between -200 - +200 HU
n=1
AdDl70 5x10⁸ pfu
AdCre 5x10⁸ pfu
AdCre 5x10⁷ pfu
AdCre 5x10⁸ pfu
AdCre 5x10⁸ pfu w/o CaPi
Week 4 (n=2)
Week 6 (n=2)
% high density
n=1
n=1
AdDl70
AdCre 5x10⁸
AdCre 5x10⁷
AdCre 5x10⁸
AdCre 5x10⁸ w/o CaPi

Chapter 5: Conclusions

In this study, two separate methods of quantification of AdCre-mediated increases in lung density were utilized. Through use of CT scans and analysis using AMIRA software, these increases in density could be quantified over the -200 → +200 HU range (density corresponding to cells/tissue and inflammation). This represents a novel means for the quantification of AdCre-mediated effects in the lung in this model. Furthermore, analysis allowed visualization of specific lung density rangesand a novel way to monitor individual animals over the time course of the model. Thus CT scanning technology represents an attractive means toward monitoring and exploring tumor development in mouse models for lung cancer. However, CT scan density ranges were not able to differentiate inflammation and epithelial hyperplasia or tumor development in the time frame examined and required histological assessment for more specific monitoring.

The mouse models used in this study represent attractive means towards understanding lung tumor development. The KRAS G12D mouse model was shown to develop increases in lung density dependent on the dose of AdCre administered as well as the time since administration and this could be followed by CT scanning and histology. Co-administration of AdCre and AdOSM (but not AdIL-6) showed a trend of increased tumor burden compared to co-administration of AdDl70 treatment controls, however this was not statistically significant. Further experiments are required in order to extend these results. To complement these studies, a separate model involving endotracheal administration of lewis lung carcinoma (LLC) cells was developed. This model had not been previously

well developed nor used to assess affects of cytokines or inflammation in the lung. In this thesis, it was shown that overexpression of IL-6 or OSM (using adenovirus vectors) were capable of promoting tumor development as evidenced by increases in total tumor number and size. These data appear to be the first to indicate that IL-6 or OSM may promote lung tumor development in animal models. Suggesting these molecules may represent attractive targets for therapeutic intervention. Additional experiments are needed to explore how gp130 cytokines IL-6 and OSM potentiate tumor development. Mechanisms involving IL-6 or OSM in directly or indirectly (through stromal cell partners) stimulating tumor cells to produce factors that promote tumor development (VEGF, IL-1β, TNF-α, MMPs) in ways involving angiogenesis or invasivenesss are possible. Furthermore, analysis of human lung adenocarcinoma samples for levels of OSM and IL-6 may also provide data that supports the proposal that these molecules are associated with the development of lung cancer.

Chapter 6: References

Alonzi, T., E. Fattori, D. Lazzaro, P. Costa, L. Probert, G. Kollias, F. De Benedetti, V. Poli, and G. Ciliberto. 1998. "Interleukin 6 is Required for the Development of Collagen-Induced Arthritis." The Journal of Experimental Medicine 187 (4): 461-468.

Amit, S. and Y. Ben-Neriah. 2003. "NF-kappaB Activation in Cancer: A Challenge for Ubiquitination- and Proteasome-Based Therapeutic Approach." Seminars in Cancer Biology 13 (1): 15-28.

Ancrile, B., K. H. Lim, and C. M. Counter. 2007. Oncogenic RAS-induced secretion of IL6 is required for tumorigenesis. Genes & Development 21 (14) (Jul 15): 1714-9.

Anton, M., and F. L. Graham. 1995. Site-specific recombination mediated by an adenovirus vector expressing the cre recombinase protein: A molecular switch for control of gene expression. Journal of Virology 69 (8) (Aug): 4600-6.

Arenberg, D. A., M. P. Keane, B. DiGiovine, S. L. Kunkel, S. R. Strom, M. D. Burdick, M. D. Iannettoni, and R. M. Strieter. 2000. Macrophage infiltration in human non-small-cell lung cancer: The role of CC chemokines. Cancer Immunology, Immunotherapy : CII 49 (2) (May): 63-70.

Asselin-Paturel, C., H. Echchakir, G. Carayol, F. Gay, P. Opolon, D. Grunenwald, S. Chouaib, and F. Mami-Chouaib. 1998. Quantitative analysis of Th1, Th2 and TGF-beta1 cytokine expression in tumor, TIL and PBL of non-small cell lung cancer patients. International Journal of Cancer.Journal International Du Cancer 77 (1) (Jul 3): 7-12.

Atsumi, T., K. Ishihara, D. Kamimura, H. Ikushima, T. Ohtani, S. Hirota, H. Kobayashi, et al. 2002. "A Point Mutation of Tyr-759 in Interleukin 6 Family Cytokine Receptor Subunit gp130 Causes Autoimmune Arthritis." The Journal of Experimental Medicine 196 (7): 979-990.

Balkwill, F. 2009. Tumour necrosis factor and cancer. Nature Reviews.Cancer 9 (5) (May): 361-71.

Ballin, M., D. E. Gomez, C. C. Sinha, and U. P. Thorgeirsson. 1988. RAS oncogene mediated induction of a 92 kDa metalloproteinase; strong correlation with the malignant phenotype. Biochemical and Biophysical Research Communications 154 (3) (Aug 15): 832-8.

Bamber, B., R. A. Reife, H. S. Haugen, and C. H. Clegg. 1998. "Oncostatin M Stimulates Excessive Extracellular Matrix Accumulation in a Transgenic

Mouse Model of Connective Tissue Disease." Journal of Molecular Medicine (Berlin, Germany) 76 (1): 61-69.

Barkett, M. and T. D. Gilmore. 1999. "Control of Apoptosis by Rel/NF-kappaB Transcription Factors." Oncogene 18 (49): 6910-6924. doi:10.1038/sj.onc.1203238.

Basseres, D. S., A. Ebbs, E. Levantini, and A. S. Baldwin. 2010. "Requirement of the NF-kappaB Subunit p65/RelA for K-Ras-Induced Lung Tumorigenesis." Cancer Research 70 (9): 3537-3546. doi:10.1158/0008-5472.CAN-09-4290.

Becker, C., M. C. Fantini, C. Schramm, H. A. Lehr, S. Wirtz, A. Nikolaev, J. Burg, et al. 2004. "TGF-Beta Suppresses Tumor Progression in Colon Cancer by Inhibition of IL-6 Trans-Signaling." Immunity21 (4): 491-501. doi:10.1016/j.immuni.2004.07.020.

Bollrath, J., T. J. Phesse, V. A. von Burstin, T. Putoczki, M. Bennecke, T. Bateman, T. Nebelsiek, et al. 2009. "Gp130-Mediated Stat3 Activation in Enterocytes Regulates Cell Survival and Cell-Cycle Progression during Colitis-Associated Tumorigenesis." Cancer Cell 15 (2): 91-102. doi:10.1016/j.ccr.2009.01.002.

Brambilla, E. and A. Gazdar. 2009. "Pathogenesis of Lung Cancer Signalling Pathways: Roadmap for Therapies." The European Respiratory Journal : Official Journal of the European Society for Clinical Respiratory Physiology 33 (6): 1485-1497. doi:10.1183/09031936.00014009.

Broers, J. L., F. C. Ramaekers, M. K. Rot, T. Oostendorp, A. Huysmans, G. N. van Muijen, S. S. Wagenaar, and G. P. Vooijs. 1988. "Cytokeratins in Different Types of Human Lung Cancer as Monitored by Chain-Specific Monoclonal Antibodies." Cancer Research 48 (11): 3221-3229.

Bromberg, J. F., M. H. Wrzeszczynska, G. Devgan, Y. Zhao, R. G. Pestell, C. Albanese, and J. E. Darnell Jr. 1999. "Stat3 as an Oncogene." Cell 98 (3): 295-303.

Bryant, A., & Cerfolio, R. J. 2007. Differences in epidemiology, histology, and survival between cigarette smokers and never-smokers who develop non-small cell lung cancer. Chest, 132(1), 185-192.

Catlett-Falcone, R., T. H. Landowski, M. M. Oshiro, J. Turkson, A. Levitzki, R. Savino, G. Ciliberto, et al. 1999. "Constitutive Activation of Stat3

Signaling Confers Resistance to Apoptosis in Human U266 Myeloma Cells." Immunity 10 (1): 105-115.

Cawston, T. E., V. A. Curry, C. A. Summers, I. M. Clark, G. P. Riley, P. F. Life, J. R. Spaull, et al. 1998. "The Role of Oncostatin M in Animal and Human Connective Tissue Collagen Turnover and its Localization within the Rheumatoid Joint." Arthritis and Rheumatism 41 (10): 1760-1771. doi:2-M.

Chen, D., C. Y. Chu, C. Y. Chen, H. C. Yang, Y. Y. Chiang, T. Y. Lin, I. P. Chiang, D. Y. Chuang, C. C. Yu, and K. C. Chow. 2008. "Expression of Short-Form Oncostatin M Receptor as a Decoy Receptor in Lung Adenocarcinomas." The Journal of Pathology 215 (3): 290-299. doi:10.1002/path.2361.

Chen, L. F., Y. Mu, and W. C. Greene. 2002. "Acetylation of RelA at Discrete Sites Regulates Distinct Nuclear Functions of NF-kappaB." The EMBO Journal 21 (23): 6539-6548.

Chen, Lf, W. Fischle, E. Verdin, and W. C. Greene. 2001. "Duration of Nuclear NF-kappaB Action Regulated by Reversible Acetylation." Science (New York, N.Y.) 293 (5535): 1653-1657. doi:10.1126/science.1062374.

Cirri, P. and P. Chiarugi. 2011. "Cancer Associated Fibroblasts: The Dark Side of the Coin." *American Journal of Cancer Research* 1 (4): 482-497.

Coussens, L. M., C. L. Tinkle, D. Hanahan, and Z. Werb. 2000. MMP-9 supplied by bone marrow-derived cells contributes to skin carcinogenesis. Cell 103 (3) (Oct 27): 481-90.

Coussens, L. M., and Z. Werb. 2002. Inflammation and cancer. Nature 420 (6917) (Dec 19-26): 860-7.

Dahmen, H., U. Horsten, A. Kuster, Y. Jacques, S. Minvielle, I. M. Kerr, G. Ciliberto, G. Paonessa, P. C. Heinrich, and G. Muller-Newen. 1998. "Activation of the Signal Transducer gp130 by Interleukin-11 and Interleukin-6 is Mediated by Similar Molecular Interactions." The Biochemical Journal 331 (Pt 3) (Pt 3): 695-702.

DiCosmo, B. F., G. P. Geba, D. Picarella, J. A. Elias, J. A. Rankin, B. R. Stripp, J. A. Whitsett, and R. A. Flavell. 1994. "Airway Epithelial Cell Expression of Interleukin-6 in Transgenic Mice. Uncoupling of Airway Inflammation

and Bronchial Hyperreactivity." The Journal of Clinical Investigation 94 (5): 2028-2035. doi:10.1172/JCI117556.

Downward, J. 1997. Cell cycle: Routine role for RAS. Current Biology : CB 7 (4) (Apr 1): R258-60.

DuPage, M., A. L. Dooley, and T. Jacks. 2009. Conditional mouse lung cancer models using adenoviral or lentiviral delivery of cre recombinase. Nature Protocols 4 (7): 1064-72.

Elizur, A., T. L. Adair-Kirk, D. G. Kelley, G. L. Griffin, D. E. Demello, and R. M. Senior. 2008. "Tumor Necrosis Factor-Alpha from Macrophages Enhances LPS-Induced Clara Cell Expression of Keratinocyte-Derived Chemokine." *American Journal of Respiratory Cell and Molecular Biology* 38 (1): 8-15. doi:10.1165/rcmb.2007-0203OC.

Erez, N., M. Truitt, P. Olson, S. T. Arron, and D. Hanahan. 2010. "Cancer-Associated Fibroblasts are Activated in Incipient Neoplasia to Orchestrate Tumor-Promoting Inflammation in an NF-kappaB-Dependent Manner." *Cancer Cell* 17 (2): 135-147. doi:10.1016/j.ccr.2009.12.041.

Ernst, M., M. Inglese, P. Waring, I. K. Campbell, S. Bao, F. J. Clay, W. S. Alexander, et al. 2001. "Defective gp130-Mediated Signal Transducer and Activator of Transcription (STAT) Signaling Results in Degenerative Joint Disease, Gastrointestinal Ulceration, and Failure of Uterine Implantation." The Journal of Experimental Medicine 194 (2): 189-203.

Ernst, M., M. Najdovska, D. Grail, T. Lundgren-May, M. Buchert, H. Tye, V. B. Matthews, et al. 2008. "STAT3 and STAT1 Mediate IL-11-Dependent and Inflammation-Associated Gastric Tumorigenesis in gp130 Receptor Mutant Mice." The Journal of Clinical Investigation 118 (5): 1727-1738. doi:10.1172/JCI34944.

Faffe, D. S., L. Flynt, M. Mellema, P. E. Moore, E. S. Silverman, V. Subramaniam, M. R. Jones, et al. 2005. Oncostatin M causes eotaxin-1 release from airway smooth muscle: Synergy with IL-4 and IL-13. The Journal of Allergy and Clinical Immunology 115 (3) (Mar): 514-20.

Faffe, D. S., L. Flynt, M. Mellema, T. R. Whitehead, K. Bourgeois, R. A. Panettieri Jr, E. S. Silverman, and S. A. Shore. 2005. "Oncostatin M Causes VEGF Release from Human Airway Smooth Muscle: Synergy with IL-1beta." *American Journal of Physiology.Lung Cellular and Molecular Physiology* 288 (6): L1040-8. doi:10.1152/ajplung.00333.2004.

Fasbender A, Lee JH, Walters RW, Moninger TO, Zabner J, Welsh MJ. Incorporation of adenovirus in calcium phosphate precipitates enhances gene transfer to airway epithelia in vitro and in vivo. J Clin Invest. 1998 Jul 1;102(1):184-93.

Fritz, D. K., C. Kerr, R. Fattouh, A. Llop-Guevara, W. I. Khan, M. Jordana, and C. D. Richards. 2011. "A Mouse Model of Airway Disease: Oncostatin M-Induced Pulmonary Eosinophilia, Goblet Cell Hyperplasia, and Airway Hyperresponsiveness are STAT6 Dependent, and Interstitial Pulmonary Fibrosis is STAT6 Independent." Journal of Immunology (Baltimore, Md.: 1950) 186 (2): 1107-1118. doi:10.4049/jimmunol.0903476.

Gao, S. P., K. G. Mark, K. Leslie, W. Pao, N. Motoi, W. L. Gerald, W. D. Travis, et al. 2007. Mutations in the EGFR kinase domain mediate STAT3 activation via IL-6 production in human lung adenocarcinomas. The Journal of Clinical Investigation 117 (12) (Dec): 3846-56.

Garassino, M. C., M. Marabese, P. Rusconi, E. Rulli, O. Martelli, G. Farina, A. Scanni, and M. Broggini. 2011. "Different Types of K-Ras Mutations could Affect Drug Sensitivity and Tumour Behaviour in Non-Small-Cell Lung Cancer." *Annals of Oncology : Official Journal of the European Society for Medical Oncology / ESMO* 22 (1): 235-237. doi:10.1093/annonc/mdq680.

Gauldie, J., C. Richards, D. Harnish, P. Lansdorp, and H. Baumann. 1987. "Interferon Beta 2/B-Cell Stimulatory Factor Type 2 Shares Identity with Monocyte-Derived Hepatocyte-Stimulating Factor and Regulates the Major Acute Phase Protein Response in Liver Cells." Proceedings of the National Academy of Sciences of the United States of America 84 (20): 7251-7255.

Gerhartz, C., B. Heesel, J. Sasse, U. Hemmann, C. Landgraf, J. Schneider-Mergener, F. Horn, P. C. Heinrich, and L. Graeve. 1996. "Differential Activation of Acute Phase Response factor/STAT3 and STAT1 Via the Cytoplasmic Domain of the Interleukin 6 Signal Transducer gp130. I. Definition of a Novel Phosphotyrosine Motif Mediating STAT1 Activation." The Journal of Biological Chemistry 271 (22): 12991-12998.

Greten, F. R., L. Eckmann, T. F. Greten, J. M. Park, Z. W. Li, L. J. Egan, M. F. Kagnoff, and M. Karin. 2004. "IKKbeta Links Inflammation and Tumorigenesis in a Mouse Model of Colitis-Associated Cancer." Cell 118 (3): 285-296. doi:10.1016/j.cell.2004.07.013.

Grivennikov, S., E. Karin, J. Terzic, D. Mucida, G. Y. Yu, S. Vallabhapurapu, J. Scheller, et al. 2009. "IL-6 and Stat3 are Required for Survival of Intestinal Epithelial Cells and Development of Colitis-Associated Cancer." Cancer Cell 15 (2): 103-113. doi:10.1016/j.ccr.2009.01.001.

Grivennikov, S. I., F. R. Greten, and M. Karin. 2010. Immunity, inflammation, and cancer. Cell 140 (6) (Mar 19): 883-99.

Guerra, C., A. J. Schuhmacher, M. Canamero, P. J. Grippo, L. Verdaguer, L. Perez-Gallego, P. Dubus, E. P. Sandgren, and M. Barbacid. 2007. Chronic pancreatitis is essential for induction of pancreatic ductal adenocarcinoma by KRAS oncogenes in adult mice. Cancer Cell 11 (3) (Mar): 291-302.

Guo, Y., F. Xu, T. Lu, Z. Duan, and Z. Zhang. 2012. "Interleukin-6 Signaling Pathway in Targeted Therapy for Cancer." Cancer Treatment Reviews. doi:10.1016/j.ctrv.2012.04.007.

Heinrich, P. C., I. Behrmann, S. Haan, H. M. Hermanns, G. Muller-Newen, and F. Schaper. 2003. "Principles of Interleukin (IL)-6-Type Cytokine Signalling and its Regulation." The Biochemical Journal374 (Pt 1): 1-20. doi:10.1042/BJ20030407.

Herbst, R. S., J. V. Heymach, and S. M. Lippman. 2008. Lung cancer. The New England Journal of Medicine 359 (13) (Sep 25): 1367-80.

Huang, M., J. Wang, P. Lee, S. Sharma, J. T. Mao, H. Meissner, K. Uyemura, R. Modlin, J. Wollman, and S. M. Dubinett. 1995. Human non-small cell lung cancer cells express a type 2 cytokine pattern. Cancer Research 55 (17) (Sep 1): 3847-53.

Huang, S. P., M. S. Wu, C. T. Shun, H. P. Wang, M. T. Lin, M. L. Kuo, and J. T. Lin. 2004. "Interleukin-6 Increases Vascular Endothelial Growth Factor and Angiogenesis in Gastric Carcinoma." *Journal of Biomedical Science* 11 (4): 517-527. doi:10.1159/000077902.

Ito, H., M. Takazoe, Y. Fukuda, T. Hibi, K. Kusugami, A. Andoh, T. Matsumoto, et al. 2004. "A Pilot Randomized Trial of a Human Anti-Interleukin-6 Receptor Monoclonal Antibody in Active Crohn's Disease." Gastroenterology 126 (4): 989-96; discussion 947.

Jackson EL, Willis N, Mercer K, Bronson RT, Crowley D, Montoya R, et al. Analysis of lung tumor initiation and progression using conditional expression of oncogenic KRAS. Genes Dev. 2001 Dec 15;15(24):3243-8.

Jackson, E. L., K. P. Olive, D. A. Tuveson, R. Bronson, D. Crowley, M. Brown, and T. Jacks. 2005. The differential effects of mutant p53 alleles on advanced murine lung cancer. Cancer Research 65 (22) (Nov 15): 10280-8.

Janakiraman, M., E. Vakiani, Z. Zeng, C. A. Pratilas, B. S. Taylor, D. Chitale, E. Halilovic, et al. 2010. "Genomic and Biological Characterization of Exon 4 KRAS Mutations in Human Cancer." *Cancer Research* 70 (14): 5901-5911. doi:10.1158/0008-5472.CAN-10-0192.

Jemal, A., R. Siegel, E. Ward, Y. Hao, J. Xu, and M. J. Thun. 2009. Cancer statistics, 2009. CA: A Cancer Journal for Clinicians 59 (4) (Jul-Aug): 225-49.

Ji, H., A. M. Houghton, T. J. Mariani, S. Perera, C. B. Kim, R. Padera, G. Tonon, et al. 2006. KRAS activation generates an inflammatory response in lung tumors. Oncogene 25 (14) (Mar 30): 2105-12.

Jiang, R., Z. Jin, Z. Liu, L. Sun, L. Wang, and K. Li. 2011. "Correlation of Activated STAT3 Expression with Clinicopathologic Features in Lung Adenocarcinoma and Squamous Cell Carcinoma." Molecular Diagnosis & Therapy 15 (6): 347-352. doi:10.2165/11599190-000000000-00000; 10.2165/11599190-000000000-00000.

Johnson, L., K. Mercer, D. Greenbaum, R. T. Bronson, D. Crowley, D. A. Tuveson, and T. Jacks. 2001. Somatic activation of the KRAS oncogene causes early onset lung cancer in mice. Nature 410 (6832) (Apr 26): 1111-6.

Jostock, T., J. Mullberg, S. Ozbek, R. Atreya, G. Blinn, N. Voltz, M. Fischer, M. F. Neurath, and S. Rose-John. 2001. "Soluble gp130 is the Natural Inhibitor of Soluble Interleukin-6 Receptor Transsignaling Responses." European Journal of Biochemistry / FEBS 268 (1): 160-167.

Kalluri, R. and M. Zeisberg. 2006. "Fibroblasts in Cancer." *Nature Reviews.Cancer* 6 (5): 392-401. doi:10.1038/nrc1877.

Kapina, M. A., G. S. Shepelkova, V. G. Avdeenko, A. N. Guseva, T. K. Kondratieva, V. V. Evstifeev, and A. S. Apt. 2011. "Interleukin-11 Drives Early Lung Inflammation during Mycobacterium Tuberculosis Infection in Genetically Susceptible Mice." PloS One 6 (7): e21878. doi:10.1371/journal.pone.0021878.

Karin, M., Y. Cao, F. R. Greten, and Z. W. Li. 2002. "NF-kappaB in Cancer: From Innocent Bystander to Major Culprit." Nature Reviews.Cancer 2 (4): 301-310. doi:10.1038/nrc780.

Kimura, A. and T. Kishimoto. 2010. "IL-6: Regulator of Treg/Th17 Balance." European Journal of Immunology 40 (7): 1830-1835. doi:10.1002/eji.201040391.

Kirsch, D. G., D. M. Dinulescu, J. B. Miller, J. Grimm, P. M. Santiago, N. P. Young, G. P. Nielsen, et al. 2007. "A Spatially and Temporally Restricted Mouse Model of Soft Tissue Sarcoma." Nature Medicine13 (8): 992-997. doi:10.1038/nm1602.

Kontakiotis T, Katsoulis K, Hagizisi O, Kougioulis M, Gerou S, Papakosta D. Bronchoalveolar lavage fluid alteration in antioxidant and inflammatory status in lung cancer patients. Eur J Intern Med. 2011 Oct;22(5):522-6.

Kopf, M., H. Baumann, G. Freer, M. Freudenberg, M. Lamers, T. Kishimoto, R. Zinkernagel, H. Bluethmann, and G. Kohler. 1994. "Impaired Immune and Acute-Phase Responses in Interleukin-6-Deficient Mice." Nature 368 (6469): 339-342. doi:10.1038/368339a0.

Kossakowska, A. E., D. R. Edwards, C. Prusinkiewicz, M. C. Zhang, D. Guo, S. J. Urbanski, T. Grogan, L. A. Marquez, and A. Janowska-Wieczorek. 1999. "Interleukin-6 Regulation of Matrix Metalloproteinase (MMP-2 and MMP-9) and Tissue Inhibitor of Metalloproteinase (TIMP-1) Expression in Malignant Non-Hodgkin's Lymphomas." *Blood* 94 (6): 2080-2089.

Kuhn, C.,3rd, R. J. Homer, Z. Zhu, N. Ward, R. A. Flavell, G. P. Geba, and J. A. Elias. 2000. "Airway Hyperresponsiveness and Airway Obstruction in Transgenic Mice. Morphologic Correlates in Mice Overexpressing Interleukin (IL)-11 and IL-6 in the Lung." American Journal of Respiratory Cell and Molecular Biology 22 (3): 289-295.

Kunz-Schughart, L. A. and R. Knuechel. 2002. "Tumor-Associated Fibroblasts (Part I): Active Stromal Participants in Tumor Development and Progression?" *Histology and Histopathology* 17 (2): 599-621.

Lafontant, P. J., A. R. Burns, E. Donnachie, S. B. Haudek, C. W. Smith, and M. L. Entman. 2006. "Oncostatin M Differentially Regulates CXC Chemokines in Mouse Cardiac Fibroblasts." *American Journal of Physiology.Cell Physiology* 291 (1): C18-26. doi:10.1152/ajpcell.00322.2005.

Langdon, C., C. Kerr, M. Hassen, T. Hara, A. L. Arsenault, and C. D. Richards. 2000. "Murine Oncostatin M Stimulates Mouse Synovial Fibroblasts in Vitro and Induces Inflammation and Destruction in Mouse Joints in Vivo." The American Journal of Pathology 157 (4): 1187-1196. doi:10.1016/S0002-9440(10)64634-2.

Langdon, C., C. Kerr, L. Tong, and C. D. Richards. 2003. "Oncostatin M Regulates Eotaxin Expression in Fibroblasts and Eosinophilic Inflammation in C57BL/6 Mice." Journal of Immunology (Baltimore, Md.: 1950) 170 (1): 548-555.

Langdon, C., J. Leith, F. Smith, and C. D. Richards. 1997. "Oncostatin M Stimulates Monocyte Chemoattractant Protein-1- and Interleukin-1-Induced Matrix Metalloproteinase-1 Production by Human Synovial Fibroblasts in Vitro." *Arthritis and Rheumatism* 40 (12): 2139-2146. doi:2-L.

Lappalainen, U., J. A. Whitsett, S. E. Wert, J. W. Tichelaar, and K. Bry. 2005. "Interleukin-1beta Causes Pulmonary Inflammation, Emphysema, and Airway Remodeling in the Adult Murine Lung."*American Journal of Respiratory Cell and Molecular Biology* 32 (4): 311-318. doi:10.1165/rcmb.2004-0309OC.

Lee, H., A. Herrmann, J. H. Deng, M. Kujawski, G. Niu, Z. Li, S. Forman, R. Jove, D. M. Pardoll, and H. Yu. 2009. "Persistently Activated Stat3 Maintains Constitutive NF-kappaB Activity in Tumors."Cancer Cell 15 (4): 283-293. doi:10.1016/j.ccr.2009.02.015.

Lewis, A. M., S. Varghese, H. Xu, and H. R. Alexander. 2006. "Interleukin-1 and Cancer Progression: The Emerging Role of Interleukin-1 Receptor Antagonist as a Novel Therapeutic Agent in Cancer Treatment." *Journal of Translational Medicine* 4: 48. doi:10.1186/1479-5876-4-48.

Lesina, M., M. U. Kurkowski, K. Ludes, S. Rose-John, M. Treiber, G. Kloppel, A. Yoshimura, et al. 2011. "Stat3/Socs3 Activation by IL-6 Transsignaling Promotes Progression of Pancreatic Intraepithelial Neoplasia and Development of Pancreatic Cancer." Cancer Cell 19 (4): 456-469. doi:10.1016/j.ccr.2011.03.009.

Libermann, T. A. and D. Baltimore. 1990. "Activation of Interleukin-6 Gene Expression through the NF-Kappa B Transcription Factor." Molecular and Cellular Biology 10 (5): 2327-2334.

Lin, E. Y., J. F. Li, L. Gnatovskiy, Y. Deng, L. Zhu, D. A. Grzesik, H. Qian, X. N. Xue, and J. W. Pollard. 2006. Macrophages regulate the angiogenic switch in a mouse model of breast cancer. Cancer Research 66 (23) (Dec 1): 11238-46.

Lin, W. W., and M. Karin. 2007. A cytokine-mediated link between innate immunity, inflammation, and cancer. The Journal of Clinical Investigation 117 (5) (May): 1175-83.

Lippincott Williams & Wilkins 2010.Wood, G. W. and G. Y. Gillespie. 1975. "Studies on the Role of Macrophages in Regulation of Growth and Metastasis of Murine Chemically Induced Fibrosarcomas." International Journal of Cancer.Journal International Du Cancer 16 (6): 1022-1029.

Livak, K. J., and T. D. Schmittgen. 2001. Analysis of relative gene expression data using real-time quantitative PCR and the 2(-delta delta C(T)) method. Methods (San Diego, Calif.) 25 (4) (Dec): 402-8.

Luppi, F., A. M. Longo, W. I. de Boer, K. F. Rabe, and P. S. Hiemstra. 2007. Interleukin-8 stimulates cell proliferation in non-small cell lung cancer through epidermal growth factor receptor transactivation. Lung Cancer (Amsterdam, Netherlands) 56 (1) (Apr): 25-33.

Manfredi, B., P. Sacerdote, L. Gaspani, V. Poli, and A. E. Panerai. 1998. "IL-6 Knock-Out Mice show Modified Basal Immune Functions, but Normal Immune Responses to Stress." Brain, Behavior, and Immunity 12 (3): 201-211. doi:10.1006/brbi.1998.0525.

Mantovani, A., A. Sica, and M. Locati. 2007. New vistas on macrophage differentiation and activation. European Journal of Immunology 37 (1) (Jan): 14-6.

Mantovani, A., S. Sozzani, M. Locati, P. Allavena, and A. Sica. 2002. Macrophage polarization: Tumor-associated macrophages as a paradigm for polarized M2 mononuclear phagocytes. Trends in Immunology 23 (11) (Nov): 549-55.

Marte, B. M., and J. Downward. 1997. PKB/Akt: Connecting phosphoinositide 3-kinase to cell survival and beyond. Trends in Biochemical Sciences 22 (9) (Sep): 355-8.

Meylan, E., A. L. Dooley, D. M. Feldser, L. Shen, E. Turk, C. Ouyang, and T. Jacks. 2009. "Requirement for NF-kappaB Signalling in a Mouse Model of

Lung Adenocarcinoma." Nature 462 (7269): 104-107. doi:10.1038/nature08462.

Mizumoto, Y., S. Kyo, T. Kiyono, M. Takakura, M. Nakamura, Y. Maida, N. Mori, Y. Bono, H. Sakurai, and M. Inoue. 2011. "Activation of NF-kappaB is a Novel Target of KRAS-Induced Endometrial Carcinogenesis." Clinical Cancer Research : An Official Journal of the American Association for Cancer Research 17 (6): 1341-1350. doi:10.1158/1078-0432.CCR-10-2291.

Moses, H. and M. H. Barcellos-Hoff. 2011. "TGF-Beta Biology in Mammary Development and Breast Cancer." *Cold Spring Harbor Perspectives in Biology* 3 (1): a003277. doi:10.1101/cshperspect.a003277; 10.1101/cshperspect.a003277.

Mozaffarian, A., A. W. Brewer, E. S. Trueblood, I. G. Luzina, N. W. Todd, S. P. Atamas, and H. A. Arnett. 2008. "Mechanisms of Oncostatin M-Induced Pulmonary Inflammation and Fibrosis." Journal of Immunology (Baltimore, Md.: 1950) 181 (10): 7243-7253.

Murao, K., T. Ohyama, H. Imachi, T. Ishida, W. M. Cao, H. Namihira, M. Sato, N. C. Wong, and J. Takahara. 2000. "TNF-Alpha Stimulation of MCP-1 Expression is Mediated by the Akt/PKB Signal Transduction Pathway in Vascular Endothelial Cells." *Biochemical and Biophysical Research Communications* 276 (2): 791-796. doi:10.1006/bbrc.2000.3497.

Murlas, C. G., A. C. Sharma, A. Gulati, and F. Najmabadi. 1997. "Interleukin-1 Beta Increases Airway Epithelial Cell Mitogenesis Partly by Stimulating Endothelin-1 Production." *Lung* 175 (2): 117-126.

Naugler, W. E., and M. Karin. 2008. The wolf in sheep's clothing: The role of interleukin-6 in immunity, inflammation and cancer. Trends in Molecular Medicine 14 (3) (Mar): 109-19.

Neurath, M. F. and S. Finotto. 2011. "IL-6 Signaling in Autoimmunity, Chronic Inflammation and Inflammation-Associated Cancer." Cytokine & Growth Factor Reviews 22 (2): 83-89. doi:10.1016/j.cytogfr.2011.02.003; 10.1016/j.cytogfr.2011.02.003.

Nishibe, T., G. Parry, A. Ishida, S. Aziz, J. Murray, Y. Patel, S. Rahman, et al. 2001. "Oncostatin M Promotes Biphasic Tissue Factor Expression in Smooth Muscle Cells: Evidence for Erk-1/2 Activation."Blood 97 (3): 692-699.

Nishimoto, N., K. Yoshizaki, N. Miyasaka, K. Yamamoto, S. Kawai, T. Takeuchi, J. Hashimoto, J. Azuma, and T. Kishimoto. 2004. "Treatment of Rheumatoid Arthritis with Humanized Anti-Interleukin-6 Receptor Antibody: A Multicenter, Double-Blind, Placebo-Controlled Trial." Arthritis and Rheumatism 50 (6): 1761-1769. doi:10.1002/art.20303.

Nozawa, H., C. Chiu, and D. Hanahan. 2006. Infiltrating neutrophils mediate the initial angiogenic switch in a mouse model of multistage carcinogenesis. Proceedings of the National Academy of Sciences of the United States of America 103 (33) (Aug 15): 12493-8.

Ochoa, C. E., S. G. Mirabolfathinejad, V. A. Ruiz, S. E. Evans, M. Gagea, C. M. Evans, B. F. Dickey, and S. J. Moghaddam. 2011. Interleukin 6, but not T helper 2 cytokines, promotes lung carcinogenesis. Cancer Prevention Research (Philadelphia, Pa.) 4 (1) (Jan): 51-64.

O'Hara, K. A., M. A. Kedda, P. J. Thompson, and D. A. Knight. 2003. "Oncostatin M: An Interleukin-6-Like Cytokine Relevant to Airway Remodelling and the Pathogenesis of Asthma." Clinical and Experimental Allergy : Journal of the British Society for Allergy and Clinical Immunology 33 (8): 1026-1032.

Ohtaki, Y., G. Ishii, K. Nagai, S. Ashimine, T. Kuwata, T. Hishida, M. Nishimura, J. Yoshida, I. Takeyoshi, and A. Ochiai. 2010. Stromal macrophage expressing CD204 is associated with tumor aggressiveness in lung adenocarcinoma. Journal of Thoracic Oncology : Official Publication of the International Association for the Study of Lung Cancer 5 (10) (Oct): 1507-15.

Okada, F., J. W. Rak, B. S. Croix, B. Lieubeau, M. Kaya, L. Roncari, S. ShiRASawa, T. Sasazuki, and R. S. Kerbel. 1998. Impact of oncogenes in tumor angiogenesis: Mutant KRAS up-regulation of vascular endothelial growth factor/vascular permeability factor is necessary, but not sufficient for tumorigenicity of human colorectal carcinoma cells. Proceedings of the National Academy of Sciences of the United States of America 95 (7) (Mar 31): 3609-14.

Parry, G. C., T. Martin, K. A. Felts, and R. R. Cobb. 1998. "IL-1beta-Induced Monocyte Chemoattractant Protein-1 Gene Expression in Endothelial Cells is Blocked by Proteasome Inhibitors."*Arteriosclerosis, Thrombosis, and Vascular Biology* 18 (6): 934-940.

Pine SR, Mechanic LE, Enewold L, Chaturvedi AK, Katki HA, Zheng YL, et al. Increased levels of circulating interleukin 6, interleukin 8, C-reactive protein, and risk of lung cancer. J Natl Cancer Inst. 2011 Jul 20;103(14):1112-22.

Pollard, J. W. 2004. Tumour-educated macrophages promote tumour progression and metastasis. Nature Reviews.Cancer 4 (1) (Jan): 71-8.

Queen, M. M., R. E. Ryan, R. G. Holzer, C. R. Keller-Peck, and C. L. Jorcyk. 2005. Breast cancer cells stimulate neutrophils to produce oncostatin M: Potential implications for tumor progression. Cancer Research 65 (19) (Oct 1): 8896-904.

Rebouissou, S., M. Amessou, G. Couchy, K. Poussin, S. Imbeaud, C. Pilati, T. Izard, C. Balabaud, P. Bioulac-Sage, and J. Zucman-Rossi. 2009. "Frequent in-Frame Somatic Deletions Activate gp130 in Inflammatory Hepatocellular Tumours." Nature 457 (7226): 200-204. doi:10.1038/nature07475.

Riely, G. J., J. Marks, and W. Pao. 2009. KRAS mutations in non-small cell lung cancer. Proceedings of the American Thoracic Society 6 (2) (Apr 15): 201-5.

Rincon, M., J. Anguita, T. Nakamura, E. Fikrig, and R. A. Flavell. 1997. "Interleukin (IL)-6 Directs the Differentiation of IL-4-Producing CD4+ T Cells." The Journal of Experimental Medicine 185 (3): 461-469.

Rodenhuis, S., M. L. van de Wetering, W. J. Mooi, S. G. Evers, N. van Zandwijk, and J. L. Bos. 1987. Mutational activation of the KRAS oncogene. A possible pathogenetic factor in adenocarcinoma of the lung. The New England Journal of Medicine 317 (15) (Oct 8): 929-35.

Rundhaug, J. E. 2005. "Matrix Metalloproteinases and Angiogenesis." *Journal of Cellular and Molecular Medicine* 9 (2): 267-285.

Sambrook, J., Fritsch, E.F., Maniatis, T. 1989. Molecular Cloning: A Laboratory Manual 2nd ed. Cold Spring Harbor Laboratory Press, Cold Spring Harbor, NY.

Sander, L. E., F. Obermeier, U. Dierssen, D. C. Kroy, A. K. Singh, U. Seidler, K. L. Streetz, et al. 2008. "Gp130 Signaling Promotes Development of Acute Experimental Colitis by Facilitating Early neutrophil/macrophage Recruitment and Activation." Journal of Immunology (Baltimore, Md.: 1950) 181 (5): 3586-3594.

Savai R, Wolf JC, Greschus S, Eul BG, Schermuly RT, Hanze J, et al. Analysis of tumor vessel supply in lewis lung carcinoma in mice by fluorescent microsphere distribution and imaging with micro- and flat-panel computed tomography. Am J Pathol. 2005 Oct;167(4):937-46.

Seike, M., N. Yanaihara, E. D. Bowman, K. A. Zanetti, A. Budhu, K. Kumamoto, L. E. Mechanic, et al. 2007. Use of a cytokine gene expression signature in lung adenocarcinoma and the surrounding tissue as a prognostic classifier. Journal of the National Cancer Institute 99 (16) (Aug 15): 1257-69.

Shigematsu, H. and A. F. Gazdar. 2006. "Somatic Mutations of Epidermal Growth Factor Receptor Signaling Pathway in Lung Cancers." International Journal of Cancer.Journal International Du Cancer118 (2): 257-262. doi:10.1002/ijc.21496.

Shojaei, F., M. Singh, J. D. Thompson, and N. Ferrara. 2008. Role of Bv8 in neutrophil-dependent angiogenesis in a transgenic model of cancer progression. Proceedings of the National Academy of Sciences of the United States of America 105 (7) (Feb 19): 2640-5.

Shojaei, F., X. Wu, X. Qu, M. Kowanetz, L. Yu, M. Tan, Y. G. Meng, and N. Ferrara. 2009. G-CSF-initiated myeloid cell mobilization and angiogenesis mediate tumor refractoriness to anti-VEGF therapy in mouse models. Proceedings of the National Academy of Sciences of the United States of America 106 (16) (Apr 21): 6742-7.

Shojaei, F., X. Wu, C. Zhong, L. Yu, X. H. Liang, J. Yao, D. Blanchard, et al. 2007. Bv8 regulates myeloid-cell-dependent tumour angiogenesis. Nature 450 (7171) (Dec 6): 825-31.

Sica, A., A. Saccani, B. Bottazzi, S. Bernasconi, P. Allavena, B. Gaetano, F. Fei, et al. 2000. Defective expression of the monocyte chemotactic protein-1 receptor CCR2 in macrophages associated with human ovarian carcinoma. Journal of Immunology (Baltimore, Md.: 1950) 164 (2) (Jan 15): 733-8.

Sica, A., T. Schioppa, A. Mantovani, and P. Allavena. 2006. Tumour-associated macrophages are a distinct M2 polarised population promoting tumour progression: Potential targets of anti-cancer therapy. European Journal of Cancer (Oxford, England : 1990) 42 (6) (Apr): 717-27.

Silver, J. S. and C. A. Hunter. 2010. "Gp130 at the Nexus of Inflammation, Autoimmunity, and Cancer." Journal of Leukocyte Biology 88 (6): 1145-1156. doi:10.1189/jlb.0410217.

Singer, C. F., N. Kronsteiner, E. Marton, M. Kubista, K. J. Cullen, K. Hirtenlehner, M. Seifert, and E. Kubista. 2002. "MMP-2 and MMP-9 Expression in Breast Cancer-Derived Human Fibroblasts is Differentially Regulated by Stromal-Epithelial Interactions." *Breast Cancer Research and Treatment* 72 (1): 69-77.

Skinnider, B. F., and T. W. Mak. 2002. The role of cytokines in classical hodgkin lymphoma. Blood 99 (12) (Jun 15): 4283-97.

Smith, D. R., P. J. Polverini, S. L. Kunkel, M. B. Orringer, R. I. Whyte, M. D. Burdick, C. A. Wilke, and R. M. Strieter. 1994. Inhibition of interleukin 8 attenuates angiogenesis in bronchogenic carcinoma. The Journal of Experimental Medicine 179 (5) (May 1): 1409-15.

Sparmann, A., and D. Bar-Sagi. 2004. RAS-induced interleukin-8 expression plays a critical role in tumor growth and angiogenesis. Cancer Cell 6 (5) (Nov): 447-58.

Suematsu, S., T. Matsuda, K. Aozasa, S. Akira, N. Nakano, S. Ohno, J. Miyazaki, K. Yamamura, T. Hirano, and T. Kishimoto. 1989. "IgG1 Plasmacytosis in Interleukin 6 Transgenic Mice." Proceedings of the National Academy of Sciences of the United States of America 86 (19): 7547-7551.

Swaak, A. J., A. van Rooyen, E. Nieuwenhuis, and L. A. Aarden. 1988. "Interleukin-6 (IL-6) in Synovial Fluid and Serum of Patients with Rheumatic Diseases." Scandinavian Journal of Rheumatology 17 (6): 469-474.

Taga, T. and T. Kishimoto. 1997. "Gp130 and the Interleukin-6 Family of Cytokines." Annual Review of Immunology 15: 797-819. doi:10.1146/annurev.immunol.15.1.797.

Takami, K., N. Takuwa, H. Okazaki, M. Kobayashi, T. Ohtoshi, S. Kawasaki, M. Dohi, et al. 2002. "Interferon-Gamma Inhibits Hepatocyte Growth Factor-Stimulated Cell Proliferation of Human Bronchial Epithelial Cells: Upregulation of p27(kip1) Cyclin-Dependent Kinase Inhibitor." *American Journal of Respiratory Cell and Molecular Biology* 26 (2): 231-238.

Tanaka, M., and A. Miyajima. 2003. Oncostatin M, a multifunctional cytokine. Reviews of Physiology, Biochemistry and Pharmacology 149 : 39-52.

Teague, T. K., P. Marrack, J. W. Kappler, and A. T. Vella. 1997. "IL-6 Rescues Resting Mouse T Cells from Apoptosis." Journal of Immunology (Baltimore, Md.: 1950) 158 (12): 5791-5796.

Tlsty, T. D., and L. M. Coussens. 2006. Tumor stroma and regulation of cancer development. Annual Review of Pathology 1 : 119-50.

Trikha, M., R. Corringham, B. Klein, and J. F. Rossi. 2003. "Targeted Anti-Interleukin-6 Monoclonal Antibody Therapy for Cancer: A Review of the Rationale and Clinical Evidence." Clinical Cancer Research : An Official Journal of the American Association for Cancer Research 9 (13): 4653-4665.

Vasse, M., J. Pourtau, V. Trochon, M. Muraine, J. P. Vannier, H. Lu, J. Soria, and C. Soria. 1999. Oncostatin M induces angiogenesis in vitro and in vivo. Arteriosclerosis, Thrombosis, and Vascular Biology 19 (8) (Aug): 1835-42.

Vicari, A. P., and C. Caux. 2002. Chemokines in cancer. Cytokine & Growth Factor Reviews 13 (2) (Apr): 143-54.

Watnick, R. S., Y. N. Cheng, A. Rangarajan, T. A. Ince, and R. A. Weinberg. 2003. RAS modulates myc activity to repress thrombospondin-1 expression and increase tumor angiogenesis. Cancer Cell 3 (3) (Mar): 219-31.

Weiss, T. W., R. Simak, C. Kaun, G. Rega, H. Pfluger, G. Maurer, K. Huber, and J. Wojta. 2011. "Oncostatin M and IL-6 Induce u-PA and VEGF in Prostate Cancer Cells and Correlate in Vivo." *Anticancer Research* 31 (10): 3273-3278.

West, N. R., L. C. Murphy, and P. H. Watson. 2012. "Oncostatin M Suppresses Oestrogen Receptor-Alpha Expression and is Associated with Poor Outcome in Human Breast Cancer." Endocrine-Related Cancer 19 (2): 181-195. doi:10.1530/ERC-11-0326.

Westra, W. H. 2000. Early glandular neoplasia of the lung. Respiratory Research 1 (3): 163-9.

White, U. A. and J. M. Stephens. 2011. "The gp130 Receptor Cytokine Family: Regulators of Adipocyte Development and Function." Current Pharmaceutical Design 17 (4): 340-346.

Wiekowski1,*, Shu-Cheng Chen*, Petronio Zalamea*, Brian P. Wilburn*, David J. Kinsley*, Wanda W. Sharif*, Kristian K. Jensen*, Joseph A. Hedrick†,

Denise Manfra* and Sergio A. Lira*. 2001. Disruption of Neutrophil Migration in a Conditional Transgenic Model: Evidence for CXCR2 Desensitization In Vivo. The Journal of Immunology 167: 7102-7110.

Wislez, M., J. Fleury-Feith, N. Rabbe, J. Moreau, D. Cesari, B. Milleron, C. Mayaud, M. Antoine, P. Soler, and J. Cadranel. 2001. Tumor-derived granulocyte-macrophage colony-stimulating factor and granulocyte colony-stimulating factor prolong the survival of neutrophils infiltrating bronchoalveolar subtype pulmonary adenocarcinoma. The American Journal of Pathology 159 (4) (Oct): 1423-33.

Wislez, M., M. L. Spencer, J. G. Izzo, D. M. Juroske, K. Balhara, D. D. Cody, R. E. Price, W. N. Hittelman, I. I. Wistuba, and J. M. Kurie. 2005. Inhibition of mammalian target of rapamycin reverses alveolar epithelial neoplasia induced by oncogenic KRAS. Cancer Research 65 (8) (Apr 15): 3226-35.

Wislez, M, Cadranel, J, Kurie, JM. 2010. Principles and Practice of Lung Cancer (4th edition) Chapter 12: Lung cancer and its microenvironment.

Yamaura T, Doki Y, Murakami K, Saiki I. Model for mediastinal lymph node metastasis produced by orthotopic intrapulmonary implantation of lung cancer cells in mice. Hum Cell. 1999 Dec;12(4):197-204.

Yeh, H. H., W. W. Lai, H. H. Chen, H. S. Liu, and W. C. Su. 2006. Autocrine IL-6-induced Stat3 activation contributes to the pathogenesis of lung adenocarcinoma and malignant pleural effusion. Oncogene 25 (31) (Jul 20): 4300-9.

Yi SM, Lee JH, Graham S, Zabner J, Welsh MJ. Adenovirus calcium phosphate coprecipitates enhance squamous cell carcinoma gene transfer. Laryngoscope. 2001 Jul;111(7):1290-6.

Yu, H. and R. Jove. 2004. "The STATs of Cancer--New Molecular Targets Come of Age." Nature Reviews.Cancer 4 (2): 97-105. doi:10.1038/nrc1275.

Yu, H., D. Pardoll, and R. Jove. 2009. "STATs in Cancer Inflammation and Immunity: A Leading Role for STAT3." Nature Reviews.Cancer 9 (11): 798-809. doi:10.1038/nrc2734.

Yuan, A., P. C. Yang, C. J. Yu, W. J. Chen, F. Y. Lin, S. H. Kuo, and K. T. Luh. 2000. Interleukin-8 messenger ribonucleic acid expression correlates with tumor progression, tumor angiogenesis, patient survival, and timing of

relapse in non-small-cell lung cancer. American Journal of Respiratory and Critical Care Medicine 162 (5) (Nov): 1957-63.

Zhong, L., J. Roybal, R. Chaerkady, W. Zhang, K. Choi, C. A. Alvarez, H. Tran, et al. 2008. "Identification of Secreted Proteins that Mediate Cell-Cell Interactions in an in Vitro Model of the Lung Cancer Microenvironment." *Cancer Research* 68 (17): 7237-7245. doi:10.1158/0008-5472.CAN-08-1529.